Point of View

How AI impacts molecular imaging

Precision Medicine

Physicians from the Netherlands and Switzerland describe how they're able to bring precision medicine to their practices

Quantification

Quantification in SPECT/CT advances precision medicine

Clinical Results

Read the latest clinical cases from around the world

Imaging Life

Your Resource for Molecular Imaging Innovation

Scaling the summit of molecular imaging

Experts discuss nuclear medicine and molecular imaging's optimistic future at the Molecular Imaging World Summit

Issue 16 · 2019

SIEMENS Healthineers

"The future will have a close collaboration between biologists, medical oncologists, and molecular imaging specialists to drive the field forward."

Olivier Michielin, MD, PhD, Centre Hospitalier Universitaire Vaudois; Swiss Institute of Bioinformatics
Read more about how experts envision the future of the field on page 6

Healthcare continues to face tremendous challenges: increasing consolidation, reduced reimbursements, and constant pressure to deliver more with less.

While it's easy to focus on these day-to-day pressures, equally important is taking time to plan and shape the future for which we are all so passionate. In order to stimulate discussion and debate on the direction of molecular imaging, we recently convened a gathering of over 240 academics, luminaries, and thought leaders from around the world: what ensued was inspiring.

Since 2011, Siemens Healthineers has hosted three Molecular Imaging World Summits. This year's gathering was a unique chance to reflect on milestones achieved and examine drivers fueling new opportunity. In recent years molecular imaging has progressed significantly with the rapid adoption of PET/CT in therapy planning, a steady shift towards SPECT/CT, and advanced quantification tools. Impressive growth has been made in physics, computing power, and scanner technology, which have enabled features like continuous bed motion, SiPM-based PET/CT with 214 picosecond time of flight, and new reconstruction techniques such as xSPECT™. Novel tracers and radiotherapeutics are likewise stimulating an industry renaissance and accelerating new approaches to care.

Looking ahead, predictions for next-generation molecular imaging include the clinical adoption of multiparametric PET/CT imaging, routine quantitative SPECT/CT, and a more decisive role in theranostics. Additionally, the future of molecular imaging will impact the management of prostate cancer, as well as neurological and orthopedic disorders. Pushing new frontiers is the advent of artificial intelligence, which creates unprecedented possibilities for radiomics and tumor heterogeneity analysis.

In this issue of *Imaging Life*, we share some of the visionary work and accomplishments made by leaders in our field. I hope their experiences leave you with a renewed sense of optimism for the ambitious future upon which we are jointly embarking.

Matt Shah,
Vice President, Global Sales & Marketing
Molecular Imaging Business Line
Siemens Healthineers

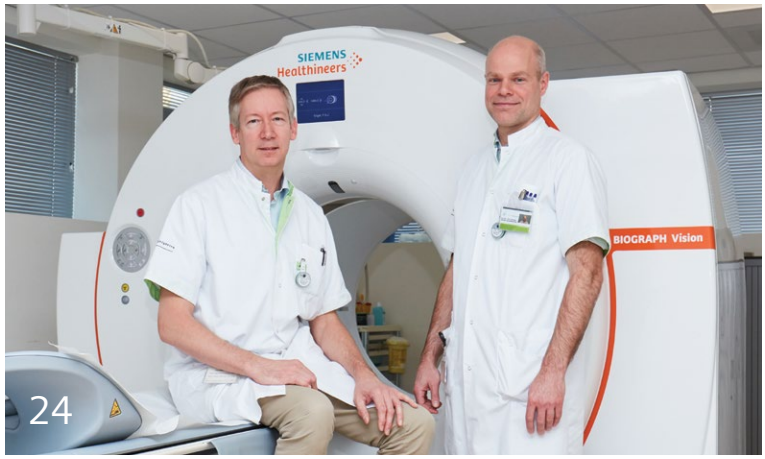

Spotlight

Point of View

Precision Medicine

Quantification

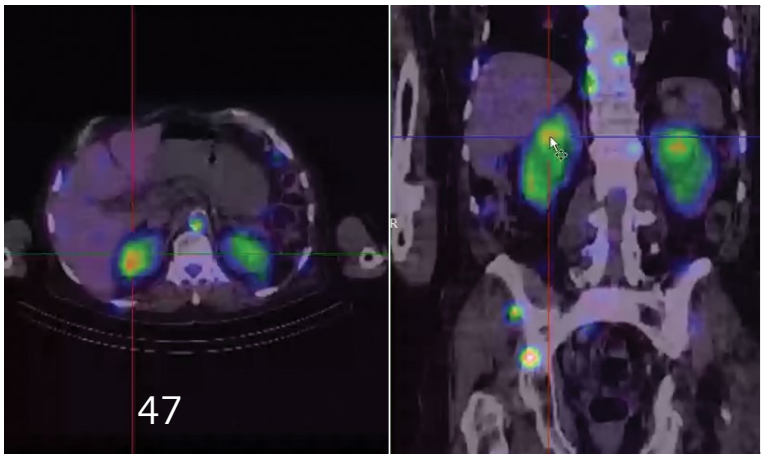

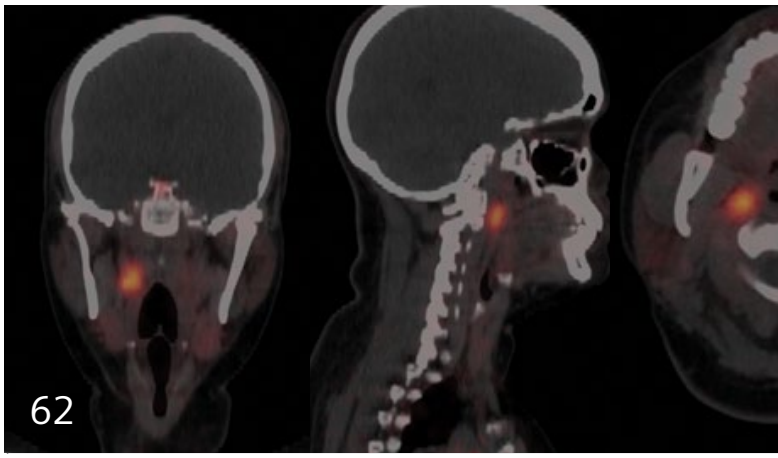

Clinical Results

^{177}Lu PSMA is not currently recognized by the U.S. Food and Drug Administration (FDA) or other regulatory agencies as being safe and effective, and Siemens does not make any claims regarding its use.

Scaling the summit of molecular imaging

At Siemens Healthineers' recent Molecular Imaging World Summit, nuclear medicine and molecular imaging professionals were optimistic about the future as they examined trends, research, and technological advancements. The Summit fostered inspired discussion around opportunities for molecular imaging and how the field contributes to the expansion of personalized care.

By Bill Hinchberger | Photography by Ronald Patrick

These are exciting times for molecular imaging and, as current applications broaden, more people benefit from today's best practices. Moving beyond diagnostics into therapy, molecular imaging propels efforts to provide personalized care that improves patient outcomes. Cutting-edge research in areas like artificial intelligence (AI) suggests that tools, such as digital avatars, will soon become available—even if some seem straight out of science fiction.

Upbeat messages dominated the dialog during the Molecular Imaging World Summit in Lausanne, Switzerland. Hosted by Siemens Healthineers, the conference brought together over 240 participants from more than 140 institutions around the world. While the mood was generally hopeful, there were a few pauses for reflection around topics such as the possibilities of AI and pressures to adapt to a changing healthcare landscape.

Optimism populated the Summit's keynote address, given by John O. Prior, MD, PhD, FEBNM, professor and head of nuclear medicine and molecular imaging at Centre Hospitalier Universitaire Vaudois (CHUV) in Lausanne, Switzerland. In his opening speech, Prior explained precision medicine occurs when physicians, "make a treatment plan based on the characteristics of the patient." The concept involves gathering sufficient data about an individual to be able to predict their reaction to a particular treatment, and to adjust treatment based on results. Continued research is needed regarding the potential of molecular imaging in precision medicine, as there are multiple pathways and possible new tracers that could be "exciting," he emphasized.

Quantified precision medicine

Looking into the future, presenters were keen to focus on quantification. Many noted the movement from a traditional


Été
Summer
Hiver
Winter
Actualités olympiques
Olympic News
LATEST
SUITE
SPECT

mixture of qualitative and subjective analysis to one that relies on quantitative and objective criteria. This approach continues to evolve as both SPECT/CT and PET/CT develop similar quantitative capabilities and analytical tools become more reliable and sophisticated, such as solutions for automated, quantitative SPECT/CT and multiparametric PET.

Quantitative and objective analysis of data are the central motivators behind the increased focus on phenotypes, which is a significant shift from a past where an emphasis was on genotypes. Molecular imaging can help physicians better understand a patient's phenotype, therefore making it easier to determine if someone is a good candidate for a certain type of treatment. In the early stages right now, this trend will develop over the next decade as experts anticipate it to engender better use of precision medicine.

Presenters participate in the quantitative imaging panel (top) and Biograph Vision panel (bottom).

Early diagnosis and planning

Presentations about early diagnosis and planning focused to a large extent on opportunities in neurology and orthopedics.

In aging nations, demand is growing for hybrid neuroimaging of degenerative diseases, said Jun Hatazawa, MD, professor of nuclear medicine at Osaka University in Japan. Quantitative SPECT/CT improves the neurological diagnosis as it provides biopsy-quality neuropathological results without the need for tissue sampling.

Exploring opportunities in orthopedics, Helmut Rasch, MD, of the department of radiology and nuclear medicine at Kantonsspital Baselland in Switzerland, explained how everyone dreams of a "one-stop shop". Biomechanics, metabolism, and morphology all affect the ability to visualize a bone bruise that causes pain, for example. As SPECT/CT offers metabolic and anatomical information in its hybrid approach, it can provide physicians a wealth of orthopedic information that aids in accurate and quick clinical decision making.

Beyond neurology and orthopedics, a panel of four physicians explored the progression of PET/CT through a review of everyday cases acquired with the Biograph Vision™ PET/CT scanner. The panel vetted the system's performance, noting the clinical impact they experience with the latest advancements in PET/CT.

Therapy management

As presenters examined the use of molecular imaging in therapy management, the topic centered around prospects for theranostics—the combination of diagnostics and therapy—and immunotherapy.

Treatments considered to have high promise include those designed, "to target a molecular pathway and activate the immune system," explained Prior. A combination of talks on cancer immunotherapy highlighted how understanding

The Molecular Imaging World Summit in Lausanne, Switzerland brought together over 240 participants from more than 140 institutions around the world.

"The fact that molecular imaging can assess heterogeneity and the dynamics of response and adaptive resistance is a key advantage over other techniques."

Olivier Michielin, MD, PhD, CHUV; Swiss Institute of Bioinformatics

the biology of individual patients can aid in selecting those who are most likely to respond favorably to a particular biomarker, and thus guide first- and second-line therapies. "The fact that molecular imaging can assess heterogeneity and the dynamics of response and adaptive resistance is a key advantage over other techniques," signaled Olivier Michielin, MD, PhD, head of the precision oncology center at CHUV and group leader at the Swiss Institute of Bioinformatics. "For me the future will have a close collaboration between biologists, medical oncologists, and molecular imaging specialists to drive the field forward."

Precision medicine, theranostics, and dosimetry loomed large in a talk given by Rodney Hicks, MD, professor of medicine and radiology at the University of Melbourne and director of the Centre for Cancer Imaging at the Peter MacCallum Cancer Centre in Melbourne, Australia. Drawing on the sentiment, "if we can see if, we can treat it," he emphasized how personalized data opens the door to tailored dosimetry. In a current practice without dosimetry—or a dose-tailored regimen for therapeutic agents—physicians utilize standard protocols even though the treatment option may not help the prognosis for the individual. Dosimetry can aide physicians in adapting the therapeutic dose to more effectively treat patients who might be able to withstand a higher dose as well as others who may be excluded as therapy candidates but may benefit from lower-dose protocols. Yet Hicks warned against excessive complexity; when talking about his work with dosimetry he said, "we like to keep it simple."

Speaking to the implementation of standardized protocols in therapeutics, an invited industry speaker articulated the viewpoint that a standardized dose regimen for therapeutic agents may accelerate a broad adoption by

"AI-assisted software applications are already working on non-small cell lung cancer and lymphoma."

Marcus Hacker, MD, PhD, Medical University of Vienna

clinicians. From his perspective, topics like dosimetry could be introduced once therapeutics are clinically routine. What followed was an active debate on dosimetry from a panel of international luminaries, moderated by Dale Bailey, PhD, principal physicist in the department of nuclear medicine at Royal North Shore Hospital in Australia.

Creating the future of molecular imaging

Progress in the realm of molecular imaging is likely to be split between important, incremental advances and industry game-changers. Examples of relevant developments ranged from continuous bed motion and motion management in PET/CT to possibilities for quantitative cardiac SPECT/CT. In his talk, Frederick Giesel, MD, vice chair of nuclear medicine at the University of Heidelberg, presented the latest results of their work with quinoline-based PET tracers that act as fibroblast activation protein (FAP) inhibitors (FAPIs). An emerging diagnostic method, FAPI PET/CT appears to be viable for imaging a broad range of cancers, while providing specific data. Exciting opportunities for a theranostic adjunct also appear to be feasible.

When shifting to game-changers that impact the future of molecular imaging, AI was a salient example. "AI-assisted software applications are already working on non-small cell lung cancer and lymphoma," said Marcus Hacker, MD, PhD, head of the clinical department of nuclear

medicine at the Medical University of Vienna. Experiments seek to apply Google's face-recognition technology to identify tumors, and machine learning seems capable of differentiating high- and low-risk tumors, as well as malignant and non-malignant ones. The joint future of AI and molecular imaging could include several major developments: the use of predictive biomarkers; convergent molecular diagnostics—a survival-prediction approach which combines molecular diagnostics with molecular imaging—and applied metabiomics.

Even outside the considerations of AI's imact, it's obvious the pace of molecular imaging is accelerating: the goal is to gain a clear understanding of disease and utilize this information to better formulate treatment plans that benefit individual patients. When leaders meet again at future world summits, it will be enlightening to see what milestones are achieved and what remains on the horizon. Yet, regardless how many predictions we check "accomplished" or not, it is clear there is a crucial place for molecular imaging and nuclear medicine in the future of healthcare, which is cause for great optimism. ●

Near-future predictions for MI

- The demand for imaging will grow due to aging populations, chronic disease, and reimbursement expansion based on success.
- Due to growing demand more injection rooms will be required.
- The number of available therapies will increase.
- There will be a shift towards predictive imaging.
- Alongside PET/CT and SPECT/CT, PET/MR will be established clinically.
- The number of personnel per patient will decrease.
- AI will aid image acquisition and interpretation.

– *Martin A. Walter, MD, PhD*
University Hospital Geneva

Bill Hinchberger is a Paris-based journalist whose work has appeared in *The Lancet, Science*, and many other publications.

Further Information

Learn more about the Molecular Imaging World Summit 2019
siemens-healthineers.com/misummit

Examine the use of SPECT/CT quantification for theranostics
siemens-healthineers.com/theranostics

Discover the use of SPECT/CT in orthopedics
siemens-healthineers.com/spectorthopedics

Explore Biograph Vision
siemens-healthineers.com/vision

Point of View

AI in molecular imaging: the vast potential

Artificial intelligence (AI) is already integrated into many facets of our daily lives and, in the medical-imaging community, new research demonstrates how it can help us on a myriad of fronts in molecular imaging.

By Univ.-Prof. Dr. Marcus Hacker | Photography by Ronald Patrick | Illustration by Dmitri Broido

The potential is vast; by applying AI algorithms to molecular imaging studies and integrating other data, we might be able to improve diagnostic accuracy. It's even on the radar that AI-aided imaging techniques may soon prove more accurate than standard biopsies.

But we're still in the early stages. Only one presentation focused on AI during the recent Molecular Imaging World Summit in Lausanne, Switzerland—the one I gave in tandem with Sven Zuehlsdorff, PhD, Senior Director, Research for Molecular Imaging at Siemens Healthineers. Yet, when the next summit takes place a few years from now, I expect at least half of the talks will feature AI.

Starting simply: classical segmentation

The clinical application of AI in molecular imaging is one of great potential. For example, AI could help physicians identify uptake patterns of glucose-analog tracers in examinations for non-small cell lung cancer. In this type of disease the presence of tracer uptake is a potential indicator of a metastasis, but sometimes there's also distinct uptake in small lymph nodes. Even with standard uptake value (SUV) thresholds, how do we confidently resolve the uncertainty around lymph node uptake? The use of AI could help differentiate a metastasis from other potential causes of uptake.

Another example is in the routine diagnosis of lymphoma. In a whole-body scan, there may be lesions in both the lymph nodes and organs. It would be useful to have algorithms that could help segment and quantify those lesions and compare imaging examinations with previous ones: the comparative data could also help determine the success of the treatment.

Radiomics

Even as current applications are still being determined, the field is moving forward at a rapid pace. One inspiring initiative is in the realm of pattern recognition with deep convolutional neural networks.

Such an initiative involves "radiomics", which is the accumulation and analysis of quantified image data to improve medical decision making. Radiomics can help quantify the heterogeneity of uptake in a certain region, for instance.

As an example, benign and malignant lesions in the cutis can sometimes look very similar. A landmark study published in 2017 used Google's face-detection algorithm to detect and rate dermal lesions. The algorithm was trained on some 130,000 images and the parameters that emerged were then trained on about 2,000 cases where histology data was available: the resulting algorithm outperformed the results of a group of board-certified dermatologists.[1]

""Medicine is a science of uncertainty and an art of probability."

Sir WIlliam Osler

"The nuclear medicine and molecular imaging field has a unique advantage over other imaging modalities."

Marcus Hacker, MD, PhD, Medical University of Vienna

Studies such as this show the potential of AI in helping determine tissue characterization in molecular imaging studies and the importance of extracting more information from images.

21st-century Bayes

"Medicine is a science of uncertainty and an art of probability," said Sir William Osler, one of the founders of modern medicine in the late-19th and early-20th century. Over a century earlier, a pioneering statistician named Thomas Bayes established a theorem in medicine: a successful diagnosis depends in large part on the known pre-examination conditions.

Since a diagnosis is a guess at the probability of a particular reality, the Bayes theorem suggests that relevant pre-test elements be factored into the equation as much as possible. Instead of just looking at images, physicians should consider demographic data—such as age—and the results of earlier examinations.

If you want to predict the mortality rates of patients with lung cancer, several factors are important: smoking, the FEV1 number (for lung capacity), and even the tumor size. But most examiners do not take such data into consideration when they analyze images. Algorithms could help prompt doctors to closely examine lesions in patients who have red-flag pre-test characteristics, for example.

What's next?

The nuclear medicine and molecular imaging field has a unique advantage over other imaging modalities as it can focus and quantify results in ways that allow physicians to determine targeted responses to disease.

However, it is also important to peruse what I call "convergence engagement" among disciplines. Professionals from different disciplines should learn how to combine their knowledge and expertise, which includes the combination of data from disparate tests and other sources. AI could prove crucial in our efforts to bring together these different parameters and optimally leverage their additional value. ●

Univ.-Prof. Dr. Marcus Hacker is the Professor for Nuclear Medicine and Head of the Clinical Department for Nuclear Medicine at the Medical University of Vienna.

The statements by Siemens Healthineers customers described herein are based on results that were achieved in the customer's unique setting. Since there is no "typical" hospital and many variables exist (e.g., hospital size, case mix, level of IT adoption) there can be no guarantee that other customers will achieve the same results.

References

[1] Esteva A, Kuprel B, Novoa RA, et al. Dermatologist-level classification of skin cancer with deep neural networks. *Nature*. 2017;542:115-118.

AI for molecular imaging, in action

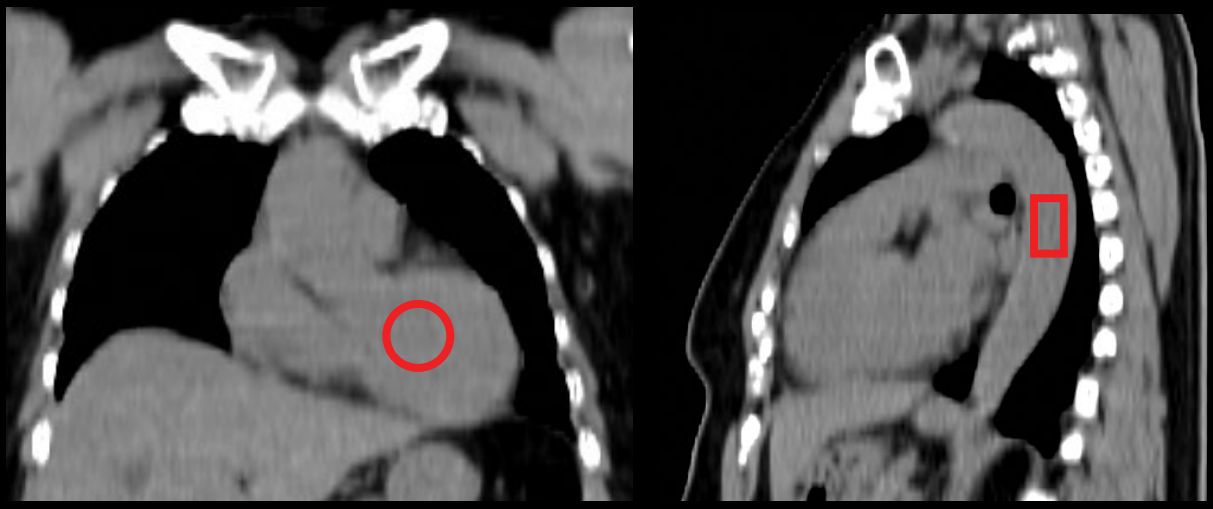

Data courtesy of Chulabhorn Hospital & Research Institute, Bangkok, Thailand

AI currently powers Siemens Healthineers' comprehensive molecular imaging approach: multiparametric PET/CT.

Patlak parametric modeling requires measurement of the arterial input function (AIF), which is the amount of tracer available in the blood pool over time.

Siemens Healthineers' AI-powered solution—driven by Anatomical Landmark Parsing of Human Anatomy (ALPHA)—uses the CT image to find anatomical landmarks and obtain the AIF from the PET images, automatically.

Discover Siemens Healthineers' approach to AI:
siemens-healthineers.com/AI

Learn about our approach to Multiparametric PET/CT:
siemens-healthineers.com/multiparametricPET

SIEMENS Healthineers

Scaling with Precisi

the Summit on Medicine

A vision realized

While imaging professionals work to contend with the progression of disease they strive to improve diagnostic accuracy that supports personalized treatment for each patient, all while maintaining operational efficiency.

By Kathryn J. McCullough | Photography by Peter J. Reese & Alex Teuscher

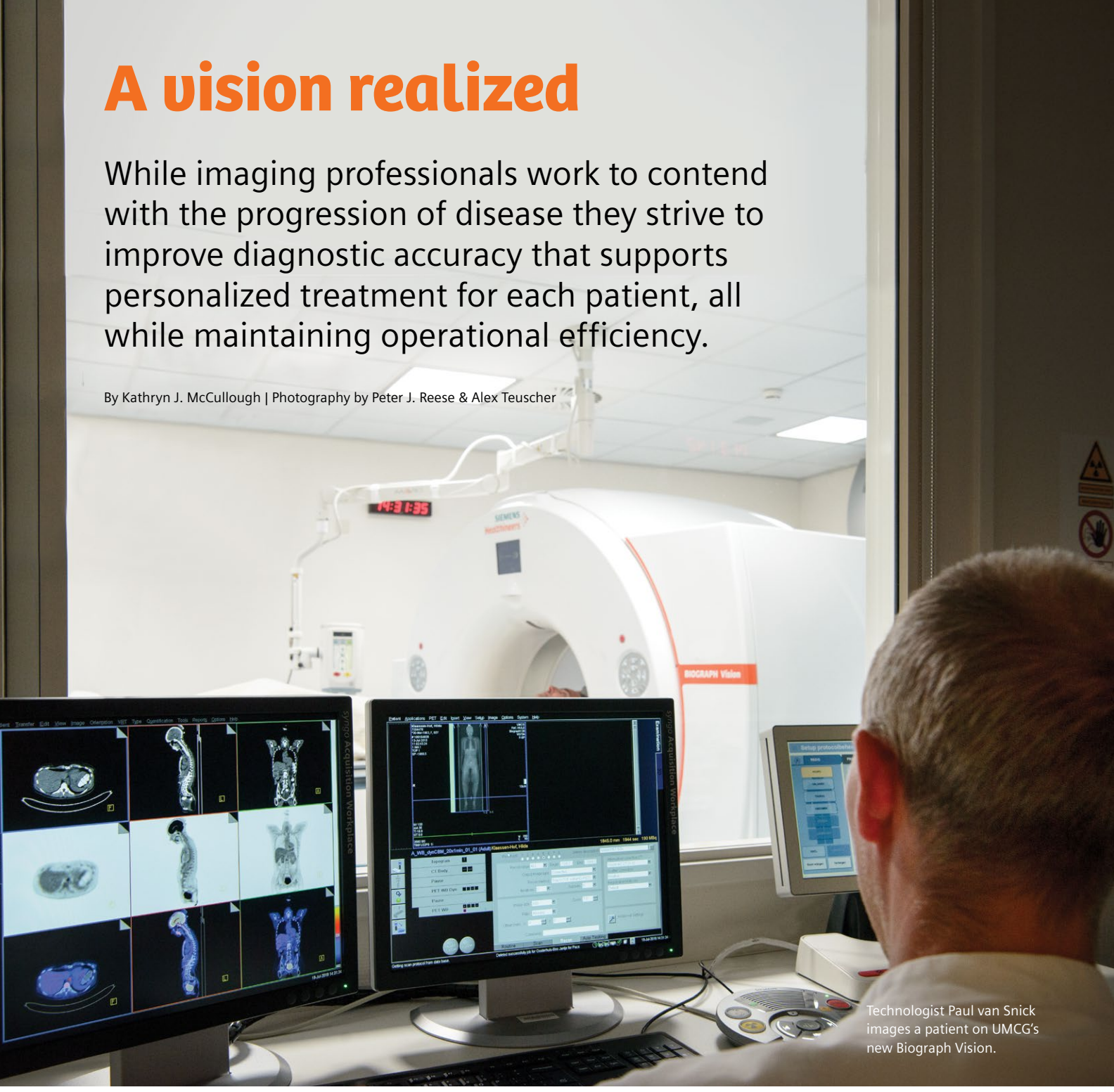

Technologist Paul van Snick images a patient on UMCG's new Biograph Vision.

The challenge is clear: medical imaging must keep pace with progressive disease. Medical imaging noninvasively visualizes the physiology of disease and provides clinicians vital information that aids them in developing and monitoring a patient's treatment strategy. Yet, the fact remains that progressive disease often outpaces medical imaging. "One of the problems with imaging is that you're always running behind. The tumor has either grown or metastasized even in a very early stage of the disease, and it's difficult to detect those very small locations of metastases," emphasizes Walter Noordzij, MD, PhD, nuclear physician at the University Medical Center Groningen (UMCG) in the Netherlands.

Addressing a medical need of such magnitude proves daunting, especially when the pressure to support precision medicine and maximize operational efficiency compounds the challenge.

Ronald Borra and Walter Noordzij walk the halls of of the diagnostic imaging department at UMCG.

For medical professionals, utilizing the latest innovations in imaging technology is a step towards overcoming this complex challenge. For Niklaus Schaefer, MD, nuclear physician at Centre Hospitalier Universitaire Vaudois (CHUV) in Lausanne, Switzerland, the approach is clear. "On one side we really want to propagate nuclear medicine as the best possible tool to visualize complex diseases, for example to better plan a treatment or assess response. For this we need the best possible scanner and for me, nuclear medicine is really facilitating precision medicine now."

Precision that changes perceptions

In medical imaging, precision medicine translates to the precise visualization of disease. Such precise visualization provides physicians detailed diagnostic information that may influence the treatment path for a patient.

For Mario Jreige, MD, a radiologist and nuclear medicine resident at CHUV, "it's very important to provide patients with the best treatment and technologies that we have. And now that we have Biograph Vision™, we are working to adapt our knowledge and capacities to provide better healthcare, diagnostic capacities, and treatment to our patients."

Technology that enables physicians to visualize disease in a way that facilitates better treatment is the fundamental cornerstone of nuclear medicine. For a field that was notoriously dubbed as "unclear medicine" in the past, the ability to deliver precise imaging changes how clinicians perceive disease. Schaefer elaborates, "over the years, nuclear medicine went from something that was seen as not very clear to really a precise form of medicine. Nuclear medicine is changing clinicians' perceptions because we can now see nodules that are three millimeters, and it's augmenting our perception of disease."

As a physician, having access to PET/CT technology that acquires images which challenge previous perceptions of nuclear medicine—the possibilities as well as the limitations—incites excitement. Noordzij recounts his enthusiasm upon seeing the precise detail of Biograph Vision's images. "When we got the image of the first patient, we were very excited. We could see lesions that were clearly outlined and also seemed fairly homogeneous, not patchy because of the different noise levels. It was a completely different kind of image."

Above: Mario Jreige and Martin Pappon walk the halls of CHUV as they discuss the day's patient scans.

Left: Technologist Martin Pappon positions a patient for a scan on CHUV's Biograph Vision.

Advanced technology enables precision

Admittedly, the science of PET/CT is impressive and complex: in one machine resides technology that combines physics, biology, medicine, engineering, and an abundance of innovation.

Examining recent PET/CT images acquired on Biograph Vision, Silvano Gnesin, PhD, medical physicist at CHUV, reflects on how the system's advanced technology enables such precision. "We would traditionally reconstruct the field of view with about 250 x 250 voxels discretization in each direction, and we had voxels of around two and a half millimeters. Now we can go down to half of this size."

Expounding on how Biograph Vision's core technology can advance precise PET/CT imaging, Ronald Boellaard, PhD, medical physicist at UMCG, offers his insights. "The high resolution makes images with more spatial detail which also means the signal, such as for a small tumor or lymph node, will be less spread. By making a PET system with smaller detectors, you improve the spatial resolution and also reduce the partial volume effect, which leads to sharper images and more accurate quantification."

The clinical impacts of precision

While there is much excitement over the technological advancements of Biograph Vision and the resulting image quality, it is important to remember the technology's ultimate

"When we got the image of the first patient, we were very excited. We could see lesions that were clearly outlined and also seemed fairly homogeneous, not patchy because of the different noise levels. It was a completely different kind of image."

Walter Noordzij, MD, PhD, University Medical Center Groningen

purpose: visualizing disease in such a way that helps physicians determine the best path of patient care.

As the first two sites with the latest PET/CT technology, UMCG and CHUV are just beginning to discover Biograph Vision's potential.

At UCMG, Ronald Borra, MD, PhD, explains, "Biograph Vision is extremely sensitive with a high resolution. We can see exactly where the tracer binds to the tumor and we see the volume and distribution much more accurately. All of those things can play a key role in steering the patient's therapy toward the best possible clinical outcome."

Physicians at CHUV also see the capacity for this new technology to aid in the determination of a patient's therapy plan. Schaefer explains, "for those patients where localized treatment plays a huge role—in prostate cancer or lung cancer—it is certainly a factor because we need the fastest and highest form of resolution. In those situations, Biograph Vision will play a big part."

Addressing operational efficiency

While the connection between advancements in imaging technology and the impact on patient care may be apparent, another vital part of the challenge is how to handle daily operational demands efficiently.

Equipped with the latest advancement in PET/CT technology, UMCG and CHUV are able to discover what it means to be precise and operationally efficient, simultaneously.

At CHUV, John Prior, MD, PhD, FEBNM, head of nuclear medicine, elaborates that Biograph Vision enables his team to acquire scans, "probably 30% faster with about 30% less dose, which is something extraordinary."

Martin Pappon and Silvano Gnesin discuss recently acquired images on CHUV's Biogaph Vision.

"Biograph Vision is extremely sensitive with a high resolution. We can see exactly where the tracer binds to the tumor and we see the volume and distribution much more accurately. All of those things can play a key role in steering the patient's therapy toward the best possible clinical outcome."

Ronald Borra, MD, PhD, University Medical Center Groningen

However, for the team at UMCG, the realization that Biograph Vision allows them to couple precision and operational efficiency came quite unexpectedly. According to Borra, "one of the things we wanted to do was push the scanner to the limits and at some point, without meaning to, we entered seven seconds per bed. So, in total, we had around a 50-second scan for seven bed positions. We all expected the quality to be very poor, but the resulting images turned out to have spectacular quality for such a short scan time. One of my nuclear research colleagues said, 'This thing is amazing. We can do so many scans.' It was not something we intended, but it was a very early sign of how extremely good Biograph Vision is."

What's next?

Technologies such as Biograph Vision are just one step in the advancement of medicine as it looks to keep pace with the progression of disease.

For Schaefer, while he recognizes the opportunities advanced PET/CT technology present, he also emphasizes that the responsibility of true progress resides with the physicians. "We have to understand what our high-resolution images mean. What is real disease? Does it play a role? I think having a great tool

Walter Noordzij and team member examine Biograph Vision's image quality at UMCG.

The lobby of UMCG bustles with activity; a common site at one of the Netherlands largest hospitals.

"We have to understand what our high-resolution images mean. What is real disease? Does it play a role? I think having a great tool certainly allows for the best possible way to measure disease, but it has to be followed by some kind of decision from a clinician."

Niklaus Schaefer, MD, Centre Hospitalier Universitaire Vaudois

certainly allows for the best possible way to measure disease, but it has to be followed by some kind of decision from a clinician. To understand its real value and its impact on management, we need clinical trials together with our clinical partners."

Jreige stresses, "it is important for us to progress; not to remain where we are, and not just do a routine clinical workup. It's crucial for patients to receive their staging, monitoring, and therapy, but it's also important for us to better understand cancer and other pathologies, as well as the continuum and difference between these entities so we can make diagnoses with more ease. It's important for us to understand the physiology of the disease, and having new technologies that help us do this is very promising and satisfying." ●

The statements by Siemens Healthineers' customers described herein are based on results that were achieved in the customer's unique setting. Since there is no "typical" hospital and many variables exist (e.g., hospital size, case mix, level of IT adoption) there can be no guarantee that other customers will achieve the same results.

Biograph Vision is not commercially available in all countries. Due to regulatory reasons, their future availability cannot be guaranteed. Please contact your local Siemens organization for further details.

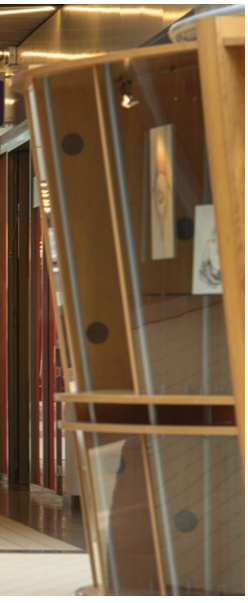

Mario Jreige and Martin Pappon study Biograph Vision's next-generation imaging capabilities.

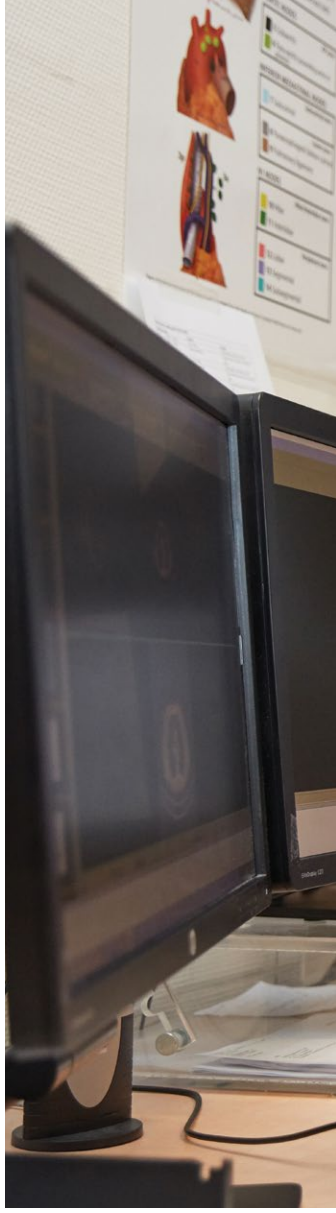

Precision at the molecular level

In molecular imaging, the smallest details can make a significant difference when it comes to reporting, sharing, and reading studies. By equipping their nuclear medicine and molecular imaging department with state-of-the-art equipment and a revolutionary reading solution, Instituut Verbeeten in the Netherlands aims to deliver accurate and efficient medical care.

By Erika Claessens | Photography by Miquel Gonzalez

Instituut Verbeeten is a center for nuclear medicine and radiotherapy, linked to the ETZ Elisabeth-Twee Steden Hospital in Tilburg," says Arjan B. van Dijk, MD, a nuclear physician at the Instituut Verbeeten. Since 2003, van Dijk has been responsible for PET/CT imaging at the institute.

"With radiotherapy offices in Tilburg, Breda, and Den Bosch, our institute is widely known as a center of excellence in the south of the Netherlands, with our nuclear medicine and molecular imaging department situated in Tilburg. We realized that in order to deliver accurate and detailed medical images, we

needed the right tools for reading, interpreting, and sharing PET and SPECT studies. And, as we play an important role in the regional healthcare industry, our executive board and management team have always looked years ahead when equipping the nuclear medicine and molecular imaging department."

"By equipping our nuclear medicine and molecular imaging department with a comprehensive reading solution, we can continue to deliver the best healthcare possible in the south of the Netherlands."

Arjan van Dijk, MD, Instituut Verbeeten

Looking ahead

"Looking ahead is critical because things move extremely fast in nuclear medicine," adds Jeroen De Jong, MD, nuclear physician and medical manager of the nuclear medicine department. "When I started my career at Instituut Verbeeten, our department already had a Symbia™ T2 SPECT/CT along with an Orbiter single-head gamma camera. Even back then, we used dedicated software to integrate all images from various departments and neighboring hospitals into one platform across all workstations."

Arjan B. Van Dijk (left) and Jeroen De Jong proudly stand in front of their department's state-of-the-art PET/CT scanner, Biograph Vision.

When looking to add the next generation of PET/CT technology to their enterprise, van Dijk's eye fell on Biograph Vision™ 600, which was installed at the Tilburg site in November 2018. "Keeping at the cutting edge of technology can dramatically improve how we work," van Dijk continues. The institute can now serve 2,200 patients annually with their newest PET/CT addition, while around 5,000 patients per year are imaged via their two SPECT/CT systems.

One application for all

"With the new device, we also needed a comprehensive reading solution, so we chose the *syngo*®.via multiuser application. We simply love the way this application works," van Dijk states. "It allows images from our latest-generation PET/CT system to be easily and efficiently read by a multidisciplinary team spread across different locations. The images are automatically prepared, digitized, and processed on a unique client/server platform no matter where the workstation is situated." He adds that when the patient data transfers from the scanner to the reading solution, the images are automatically added to the patient's folder and ready to view.

Virtual collaboration

"Furthermore, it is important to know that our picture archiving and communication system (PACS) differs from other hospital PACS. Thus, we need to be very flexible, and the *syngo*.via reading solution is of great help in supporting our processes," explains van Dijk. According to van Dijk, most of the multidisciplinary team meetings are now held virtually with video conferencing, while patient studies and reports are projected on a large screen. "With the virtual *syngo*.via server we can add a patient's previous scans and share the images with all participating members. And other information, such as a past gastric-emptying study, can be easily uploaded from a CD-ROM and integrated into the platform." The reading solution is also equipped with a Findings Navigator, which automatically stores and displays previous findings. This solution can shorten the time needed to compare pre- and post-therapy exams, a feature which van Dijk warmly welcomes.

Layouts improve quality

For De Jong, viewing images in the reading solution layout makes all the difference. "It's a huge step forward," he states. "Pre-fetching the digitalized images from a patient's history, even when these are made in another hospital, is instant and effortless. And comparing studies can be done in next-to-no time." Choosing a specific layout instead of a standard one is another advantage of the reading solution, according to De Jong. "I can easily adjust image saturation to highlight the patient's follow-up scan. By scaling it myself, I can immediately detect if a patient is reacting positively to a treatment."

An eye opener

Learning how to incorporate the robust reading solution into his established working method took time, De Jong admits, "but now I only see the advantages." With the elimination of many manual pre-processing steps, the workflow is more efficient. "The adaptability of the layout is certainly a plus. If I am not satisfied with an image, I can still correct it manually. The images are our end product and if we can highlight the key details at a molecular level, it increases their value." Van Dijk and De Jong are proud of the outstanding image quality they are able to deliver. Before, when they attended multidisciplinary meetings, they only had a

The architecture and design within Instituut Verbeeten mirror the institute's healing-environment philosophy.

laptop with them and, as the image could not be scaled and the quality was not always perfect, there was little room for discussion around diagnosis.

"*syngo*.via has been an eye-opener to me," De Jong emphasizes. "We are proud to show the high-quality images it produces. Why would we have a state-of-the-art, high-resolution scanning device like Biograph Vision if we didn't also have a comprehensive reading solution that brings precision to our images."

Motivation and ambition

Arjan van Dijk agrees. He says the dedication to precision and patient care is likewise reflected in the healing-environment philosophy of Instituut Verbeeten, where it is believed architecture and design contribute to patient health. Instituut Verbeeten's excitement to utilize the latest generation of technology mirrors this philosophy. "Our patients and staff must feel and experience our motivation and ambition. By equipping our nuclear medicine and molecular imaging department with a comprehensive reading solution, we can continue to deliver the best healthcare possible in the south of the Netherlands." ●

Erika Claessens is an independent journalist and editor based in Belgium. Her principal topics are entrepreneurial innovation and (medical) technology. She works from Antwerp, Belgium.

Scaling with Qu

the Summit antification

CHUV team members examine a ^{177}Lu xSPECT Quant image.

Defining the quantitative future of SPECT/CT

SPECT/CT imaging, with its innate ability to detect and characterize abnormalities in their earliest forms, is a meaningful tool for determining prompt diagnoses and developing personalized treatment strategies. Such a tool is invaluable as we move toward precision medicine, and the significant addition of reliable quantitative measurements only enhances SPECT/CT's opportunities. But as quantitative SPECT/CT looks to establish an active role in the next era of healthcare, the extent of its impact continues to be defined.

By Colleen R. Smith, MBA | Photography by Alex Teuscher

While the concept of quantitative SPECT/CT has existed for years, SPECT/CT systems are not intrinsically quantitative; their means for measuring activity concentration are limited without additional efforts such as manual, complex calibrations. While publications stress the benefits of quantification, they simultaneously reinforce the importance of accuracy by sharing tips for more easily obtaining measurements and minimizing chances for error.

These obstacles are far less discouraging now that technologies are in place to address them. Today's automated measurement tools allow us to go beyond questioning whether quantitative SPECT/CT will impact the future of medicine and instead ask how much of an impact it will have.

As we evaluate how quantitative SPECT/CT will influence care, the emphasis remains on the validation of:

- how quantification can be utilized in routine care paths
- the contribution to a more precise diagnosis
- the value in treatment management.

Around the world there are now individuals and teams who drive this debate, with the ultimate goal of reaching a consensus within the scientific community. One such team resides in the nuclear medicine and molecular imaging department at Centre Hospitalier Universitaire Vaudois (CHUV), situated on the shores of Lake Geneva in Lausanne, Switzerland.

Simplifying quantification

Over the past decade, the team at CHUV devoted a portion of their work to better understand the potential, and constraints, of SPECT/CT quantification. While applying quantitative SPECT/CT in select therapeutic situations, they identified the opportunity for more diagnostic and treatment applications. Simultaneously, they recognized the potential benefits of incorporating quantitative SPECT/CT as a standard imaging practice. Yet, without a simplified way to obtain reliable and accurate quantitative results, their progress toward routine, clinical implementation was difficult.

"Ten years ago, it was very complicated. We had to have technicians and medical physicists do the calibration to have an equivalence of how many megabecquerel were making how many counts. So, we had to establish a standard with a known activity and a known volume. From the imaging, we could then derive how many counts equal how many megabecquerel," recalls John Prior, MD, PhD, FEBNM, head of nuclear medicine at CHUV.

In 2014, Prior and his team adopted technology that was able to assist them as they forged a path towards routine quantification in SPECT/CT. With the installation of xSPECT Quant™, CHUV began to apply this new form of automated quantification in their Technetium-99m (^{99m}Tc) SPECT/CT studies. In 2016, their quantification work expanded to other isotopes, such as Iodine-123 (^{123}I), Indium-111 (^{111}In),and Lutetium-177 (^{177}Lu).

When referencing xSPECT Quant, Prior asserts, "it's done automatically, so the machine is intrinsically quantitative. In everyday SPECT/CT, we now get this valuable quantitative information with much less effort."

"Before, our number of quantitative procedures were just a few because we calibrated the system only for specific patients," admits Silvano Gnesin, PhD,

John Prior, Michael Da Mota, and Silvano Gnesin (pictured left to right) gather around CHUV's workstations to assess recent quantitative SPECT/CT images.

Michael Da Mota views recently acquired xSPECT Quant SPECT/CT images on CHUV's Symbia Intevo™ scanner.

a medical physicist at CHUV. "But since it is easier to obtain absolute quantification, most of our SPECT/CT procedures are quantitative."

"We do a lot more SPECT/CT than before, because of the quantification that goes with it," affirms Michael Da Mota, technologist in charge of molecular therapy at CHUV. "We now have doctors that write xSPECT Quant in their examination demands." Referring to the pressure to keep up with the increase in studies, Da Mota jokes, "we have to run a little bit more to schedule all the patients."

Demonstrating the diagnostic value

CHUV's work includes evaluating the utility of quantitative SPECT/CT in diagnosis. "We are now using xSPECT quantification in our clinical routine," states Mario Jreige, MD, radiologist and nuclear medicine resident at CHUV. "We often have cases that are borderline, where visual interpretation is limited. Quantification helps us get a more precise diagnosis," he explains. "One of the cases we communicated in an abstract at the 2018 Society of Nuclear Medicine and Molecular Imaging (SNMMI) meeting is where the patient had changes in the vertebrae and was referred for staging. Based on the SUV, it was clear the lesion had very low uptake and tended more towards osteoarthritis, rather than metastatic disease."

"If physicians do not have quantitative SUV measurements, they look at the darkness in an image and when it's really, really dark they say, 'Well, it's probably metastatic,'" adds Prior. "We made some first measurements with ^{99m}Tc bone scans and it looks like everything that has an SUV higher than 20 would be more metastatic and everything that stays below 20 would be more degenerative disease. With SUV we can characterize with more certainty a lesion that has an SUV of 15 or 25 and, for the patient, it makes a lot of difference."

"It is important for us to define criteria because this will lead to very accurate diagnostic capabilities for examinations," Prior points out. "This will help patients to have their diagnoses earlier, and with more precision," underscores Jreige.

When questioned on their impressions of the technology, Prior replies, "we've

"It's important that we deliver numbers, because one of the key points to treating disease is to really measure the degree of disease and treatment response."

Niklaus Schaefer, MD, Centre Hospitalier Universitaire Vaudois

had many 'aha moments,' with xSPECT quantification. One example was when we were able to quantify the uptake from the striatum in patients with potential Parkinson's disease. We know we can see this, and usually also do a ratio between the striatum and the occipital region. It's very technical, but it's a way of getting an index of normality. So having an absolute value, and not needing to make a ratio, was something we found interesting and thought maybe, with this, we can catch disease earlier."

Building off the interest generated by their findings, Prior and team designed an ^{123}I xSPECT Quant study to compare the absolute quantification with conventional relative analysis. Also presented at SNMMI 2018, their results indicate absolute quantification is capable of measuring direct activity and reflecting slight differences between the pathological and non-pathological patient population, which they believe can help define disease earlier.

"In my opinion, physicians are more and more confident as they use xSPECT Quant. We are moving towards a future where quantification is standard," Gnesin reflects when asked about the potential for routine clinical use.

Advancing therapy outcomes

Beyond diagnostics, the team at CHUV spends considerable time investigating the influence quantitative SPECT/CT has on therapy planning and assessment. "We are trying to tailor each treatment, and quantitative imaging with SPECT allows us to get more precise information about how to do it better for each patient," shares Prior. Currently, CHUV applies quantitative SPECT/CT to their ^{177}Lu and Iodine-131 (^{131}I) studies, both of which appear to hold promise.

"I think it's significant that we are not just judging on gray stuff appearing on images. It's important that we deliver numbers, because one of the key points to treating disease is to really measure the degree of disease and treatment response," stresses Niklaus Schaefer, MD, a nuclear medicine physician at CHUV.

For therapy monitoring Schaefer conveys, "after the second cycle of treatment, we want to be sure the patient is responding. First, it really helps the patient to understand

A glance at CHUV

CHUV, an institution that leads the way in SPECT/CT quantification research and clinical implementation, is one that:

- performs 8,400 molecular imaging studies a year
  - nearly half are SPECT-based exams.
- utilizes a Symbia Intevo with xSPECT Quant to perform their SPECT/CT quantification studies.
- employs a staff of:
  - three senior physicians
  - three fellows and three residents
  - 15 technologists
  - two clinical radiopharmacists
  - one medical physicist.
- participates in several research collaboration efforts centered around:
  - radiopharmaceutical development for diagnosis and therapy
  - medical physics for quantitative imaging and dosimetry.

What is xSPECT Quant?

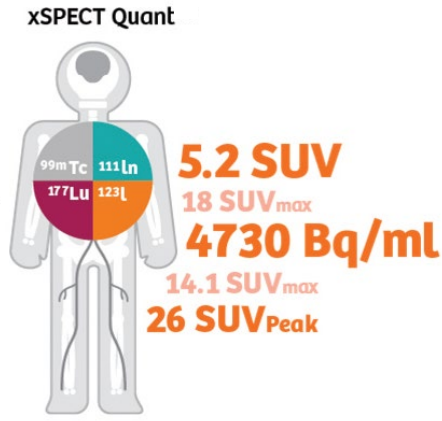

Introduced in 2013, xSPECT Quant was the first solution capable of delivering absolute SPECT/CT quantification that allows for accurate, reproducible, and standardized quantitative clinical studies.

xSPECT Quant uses a patented calibrated sensitivity source, traceable to the National Institute of Standards and Technology (NIST) to standardize system sensitivity, which enables comparable quantitative results. This ability leads to consistency across systems and time, with quantification that is independent of patient variability.

Accurate to within 5%[a], xSPECT Quant continues to be the industry's most precise and reproducible SPECT/CT quantitative solution.

---

what's happening and second, we know if the treatment is effective." Schaefer further explains, "in some cases, I see almost exactly the same image after four cycles so it's very important to measure if there is any difference. When you treat a patient with neuroendocrine tumors and see that the lesions are still there, you may think there's no response. But once you measure and quantify your images, you start to understand that that they are responding quite well with 10, 20, or even more percent reduction."

However, Schaefer acknowledges this evaluation is an ongoing process. "We need to better understand what these figures mean. We have to be able to tell if a reduction of 10% is meaningful or not. These figures need to be put into context with real clinical outcomes." Reinforcing this sentiment, Prior adds, "we need to design more studies to see where and how SPECT/CT quantification can help us. We have many ideas, we're doing research, and we're writing protocols."

When considering upcoming applications, Prior shares, "it's a tricky question but I think it's really a

Silvano Gnesin and Michael Da Mota utilize xSPECT Quant images to plan therapy.

Nicklaus Schaefer, John Prior, and Mario Jreige gather around CHUV's Symbia Intevo SPECT/CT scanner.

breakthrough that xSPECT Quant can be performed with ^{177}Lu, because many of our future therapies will be done with this isotope." Jreige highlights that they anticipate testing PSMA-Lutetium targeted therapy for prostate cancer patients.[b] "We want to see if we can adjust the doses of therapy based on the initial quantification of the tracer."

As CHUV and others continue to explore and share their insights, we come closer to understanding the value of SPECT/CT quantification in diagnostics and therapy management. Fortunately, as evidence mounts, so does enthusiasm for molecular quantitative imaging becoming the gateway to precision medicine. ●

[a] Data on file.

[b] ^{177}Lu PSMA is not currently recognized by the U.S. Food and Drug Administration (FDA) or other regulatory agencies as being safe and effective. Siemens Healthineers does not make any claims regarding its use.

The statements by Siemens Healthineers' customers described herein are based on results that were achieved in the customer's unique setting. Since there is no "typical" hospital and many variables exist (e.g., hospital size, case mix, level of IT adoption) there can be no guarantee that other customers will achieve the same results.

For more information

siemens-healthineers.com/xspectquant
siemens-healthineers.com/theranostics

Evaluating SPECT/CT Quantification in Clinical Practice

By Claudette Lew | Data courtesy of Centre Hospitalier Universitaire Vaudois (CHUV), Lausanne, Switzerland

As healthcare providers strive to improve outcomes through the development of personalized treatment strategies, quantitative SPECT/CT imaging supplies clinicians standardized, reproducible measurements of activity concentrations that help guide more accurate diagnoses.

The team of nuclear medicine and molecular imaging clinicians at Centre Hospitalier Universitaire Vaudois (CHUV) in Lausanne, Switzerland strives to evaluate how much quantitative SPECT/CT is able to influence diagnoses—and subsequent treatment management—when utilized as part of daily clinical routine. The team employs xSPECT Quant™ technology to evaluate the utility of quantitative Technetium-99m (^{99m}Tc), Indium-111 (^{111}In), Iodine-123 (^{123}I), and Lutetium-177 (^{177}Lu) SPECT/CT studies. To progress the implementation of quantitative SPECT/CT, the team regularly shares their findings with clinical peers at congresses such as the European Association of Nuclear Medicine (EANM) and the Society of Nuclear Medicine and Molecular Imaging (SNMMI).

"With xSPECT Quant we perform quantitative analysis using four tracers," explains Mario Jreige, MD, radiologist and nuclear medicine resident at CHUV. "We are currently quantifying not just Technetium in bone scans, but also Indium, DaTscan™, and Lutetium. Our research projects test the clinical application of quantification and we find the results very satisfying."

^{99m}Tc in SPECT/CT Quantification

"For ^{99m}Tc quantification, we were interested in evaluating if quantification can improve the specificity of bone scans." says Jreige.

To determine if ^{99m}Tc quantification can indeed aid in specificity, the CHUV team performed a retrospective evaluation, which examined a total of 128 metastatic and 17 osteoarthritic lesions.[1] Based on the SUV_{mean} and SUV_{max} quantifications, they established an optimal SUV_{max} threshold of 20 g/mL to define metastatic bone lesions. The team was also able to determine sensitivity (94%), specificity (94%), as well as positive (99%) and negative (67%) predictive values.

The quantitative analysis showed significant differences in ^{99m}Tc uptake on bone scans with notably higher SUV_{max} and SUV_{mean} in metastatic lesions, and a better accuracy for SUV_{max}. The team's findings support the use of quantitative SPECT/CT bone imaging to aid in the diagnosis of malignant lesions. The findings also demonstrate that the integration of SUV information has a clinical impact and can help diagnose indeterminate lesions.

Jreige emphasizes, "we have borderline cases and we need clues to define whether the lesion is metastatic or not. Having this quantitative information is very important for us to establish the diagnosis and become more accurate in our diagnostic capacities."

"Having this quantitative information is very important for us to establish the diagnosis and become more accurate in our diagnostic capacities."

Mario Jreige, MD, Centre Hospitalier Universitaire Vaudois

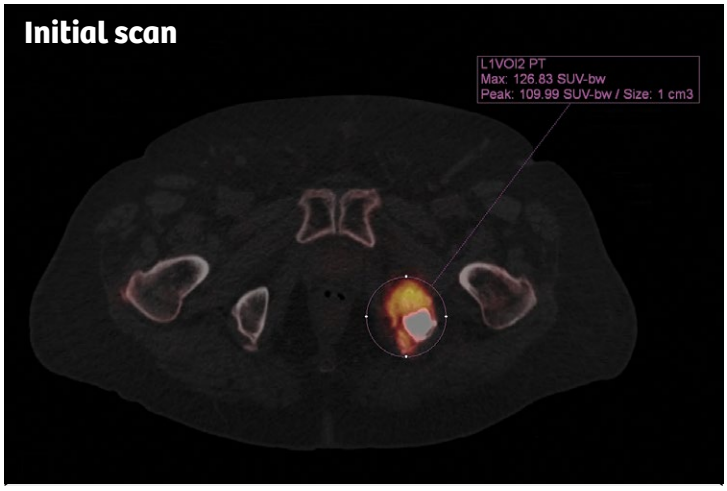

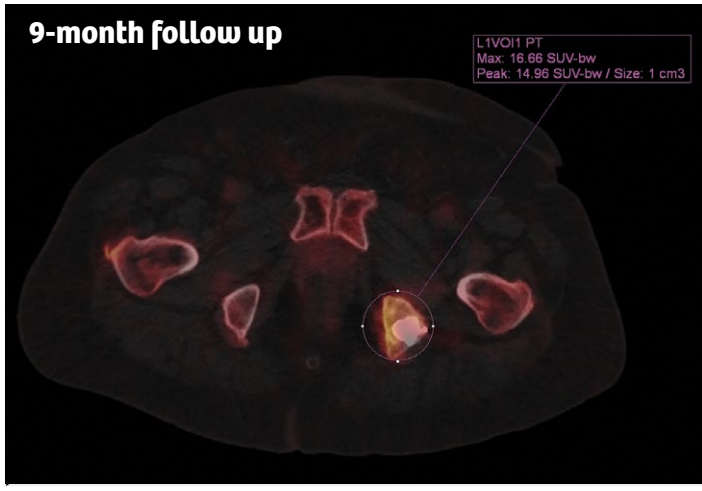

A follow-up xSPECT/CT of a prostatic adenocarcinoma with bone metastasis shows a decrease in tracer uptake at the level of the left ischium, corresponding to a positive response to therapy with radiofrequency ablation and cementoplasty (SUV_{max} 15.4 g/mL versus 84.2g/mL). No new lesions were detected.

The patient was scanned with a Symbia Intevo™ 16 SPECT/CT; 25 mCi [945 MBq] ^{99m}Tc initial scan, 25.7 mCi [953 MBq] ^{99m}Tc nine-month follow up scan. CT: 130 kV, 90 ref mAs.

^{111}In in SPECT/CT Quantification

As part of the CHUV team's research, they evaluated the potential clinical impacts of using SPECT/CT quantification with an octreotide scan. In a retrospective study, the team measured mean ± SD and 95% confidence interval (95% CI) SUV_{max} and SUV_{mean} in nine patients that underwent quantitative ^{111}In-Octreotide scan imaging for neuroendocrine tumor (NET) assessment.[2]

They found a significant difference in the measured activity of tumoral and non-tumoral tissue. Where the SUV_{mean} and SUV_{max} of the primary and metastatic sites were reduced by 50% 24-hours after tracer injection, these areas remained higher than the mean splenic uptake. Patients' digestive activity increased with time but remained lower than normal hepatic uptake.

"From this study, we can conclude that quantification allows us to better distinguish between tumoral and non-tumoral activity," states Jreige. "And this not only has an impact on the initial diagnosis, but also on therapy planning and monitoring. We are looking forward to continuing our investigation. Quantifying an octreotide scan is important before treatment, especially in the centers where DOTATATE PET/CT is not available, as it could be an alternative."

As the first team to evaluate the impact of quantitative SPECT/CT using ^{111}In in a clinical setting, the team concluded that octreotide scan with SPECT/CT quantification provides relevant insight regarding normal and pathologic SUV ranges. The results from their study also showed that time variations might offer clarity into the nature of SPECT abnormalities and enhance the specificity of indeterminate neuroendocrine lesions.

"From this study, we can conclude that quantification allows us to better distinguish between tumoral and non-tumoral activity. And this not only has an impact on the initial diagnosis, but also on therapy planning and monitoring."

Mario Jreige, MD, Centre Hospitalier Universitaire Vaudois

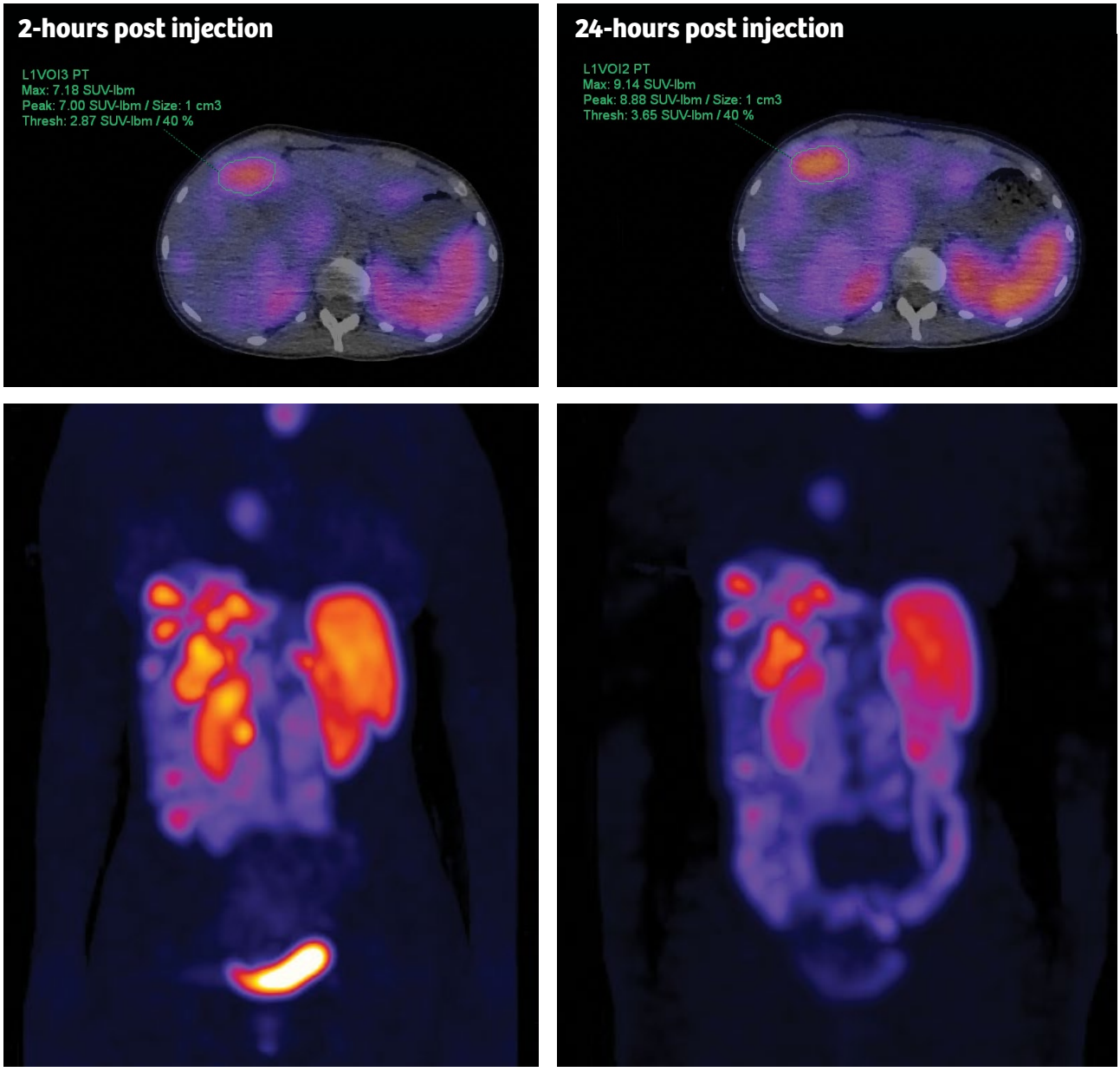

A follow-up xSPECT/CT of a well-differentiated pancreatic neuroendocrine tumor, treated with four cycles of ^{111}In metabolic radiotherapy, showed mild regression of tumoral uptake. SUV_{max} decreased from 11.8 g/mL to 8.3 g/mL, thus allowing for accurate quantification of the response to therapy.

The patient was scanned with a Symbia Intevo 16 SPECT/CT; 4.6 mCi [170 MBq] ^{111}In; 2- and 24-hour post-injection delay. CT: 130 kV, 14 ref mAs.

^{123}I in SPECT/CT Quantification

To examine whether quantitative SPECT/CT data would add precision in the diagnosis of neurodegenerative diseases of the nigro-striatal pathway, the CHUV team evaluated SPECT/CT quantification using ^{123}I within the basal ganglia.

The team investigated the role of absolute and relative SUV quantification of ^{123}I-Ioflupane (DaTscan™) in comparison to relative semi-quantitative metric methods in the differentiation between a normal and pathologic scan.[3] The data from seven patients were analyzed using Siemens Healthineers' Scenium software, which combines standard anatomy and a comprehensive database of "normal" brain scans and matches those against newly acquired clinical scans. Groups were compared using the striatal binding ratio (SBR) approach, normalized to the occipital region and absolute SUV_{mean} of the striatal, caudate, and putaminal regions. The team was able to compare the SUV_{mean} and relative metric techniques, and uptake symmetry in normal and abnormal subgroups, for each region of interest including left and right caudate nucleus, putamen and striatum, as well as the occipital region.

Only by using the absolute SUV_{mean}, and not standard iterative reconstruction methods, was the team able to differentiate between normal and pathological results in the caudate nucleus. However, all methods detected the difference between normal and pathological findings but with more pronounced significance using absolute SUV_{mean} for the putamen and striatum. xSPECT Quant was also able to detect significant asymmetry in the caudate, putamen, and striatum in a pathological scan.

The CHUV team concluded that quantitative SPECT/CT holds potential as an emerging tool for ^{123}I-Ioflupane analysis because absolute SUV can distinguish smaller differences in uptake over the standard SBR approach, making it possible to detect pathological changes earlier.

"Early identification of this neurological disease is important," emphasizes Jreige. "It helps the patient receive medications earlier, which can positively impact the treatment outcome."

"Early identification of this neurological disease is important. It helps the patient receive medications earlier, which can positively impact the treatment outcome."

Mario Jreige, MD, Centre Hospitalier Universitaire Vaudois

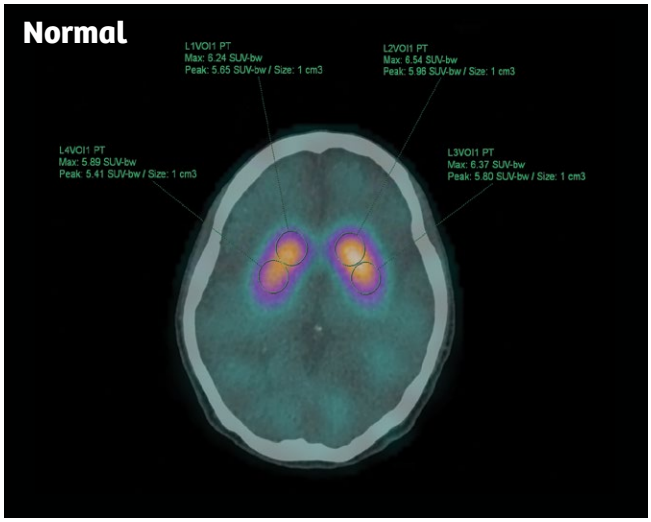

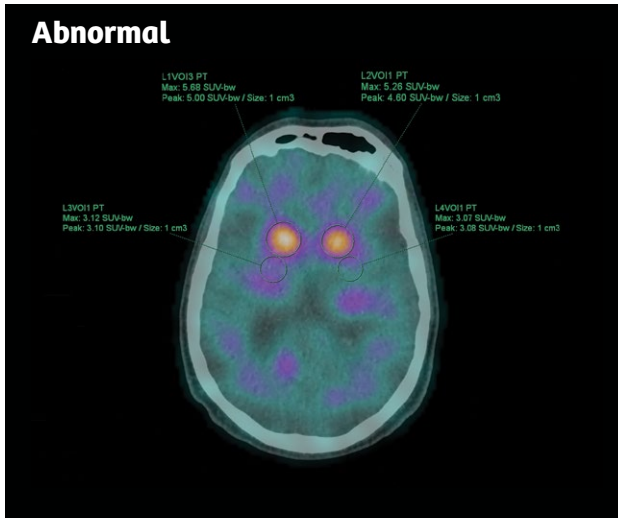

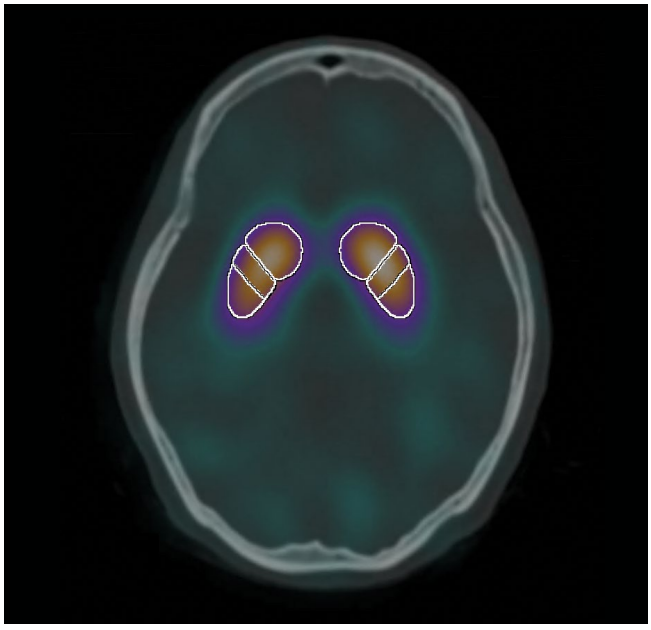

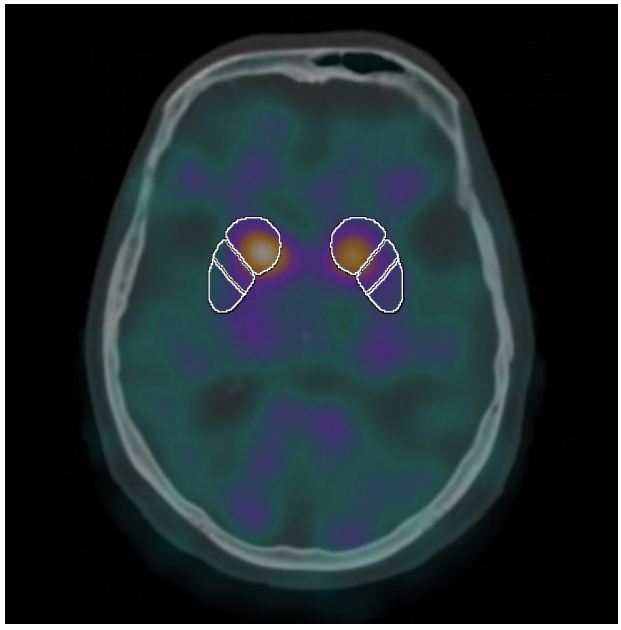

A DATscan showed normal and symmetric striatal uptake with absolute SUV quantification reported. The patient was addressed for workup of an intermittent resting and action tremor of both upper limbs, predominantly on the right side.

The patient was scanned with a Symbia Intevo 16 SPECT/CT; 4.9 mCi [183 MBq] ^{123}I. CT: 110 kv, 12 ref mAs.

Patient uptake	Right	Left
Striatum	6.24	6.54
Putamen	5.89	6.37
Caudate	6.24	6.54
Putamen/Caudate Ratio	0.96	1.01

An abnormal DATscan showed bilateral striatal dopaminergic denervation, predominantly on the putamens, with absolute SUV quantification reported. The patient was addressed for workup of an atypical extrapyramidal syndrome disorder of balance, and recurring falls.

The patient was scanned with a Symbia Intevo 16 SPECT/CT; 4.6 mCi [171 MBq] ^{123}I. CT: 110 kV, 12 ref mAs.

Patient uptake	Right	Left
Striatum	5.68	5.26
Putamen	3.12	3.07
Caudate	5.68	5.26
Putamen/Caudate Ratio	0.85	0.92

^{177}Lu SPECT/CT quantification to assist theranostic procedures

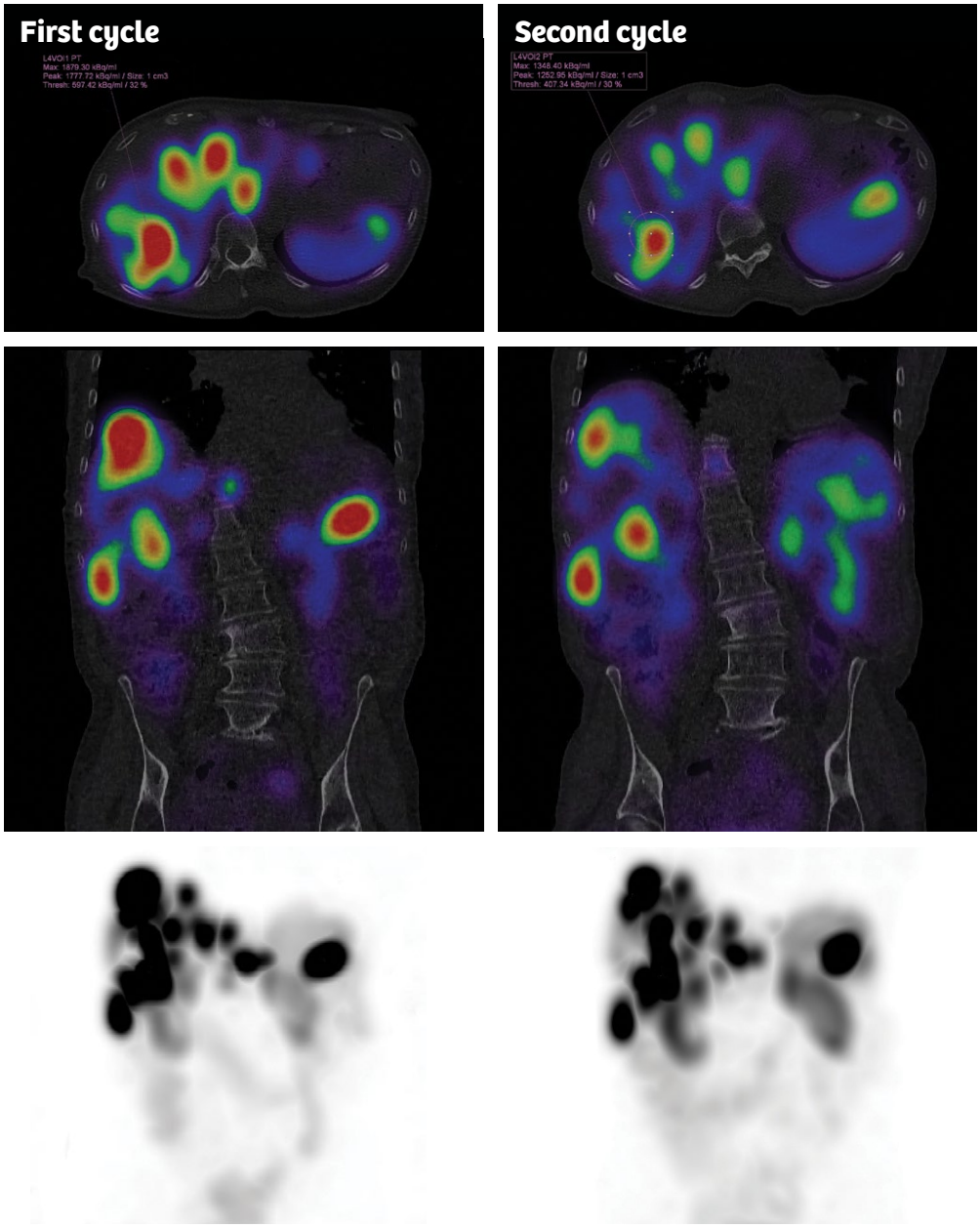

A follow-up xSPECT/CT captured a well-differentiated neuroendocrine tumor with liver metastasis after the first (left) and the second (right) cycles of ^{177}Lu DOTATATE therapy (3.8 MBq). Quantitative evaluation of the liver metastasis uptake showed a 45% reduction in SUV_{max} after the second cycle, favoring a good response to therapy.

The patient was scanned with a Symbia Intevo 16 SPECT/CT; 157 mCi [5804 MBq] ^{177}Lu DOTATATE first cycle, 100 mCi [3717 MBq] ^{177}Lu DOTATATE second cycle. CT: 130 kV, 19 ref mAs first cycle; 130 kv, 11 ref mAs second cycle.

^{177}Lu, used as a theranostics agent, is able to successfully target inoperable or metastatic neuroendocrine tumors, yet irradiation of the kidney limits the absorbed dose to the tumor. As patients typically receive a standard dose of ^{177}Lu every two months, repeated four to six times, it is vital to monitor the patient's internal dosimetry due to this repeated irradiation of the kidneys.[4] Using quantitative SPECT/CT, clinicians can follow the ^{177}Lu treatments to support patient dosimetry.

"Having accurate values derived from quantification, and from absolute quantification of the tracers, is important to define the necessary dose that should be delivered to the tumor, and also to reduce dose that is delivered to non-targeted organs," states Jreige. "This is important in the reduction of treatment side effects and the optimization of dose delivered to the patient."

The CHUV team generated a dosimetry evaluation for ^{177}Lu theranostic procedures.[5] Quantitative ^{177}Lu acquisitions were performed using xSPECT Quant, whose calibration relies on a National Institute of Standards and Technology (NIST) Selenium-75 (^{75}Se) source. Average activity recovery in organs and lesions, as a function of iteration number, was measured in a SPECT/CT acquisition of a patient three hours after therapeutic administration of 6 GBq of ^{177}Lu DOTATATE.

The results of the study concluded that quantitative phantom validation showed standardized procedures—when applied to ^{177}Lu xSPECT Quant acquisition/reconstruction protocols—enable accurate activity recovery within six percent of actual values in organs. Protocol optimization and recovery coefficients evaluations were performed to assess quantitative activity recovery in lesions. The validated xSPECT Quant workflow potentially reduces quantitative variability in dosimetry assessment of theranostic procedures aimed at improving patient care.

Changing patient care with SPECT/CT quantification

Reflecting on how their work with SPECT/CT quantification aids the progression of patient care at CHUV, Jreige elaborates, "an interesting thing we learned from the introduction of SPECT/CT quantification is that we should not only use conventional methods, but also move forward and adapt to new technology for the benefit of our patients. In the case of xSPECT Quant, it was very important to understand how to apply this tool to maximize the diagnostic capacities, and therefore to positively impact patient care." ●

The statements by Siemens Healthineers customers described herein are based on results that were achieved in the customer's unique setting. Since there is no "typical" hospital and many variables exist (e.g., hospital size, case mix, level of IT adoption) there can be no guarantee that other customers will achieve the same results.

References

[1] Tabotta F, Jreige M, Schaefer N, Prior JO, Nicod-Lalonde M. Tc-99m-DPD bone scan quantification: Metastasis of prostate cancer vs. osteoarthritis. *Eur J Nucl Med Mol Imaging*. 2017;44(Suppl 2):S351-S352.

[2] Jreige M, Tabotta F, Nicod-Lalonde M, Schaefer N, Prior J. In-111 Octreoscan scintigraphy quantification with xSPECT: first report on data of tumoral and non-tumoral SUV range. *J Nucl Med*. 2017;58(Suppl 1):924.

[3] Jreige M, Tabotta F, Nicod-Lalonde M, et al. xSPECT derived absolute SUV: An emerging accurate tool for I-123-ioflupane analysis. *Eur J Nucl Med Mol Imaging*. 2017;44(Suppl 2):S616.

[4] Van Wyk BP, Vangu WDTH, Purbhoo K, Africa L, Mosley R. Lutetium-177 (^{177}Lu) dosimetry in patients treated for neuroendocrine tumours (NETs) in Johannesburg, South Africa. *Physica Medica:Eur J Med Phys*. 2015;31(Suppl 1):S20.

[5] Gnesin S, Lima T, Malterre J, Verdun FR, Schaefer N, Prior JO. Quantitative Lu-177 SPECT/CT validation to assist theragnostic procedures. *Eur J Nucl Med Mol Imaging*. 2017;44(Suppl 2):S178.

Evaluation of therapy response using sequential xSPECT Quant in a child with a mediastinal neuroblastoma

By Mario Jreige, MD; Marie Nicod Lalonde, MD; Niklaus Schaefer, MD; John O. Prior, MD, PhD
Data courtesy of Centre Hospitalier Universitaire Vaudois, Lausanne, Switzerland

History

A 7-year-old girl was diagnosed in October 2016, with stage IV mediastinal neuroblastoma with osteo-medullary bone infiltration. During the first year following diagnosis, the patient underwent different chemotherapy regimens and received treatment according to protocol NRNBL 1.7/SIOPEN (November 2016-January 2017) and TVD followed by TOTEM (February 2017-December 2017).

A follow-up MIBG scintigraphy (December 2017; images not shown) exhibited positive response to chemotherapy and displayed a decrease in the tracer uptake and number of bone lesions. However, there was persistent uptake in the left upper thoracic-paravertebral mass.

Subsequent treatment included the administration of 6.9 GBq of Iodine-131 (^{131}I) MIBG (January 2018-February 2018), followed by stem cell reinfusion (February 2018). A follow-up Iodine-123 (^{123}I) MIBG scintigraphy was performed in March 2018, with SPECT/CT using a Symbia Intevo™ with xSPECT Quant™ (the first xSPECT acquisition) for absolute quantification of ^{123}I MIBG uptake. An intravenous injection of 111.6 MBq of ^{123}I MIBG (patient weight 48.5 lb/22 kg) was administered for a whole-body planar and SPECT/CT acquisition of the thorax and abdomen, performed 24 hours post injection. An initial CT was performed (80 kV, 30 eff mAs, 16 x 1.2 mm collimation), followed by a SPECT acquisition at 30 stops with 30 seconds per stop; the study was reconstructed with xSPECT Quant.

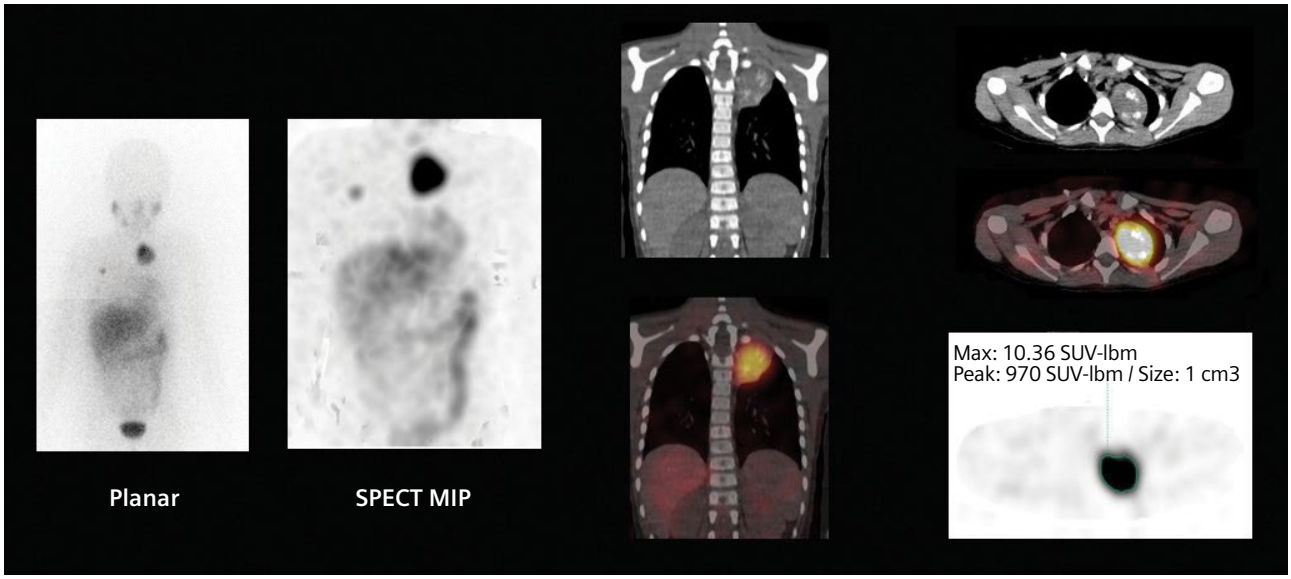

1 **Whole-body planar, SPECT/CT, and xSPECT Quant images (acquired in March 2018, one month after the administration of a large-dose ^{131}I MIBG therapy) show high uptake in the left upper-mediastinal mass, which demonstrates significant areas of focal calcification on CT that are often associated with neuroblastoma lesions. The SUV_{max} was 10.36 with a small focal area of uptake in the right chest region that is related to uptake in the chemotherapy port attached to the chest wall.**

Findings

Compared to the initial ^{123}I MIBG scintigraphy (December 2017), the follow-up ^{123}I MIBG SPECT/CT (March 2018)—performed one month after 6.9 GBq ^{131}I MIBG therapy—showed decreased uptake in the 5th rib bone lesion and stable uptake in the mediastinal lesion, without any new bone uptake on visual assessment. The SUV_{max} values obtained from the xSPECT Quant study provided a quantitative benchmark for subsequent evaluation of the MIBG-avid thoracic lesion.

The patient underwent a new cycle of high-dose chemotherapy with Busilvex®/melphalan (April 2018), followed by autologous stem-cell reinfusion that same month.

A follow-up ^{123}I MIBG SPECT/CT study with xSPECT Quant was performed in May 2018, (the second xSPECT acquisition) using a similar injected dose with the same acquisition parameters as the initial xSPECT Quant study.

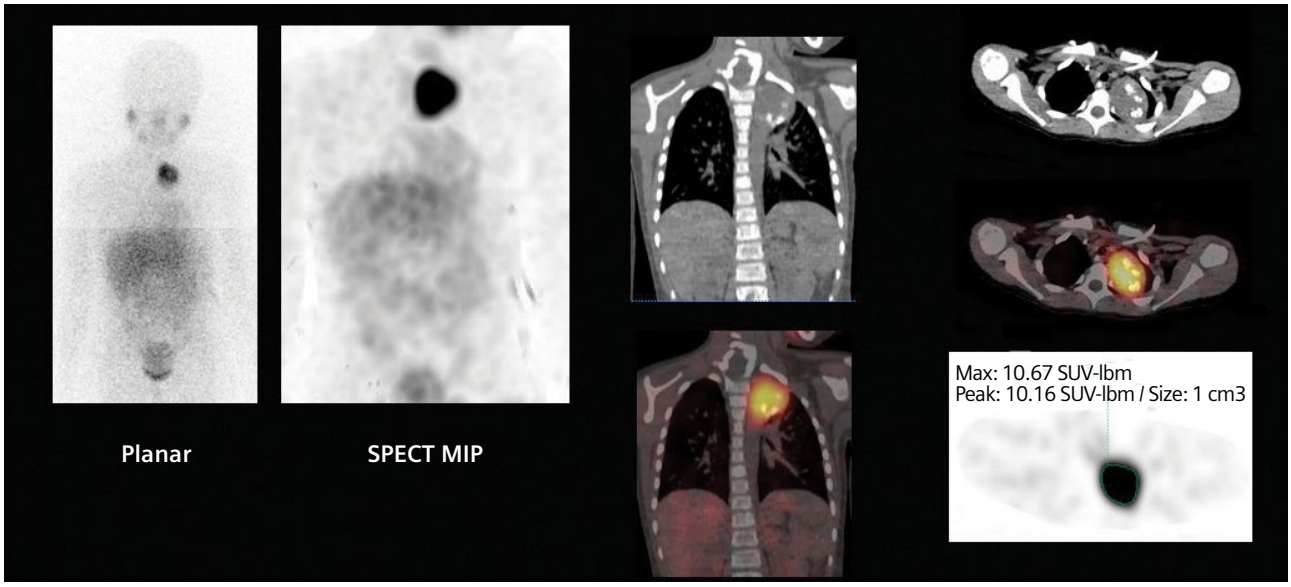

2 **The second follow-up ^{123}I MIBG SPECT/CT study with xSPECT Quant, performed in May 2018, shows relatively stable size and intensity of uptake in the left-upper mediastinal mass without any new functioning lesions.**

As noted in Figure 2, the second follow-up ^{123}I MIBG SPECT/CT study showed mediastinal lesion stability based on both visual and quantitative assessment (SUV_{max}: 10.67 versus 10.36 g/ml). In the absence of progression, the patient underwent surgical resection of the left superior mediastinal tumoral mass (June 2018). Post-surgery thoracoabdominal MRI (July 2018) showed no residual lesion in the resection site, which was filled by a loculated pleural effusion.

A follow-up ^{123}I MIBG SPECT/CT study (August 2018, the third xSPECT acquisition) confirmed the absence of tracer uptake in the resection site with minimal postoperative remodeling. No new suspicious lesions were detected on the whole-body images.

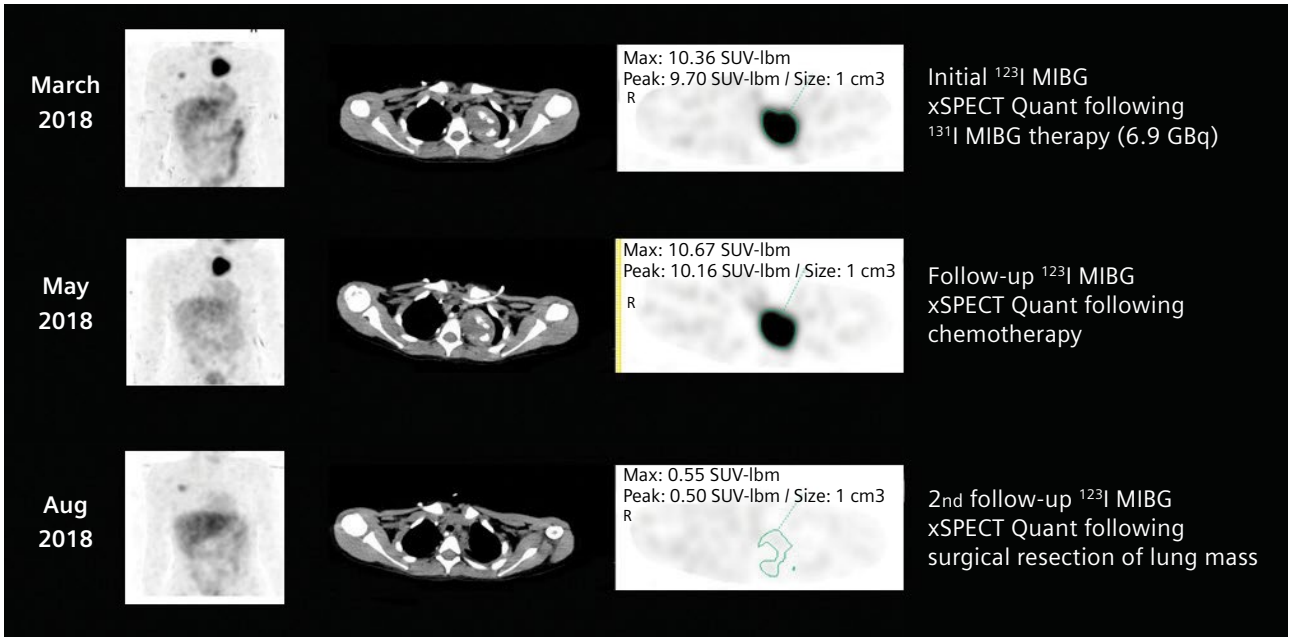

3 **SPECT maximum intensity projection (MIP), CT, and xSPECT Quant images of the sequential SPECT/CT studies show stable uptake intensity and SUV_{max} between the studies performed in March and May 2018. A post-surgical resection ^{123}I MIBG SPECT/CT study, performed in August 2018, shows complete removal of the functioning thoracic mass without any residual and no new metastases.**

Comments

In this case, the visual impression between the sequential ^{123}I MIBG SPECT/CT studies performed in March 2018 and May 2018 suggested an absence of any significant change in tumor size and intensity of uptake. However, the SUV_{max} values provided quantitative confirmation of the stable nature of the mediastinal lesion, which did not decrease in size or uptake intensity despite the high-dose ^{131}I MIBG therapy and additional chemotherapy.

In view of the absence of new metastases and the relatively stable volume and functioning tumor burden of the mediastinal lesion, which was quantitatively evaluated by sequential xSPECT Quant, the decision for surgical removal of the tumor was adopted. Post-surgery scintigraphy shows positive results with a complete removal of the functioning tumor mass and an absence of new metastases as well as post-operative fibrosis.

Conclusion

This case demonstrates the value of xSPECT Quant to act as a precise and objective tool for evaluating neuroblastoma patients—allowing for the assessment of tumoral activity on baseline MIBG scintigraphy, chemotherapy, or metabolic radiotherapy response, as well as remission after surgical treatment. Accurate knowledge of tracer uptake can guide a successful therapeutic plan by helping establish an appropriate treatment modality dependent on tumoral-activity evolution. ●

The outcomes achieved by the Siemens customers described herein were achieved in the customer's unique setting. Since there is no "typical" hospital and many variables exist (e.g. hospital size, case mix, level of IT adoption) there can be no guarantee that others will achieve the same results.

Examination protocol

Scanner: Symbia Intevo

SPECT		CT	
Injected dose	^{123}I MIBG 111.6 MBq	Tube voltage	80 kV
Scan delay	No delay	Tube current	30 eff mAs
Scan acquisition	Whole-body	Slice collimation	16 x 1.2 mm

xSPECT Quant-based dosimetry following ^{177}Lu PSMA therapy in metastatic prostate cancer

By Michael Hoffman, MD, Associate Professor
Data courtesy of Peter MacCallum Cancer Center, Melbourne, Australia

History

An 82-year-old man with castration-resistant prostate cancer and multiple skeletal metastases, demonstrated by ^{68}Ga PSMA PET/CT to be PSMA-avid, was referred for ^{177}Lu PSMA[a] therapy. The patient was treated with an intravenous infusion of 8.7 GBq of ^{177}Lu PSMA, preceded by amino acid infusion. Five hours following therapeutic administration, the patient underwent a quantitative multi-bed SPECT/CT to image the distribution of ^{177}Lu PSMA within the body. The study was performed on a Symbia Intevo™ 16. Following an initial low-dose CT acquisition (130 kV, 25 eff mAs), a three-bed SPECT/CT study using xSPECT Quant™ was acquired with 60 stops per detector and 10 seconds per stop. The study was reconstructed using xSPECT Quant to quantify ^{177}Lu tracer concentration within the lesions and critical organs. Following the initial SPECT/CT acquisition at 5 hours post-therapy, sequential studies using identical acquisition and reconstruction protocols were performed at 24 hours and again at 96 hours.

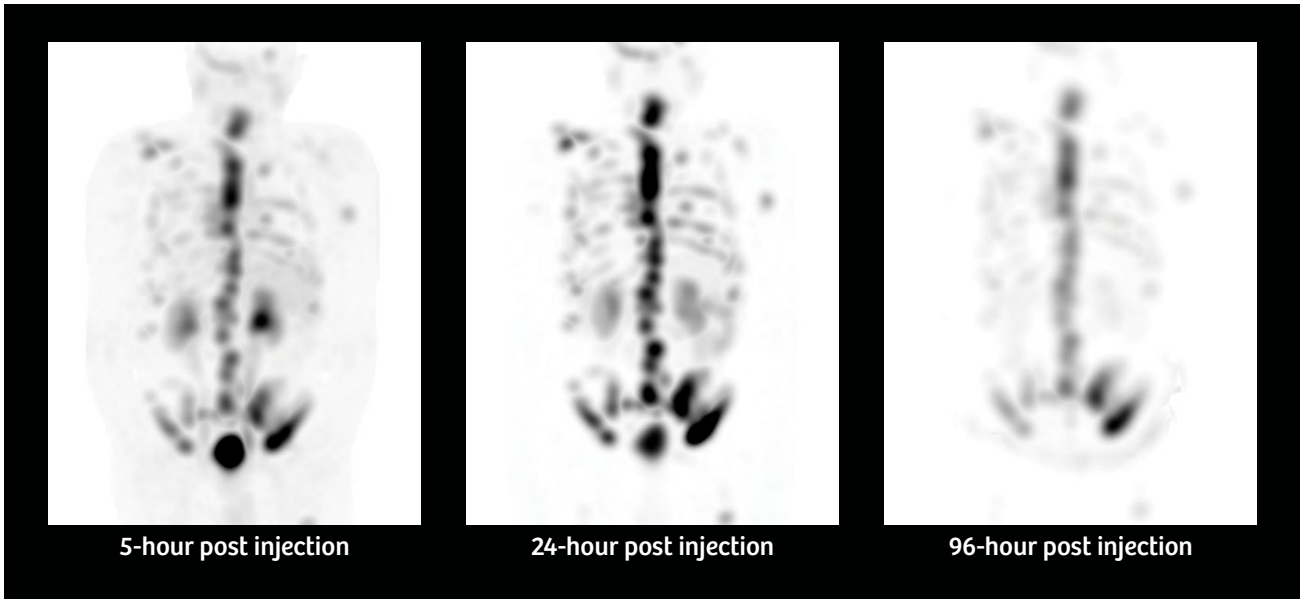

1 **MIP images of sequential ^{177}Lu PSMA multi-bed SPECT studies show a progressive increase in tracer uptake within multiple skeletal metastases in the thoracic and lumbar vertebrae, ribs, and pelvis with maximum tracer retention seen 24 hours post injection. The 96-hour image shows slow washout of tracer within the metastases. The 5-hour images show significant renal cortical uptake and tracer retention in the bilateral renal pelvis, but the fast washout at 24 hours followed by a low level of cortical retention at 96 hours suggests good renal clearance of the tracer.**

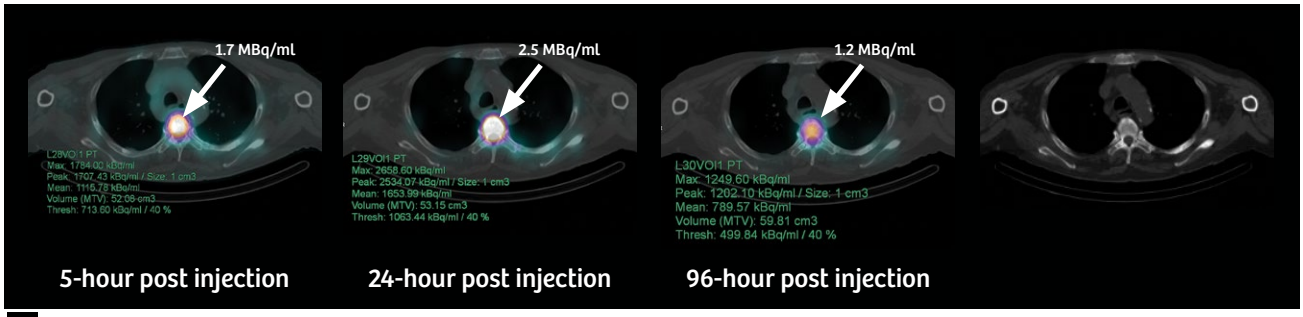

2 Fused images at the level of thoracic vertebral metastases show high initial tracer concentration within ^{177}Lu PSMA-avid metastases with further tracer retention by 24 hours, followed by slow washout. The peak tracer concentration at 24 hours was 2.5 MBq/ml, which decreased by more than 50% at 96 hours. The CT images show significant sclerosis within the metastatic vertebral body.

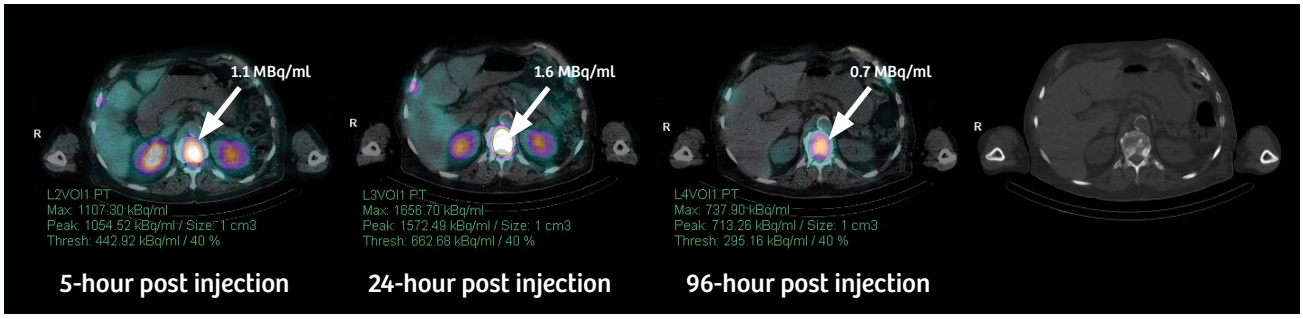

3 Similar display of maximum tracer concentration in sequential fused images at the level of lumbar vertebral metastases show slightly lower peak concentration as compared to the thoracic vertebrae but with similar increase up to 24 hours with slow clearance. The degree of sclerosis is slightly lower in the lumbar vertebral body as compared to that of the thoracic vertebrae.

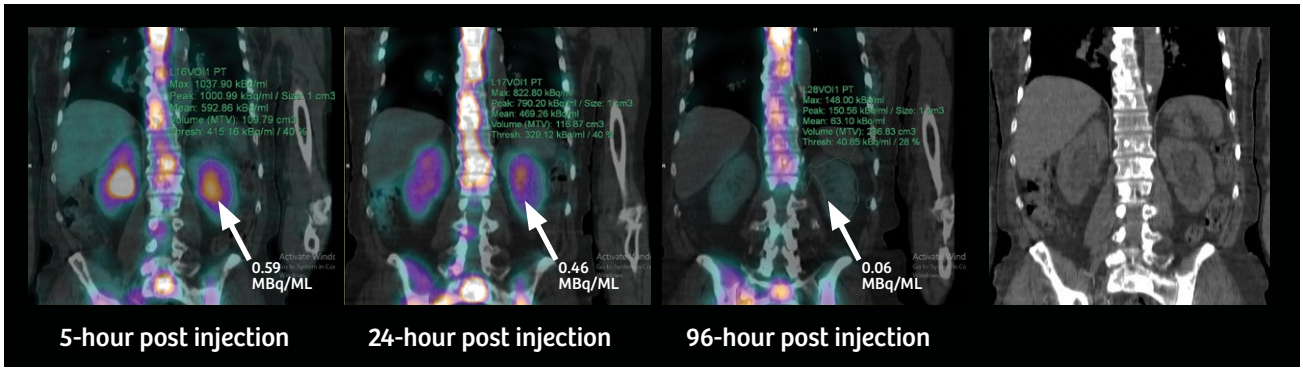

4 Coronal-fused images display the maximum tracer concentration in the left kidney along with the renal volume. The peak tracer concentration is 0.59 MBq/ml at 5-hours post injection with fast washout, such that only 10% of the peak concentration is retained in the renal cortex and pelvis after 96 hours. The coronal CT images show normal cortical thickness in both kidneys with normal calyces and pelvis.

Findings

Sequential SPECT/CT images with tracer concentration values in thoracic and lumbar vertebral metastases obtained using xSPECT Quant (as displayed in Figures 1-3) clearly highlight the high initial tracer concentration within the metastases with a gradual increase in concentration up to 24 hours post injection. There was slow washout from the metastases with nearly 50% of tracer retention even at 96-hours post injection. This pattern of initial high uptake and subsequent slow washout within the metastases reflects the potential of high radiation dose delivered by ^{177}Lu PSMA therapy.

The renal uptake appears normal in the initial 5-hour image (Figure 4) with fast washout that left only 10% of the initial concentration at 96 hours. This fast clearance suggests a low residence time of tracer within the renal cortex and a consequently low level of radiation dose to the kidneys. The normal cortical thickness and absence of pelvicalyceal enlargement on CT reflect normal renal morphology and absence of pelvicalyceal stasis or obstruction.

The sequential xSPECT Quant and CT data was fed into Siemens Healthineers' Dosimetry Research Tool (DRT), which enables the automated generation of a volume-of-interest (VOI) that includes the tumor as well as critical organs—such as the kidney, liver, and spleen—SPECT/CT. DRT performs voxel-based dosimetry using absolute tracer concentration values obtained from sequential xSPECT Quant datasets across multiple time points. These time points calculate time-activity curves and tracer residence times within individual voxels as well as within automatically generated VOIs to generate absorbed dose values, dose volume histograms, and absorbed dose maps.

The mean left and right kidney dose (as calculated by the DRT) appears within expected levels. Due to high tracer retention within metastases and the substantial metastatic burden, the circulating tracer available for renal clearance is low and that indicates the potential for low renal cortical dose, also known as a tumor sink effect. This is appropriately reflected in the mean renal dose of 2.52 Gy and 3.6 Gy to the left and right kidneys, respectively. In view of the low renal dose and the high tracer retention within the metastatic lesions, the delivered tumor dose is expectedly high and multiple therapies would be possible in this patient without undue concern for renal toxicity.

Comments

This study demonstrates 3D dosimetry performed using sequential quantitative SPECT/CT (xSPECT Quant) following therapeutic administration of ^{177}Lu PSMA. In this patient, due to extensive skeletal metastases, the majority of administered tracer is absorbed within PSMA-avid metastases with a low level of circulating ^{177}Lu PSMA available for renal clearance. A low level of renal cortical uptake with fast clearance is reflected on xSPECT Quant data, which shows only 10% of peak renal cortical activity concentration retained after 96 hours. This pattern of low cortical uptake and fast clearance reflects the low overall renal tracer residence time and consequently low levels of renal cortical absorbed dose are expected from dosimetry calculations. This expectation is confirmed by the actual renal cortical dose calculated using

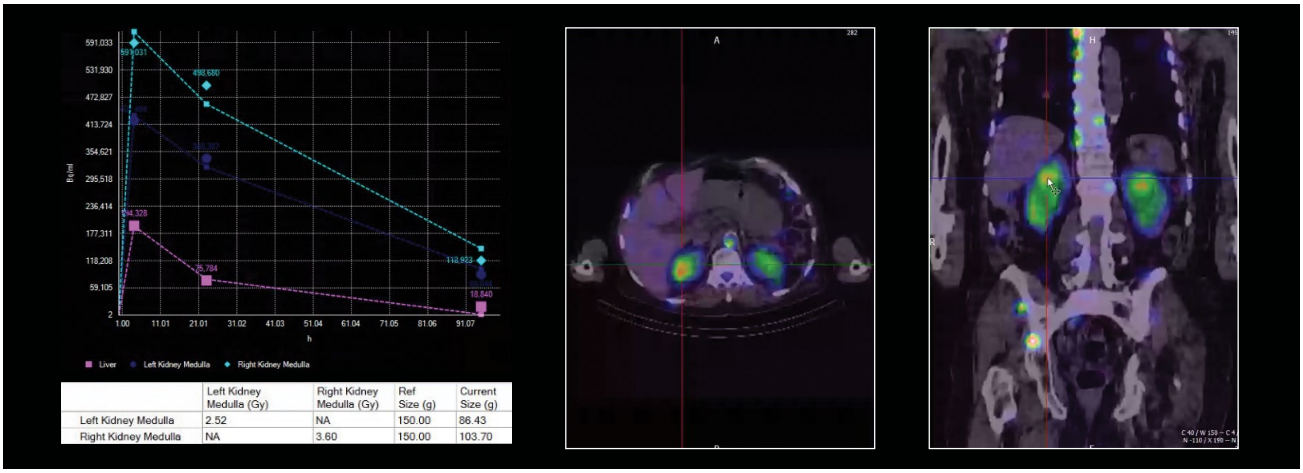

	Left Kidney Medulla (Gy)	Right Kidney Medulla (Gy)	Ref Size (g)	Current Size (g)
Left Kidney Medulla	2.52	NA	150.00	86.43
Right Kidney Medulla	NA	3.60	150.00	103.70

5 **A time-activity curve of the right and left kidney, derived from research dosimetry software, along with an absorbed dose map with the cursor in the upper right renal cortex, which displays an absorbed dose value of 4.34 Gy. The table of absorbed dose values of the left and right kidney obtained from the DRT shows a mean left renal dose to be 2.52 Gy and a mean right renal dose to be 3.6 Gy.**

sequential xSPECT Quant data and DRT, which shows a mean renal dose of 2.52 Gy and 3.6 Gy to the left and right kidneys respectively. The dose map in Figure 5 shows heterogeneity of renal cortical dose with an individual voxel in the right upper renal cortex, which displays an absorbed dose of 4.34 Gy, while the mean right renal cortical dose was 3.6 Gy.

A recent study simulated the effect of an increase in PSMA-avid tumor volume to the tumor and renal dose using the data of 13 patients treated with ^{177}Lu PSMA I&T.[1] According to the simulation, a 10-fold increase in total tumor volume (0.3 L to 3 L) was associated with a reduction of mean renal absorbed dose from 6.5 Gy to 3.7 Gy: a decrease of slightly less than 50%. The conclusion of this study demonstrates that in patients with large PSMA-positive tumor volumes, higher activities can be safely administered to maximize tumor dose without exceeding maximum dose thresholds to critical organs. Dosimetry was performed using sequential planar scintigraphy in the referenced study. In comparison, the present case example utilizes xSPECT Quant with high accuracy of calculated tracer concentration along with dosimetry software, which enables automated segmentation of critical organs. A low level of renal cortical absorbed dose (3.6 Gy to the right kidney) therefore suggests the potential of multiple therapies in order to achieve higher tumor dose without crossing the renal absorbed dose threshold of 23 Gy. Since the patient has normal renal cortical thickness with absence of pelvicalyceal stasis, there is also the possibility of accepting a higher renal cortical dose threshold of 40 Gy, which would enable a significantly higher therapeutic window.

Using sequential quantitative SPECT/CT, based on calibration using a phantom with known concentration of ^{177}Lu to enable conversion of counts to tracer concentration, a study evaluated renal absorbed dose in five patients with metastatic castration-resistant prostate cancer treated with two cycles (approximately 3.6 GBq each cycle) of ^{177}Lu PSMA therapy.[2] A mean renal absorbed dose was 2.2 Gy +/- 0.6 Gy. 3D volumes of the kidney, generated from sequential SPECT/CT images, were used to calculate total tracer concentration and generate time-activity curves for dose estimation using tracer-specific S values. All patients showed overlap of intestinal and liver activity with the kidney on planar images, which was eliminated using SPECT/CT data, therefore the authors categorically recommended utiliizing 3D SPECT/CT-based dosimetry for all ^{177}Lu PSMA studies to avoid this issue with planar scintigraphy. The present case example shows renal dose even lower than the study by Delker et al., with a mean renal cortical dose as low as 0.4 Gy/GBq (right kidney).

Tumor tracer concentration, as shown by xSPECT Quant, was high in the initial study with progressive increase up to 24 hours after injection followed by slow washout with almost 50% of peak tracer concentration retained at 96 hours. This suggests longer tracer residence time within metastatic lesions and consequently higher tumor absorbed dose. Since the present dosimetry study was based on the first therapy, subsequent therapy administrations need to be similarly evaluated using sequential xSPECT Quant studies and dosimetry to determine change in renal and tumor dose with respect to change in overall tumor burden.

Conclusion

Sequential xSPECT Quant studies following therapeutic dose of ^{177}Lu PSMA enables 3D voxel-based dosimetry in a patient with multiple skeletal metastases from prostate cancer, which show normal renal cortical dose with high tumor retention of tracer. ●

References

1 Begum NJ, Thieme A, Eberhardt N, et al. The effect of total tumor volume on the biologically effective dose to tumor and kidneys for ^{177}Lu-labeled PSMA peptides. *J Nucl Med.* 2018;59:929–933.

2 Delker A, Fendler WP, Kratochwil C, et al. Dosimetry for ^{177}Lu-DKFZ-PSMA-617: a new radiopharmaceutical for the treatment of metastatic prostate cancer. *Eur J Nucl Med Mol Imaging*. 2016;43(1):42-51.

[a] ^{177}Lu PSMA is not currently recognized by the U.S. Food and Drug Administration (FDA) or other regulatory agencies as being safe and effective. Siemens does not make any claims regarding its use.

The Dosimetry Research Tool is an investigational device. Limited by Federal (or United States) law to investigational use. This device is exclusively for clinical investigations. This investigational device does not fulfill all the essential requirements according to the European Medical Device Directive (93/42/EEC) and its national implementations. It is not commercially available in the European Union, or other countries worldwide.

Examination protocol

Scanner: Symbia Intevo 16

SPECT	
Injected dose	8.7 GBq
Scan acquisition	60 stops at 10 seconds/stop
CT	
Tube voltage	130 kV
Tube current	25 eff mAs
Slice thickness	3 mm

xSPECT Quant-based dosimetry over four ^{177}Lu DOTATATE therapy cycles for treatment of neuroendocrine tumor metastases

By Partha Ghosh, MD and Michal Cachovan, PhD
Data courtesy of Royal North Shore Hospital, Sydney, Australia

History

A patient with a neuroendocrine tumor and multiple functioning liver metastases, demonstrated by ^{68}Ga DOTATATE PET/CT, was referred for ^{177}Lu DOTATATE peptide receptor radionuclide therapy (PRRT). The first therapy dose of 7.7 GBq of ^{177}Lu DOTATATE was administered in May of 2017 with an amino-acid infusion for renal protection started 30 minutes prior that continued until the completion of therapy infusion. Thirty minutes after the ^{177}Lu DOTATATE infusion, the patient underwent an abdominal SPECT/CT study on a Symbia Intevo™ 6, utilizing xSPECT Quant™ technology. Following the initial low-dose CT acquisition (130 kV, 45 eff mAs, 6 x 1.0 mm collimation), a SPECT study was performed using 60 stops per detector with an acquisition time of 20 seconds per stop. xSPECT Quant reconstruction was performed using CT attenuation and scatter correction, which yielded quantitative data from which absolute tracer concentration in kBq/ml was derived.

Following the initial SPECT/CT, the patient underwent subsequent SPECT/CT studies using the same acquisition protocol at 4, 24, and 120 hours post infusion in order to generate sequential xSPECT Quant data.

The sequential xSPECT Quant datasets were evaluated on *syngo*®. via software in order to measure absolute tracer concentration within the tumor and critical organs, such as the renal cortex. The xSPECT Quant datasets were then loaded into Siemens Healthineers' Dosimetry Research Tool (DRT). The research dosimetry software aligns multi-timepoint SPECT/CT data and performs automatic organ segmentation based on CT and SPECT datasets to generate critical organ and tumor volumes of interest (VOI). The software also uses xSPECT Quant datasets with integrated absolute tracer concentrationto generate voxel- and VOI-specific time-activity curves. With these time-activity curves, the software can perform 3D voxel-based dosimetry from the quantitative SPECT/CT data. Dose-volume histograms and absorbed-dose maps are also generated, which help assess the heterogeneity of dose distribution.

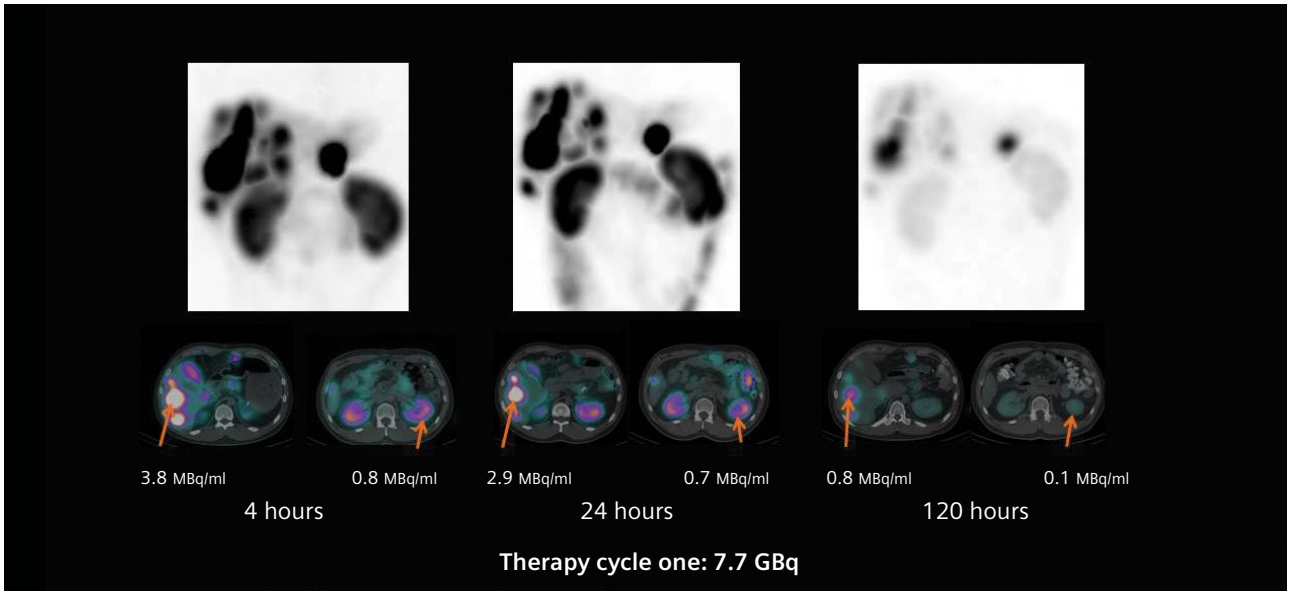

1 Maximum intensity projection (MIP) and fused SPECT/CT images of the xSPECT Quant study, acquired at 4, 24, and 120 hours after 7.7 GBq infusion of ^{177}Lu DOTATATE (first therapy cycle), show multiple tracer-avid liver metastases with maximum tracer concentration at 4-hours post infusion with a slow washout and significant retained tracer within tumor even after 120 hours. Maximum tracer concentration in the most tracer-avid liver metastases, at 4-hours post infusion, was 3.8 MBq/ml with slow washout resulting in a 23% reduction in tracer concentration by 24 hours. The concentration further decreased to 0.8 MBq/ml at 120 hours (78% decrease over 120 hours). Both renal cortices show normal levels of tracer concentration at 4 hours (0.8 MBq/ml max tracer concentration in left renal cortex) with similar levels of cortical uptake at 24 hours with only 0.1 MBq/ml of the left renal cortical concentration retained at 120 hours (87% reduction from peak concentration).

Findings

Visual and quantitative evaluations of the sequential xSPECT Quant datasets confirm the high uptake and slow clearance from the liver tumor, normal renal cortical retention, and fast washout. This suggests the possibility of a high tumor dose with normal levels of renal cortical absorbed-dose. Using the accurate quantitative data generated by xSPECT Quant as the basis, actual absorbed dose calculations were performed using the DRT.

From the dosimetry calculations (Figure 2), it is clear the renal dose is within the normal limits in spite of a high tumor dose. In view of the generally accepted threshold of 23 Gy as the maximum cumulative renal dose, a mean renal dose of 3.5 Gy supports the possibility of delivering at least 4 to 5 therapies of ^{177}Lu DOTATATE dose. However, as tumor size and intensity of uptake often change following therapy, the renal dose delivered in subsequent therapies can easily be different from what is received during the initial therapy. As such, multi-time-point quantitative SPECT/CT imaging was performed in conjunction with subsequent therapies.

Eight weeks following completion of the first therapy, the patient was administered the second cycle of ^{177}Lu DOTATATE therapy (July 2017). A dose of 7.4 GBq ^{177}Lu DOTATATE was administered, as per standard protocol. xSPECT Quant acquisitions were performed 0.5, 4, 24, and 120 hours post-therapy administration, with acquisition and reconstruction protocols identical to the imaging performed following the first therapy. The DRT was used to generate absorbed dose values from the sequential xSPECT Quant data.

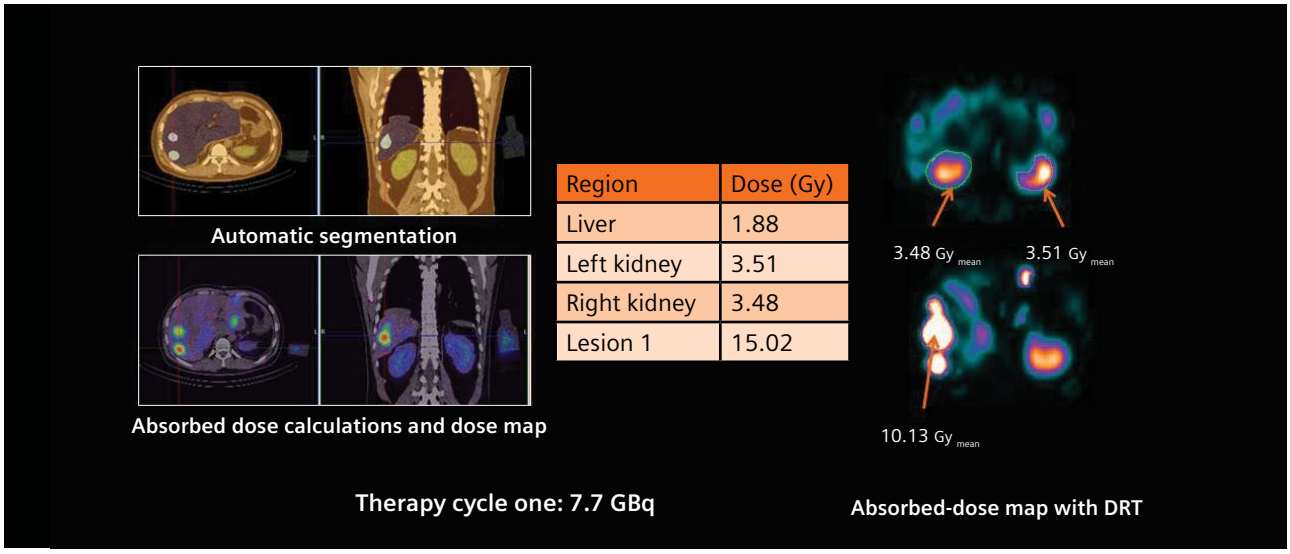

2 Absorbed-dose maps and mean dose values to both kidneys and largest liver metastases, generated from the DRT, show a mean renal dose of 3.51 Gy in the left kidney and 3.48 Gy in the right kidney, both of which fall within expected normal levels. The mean dose to a large metastatic lesion was 15 Gy, suggesting the possibility of high tumor-cell killing based on absorbed dose without undue renal or other critical organ toxicity. In spite of multiple liver metastases, the mean dose to normal liver (1.88 Gy) was within normal limits. The DRT performs automatic segmentation of critical organs and tumor along with the generation of an absorbed-dose map superimposed on CT images.

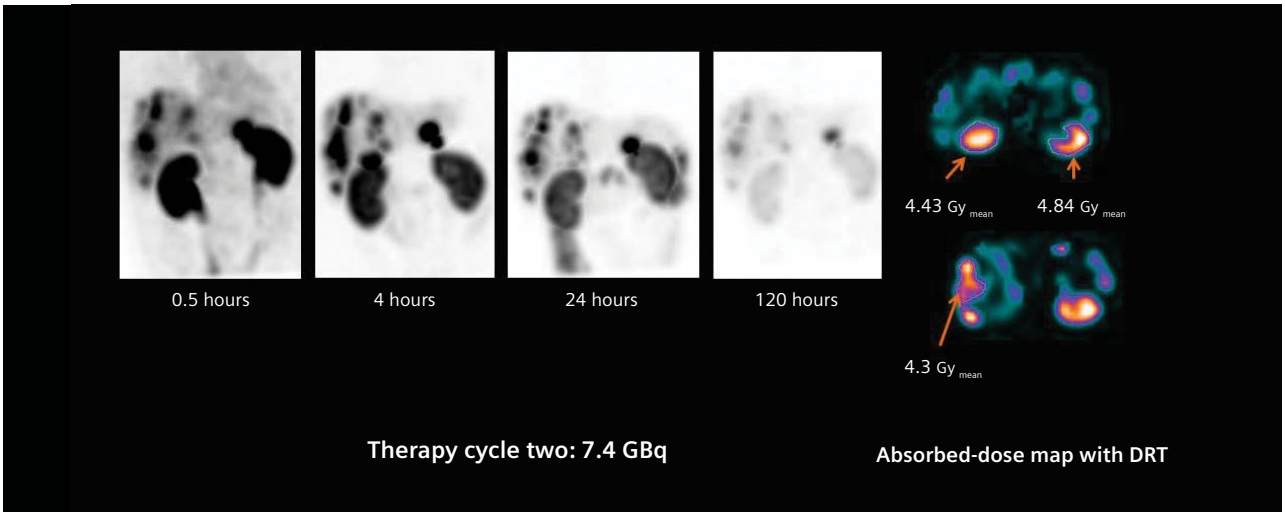

3 Sequential xSPECT Quant MIP images acquired following administration of the second ^{177}Lu DOTATATE therapy cycle.

The second therapy cycle results in an increased uptake in the liver metastases with slow washout, as demonstrated by the retained tracer within metastatic lesions at 24 and 120 hours. The tracer concentration within the metastases is slightly lower after the first therapy cycle with a slight decrease in metastatic volume, which reflects a positive response to the first therapy. Bilateral renal-cortical uptake appears normal with slow initial washout and a significant amount of retained tracer at 24 hours but then subsequent fast clearance with minimal cortical retention at 120 hours. The dosimetry research software generated absorbed-dose maps that show a calculated mean renal-cortical absorbed dose of 4.43 Gy for the right kidney and 4.84 Gy for the left kidney, which are considerably higher than that received by the kidneys following the first therapy. This may be due to the slightly lower level of tumor uptake and higher level of circulating tracer available for renal clearance, with consequent higher renal dose. The tumor dose

(for the same lesion in which dosimetry was performed after first therapy) shows significant reduction with mean absorbed dose of 4.3 Gy compared to mean dose of 15 Gy delivered after the first therapy. This reflects reduction in tumor size and number of functioning tumor cells following the first therapy.

The results for the second therapy cycle clearly indicate a slightly higher renal dose, but this was not considered excessive given the 7.4 GBq ^{177}Lu DOTATATE administered. The tumor dose, however, was significantly lower, at least for the largest initial lesion studied. Given the level of tumor size reduction and intensity following the first therapy, second, and subsequent therapies are expected to deliver high tumor doses and further impact the tumor response.

The third therapy cycle administered 7.7 GBq of ^{177}Lu DOTATATE in October 2017, 12 weeks after the second therapy. This cycle used identical protocols for therapy administration as well as sequential xSPECT Quant studies.

The images acquired following the third therapy cycle (Figure 4) indicate substantially reduced size and uptake intensity in the liver metastases. There is fast washout of tracer from within the tumor with a low level of retained tracer at 120 hours. The renal cortical uptake is normal at 0.5 hours post therapy with fast clearance with negligible retention at 120 hours. The DRT calculates a mean renal dose of 4.3 Gy in the right kidney and 3.84 Gy in the left kidney, which are comparable to that received after the second therapy. The tumor dose is expectedly lower in the liver lesion that was considered for dosimetry in the first and second therapies, showing a much lower mean dose of 2.8 Gy with significant reduction in tumor volume.

As evident from the sequential images and absorbed-dose maps in Figure 4, there was further shrinkage in the liver metastases with significant decrease in intensity of uptake reflecting positive tumor response to radionuclide therapy. The right renal dose is comparable to that of the second therapy although the left renal cortical dose was significantly lower. Both renal doses correlate with expected results of normal cortical uptake and fast washout (as seen in the images).

Although the patient showed significant response of the functioning liver metastases with tumor shrinkage as well as notable reduction in intensity of tracer uptake, a fourth therapy cycle was administered in order to complete the therapy protocol and to deliver the maximum dose possible to the remaining functioning tumor tissue with negligible risk of exceeding critical organ toxicity thresholds as evident from the dosimetry calculations generated after the first three cycles.

The fourth therapy cycle of 7.05 GBq of ^{177}Lu DOTATATE was administered in December 2017, 8 weeks following the third cycle. Sequential xSPECT Quant studies were acquired as per previous acquisitions. Reconstruction protocols and dosimetry were also performed using the DRT.

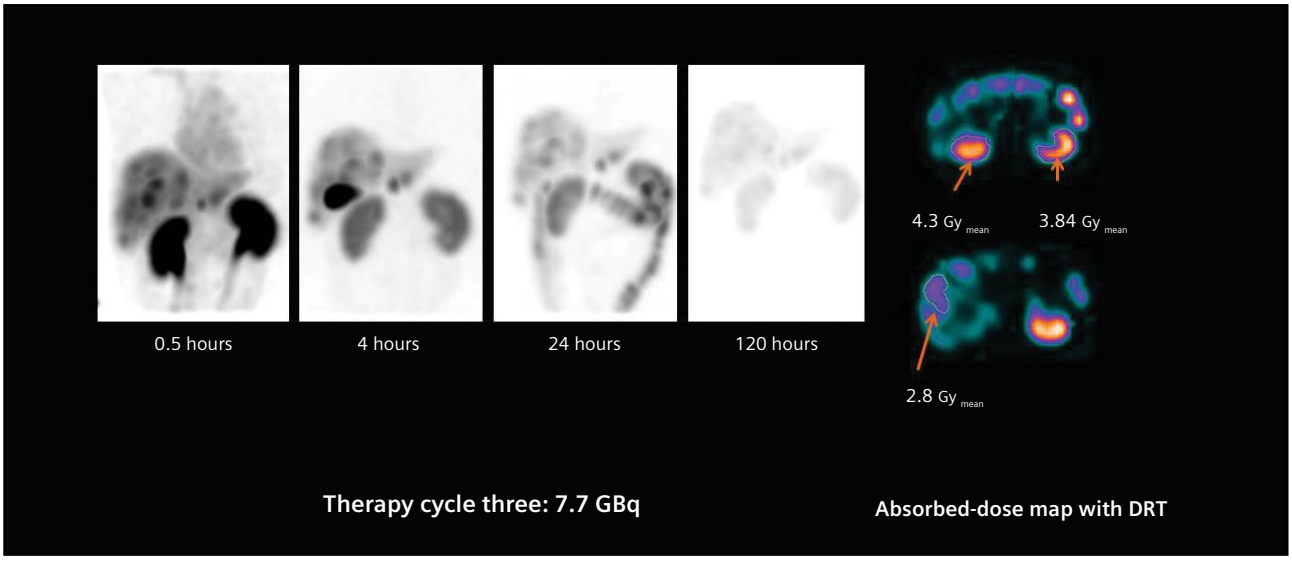

4 Sequential xSPECT Quant MIP images acquired following administration of the third ^{177}Lu DOTATATE therapy cycle.

Sequential xSPECT Quant images following the fourth therapy cycle (Figure 5) show further decrease in size and uptake intensity of the liver metastases; reflecting additional response to radionuclide therapy. There is low tracer uptake within the liver lesions, which are much reduced in size compared to the previous study. Fast washout is reflected in low tumor absorbed dose calculations. The liver lesion considered for dosimetry in the previous therapy cycles shows a mean absorbed dose of only 2.1 Gy and a further reduction of size, thus reflecting impressive response to radionuclide therapy. The low uptake of the tracer, smaller lesion dimensions, and faster washout within the liver metastases as seen in sequential xSPECT Quant correlate well with the low tumor-absorbed dose calculated on the DRT. The absorbed dose to the renal cortices, calculated with the DRT, is comparable to the previous study and confirms normal initial uptake levels followed by fast washout.

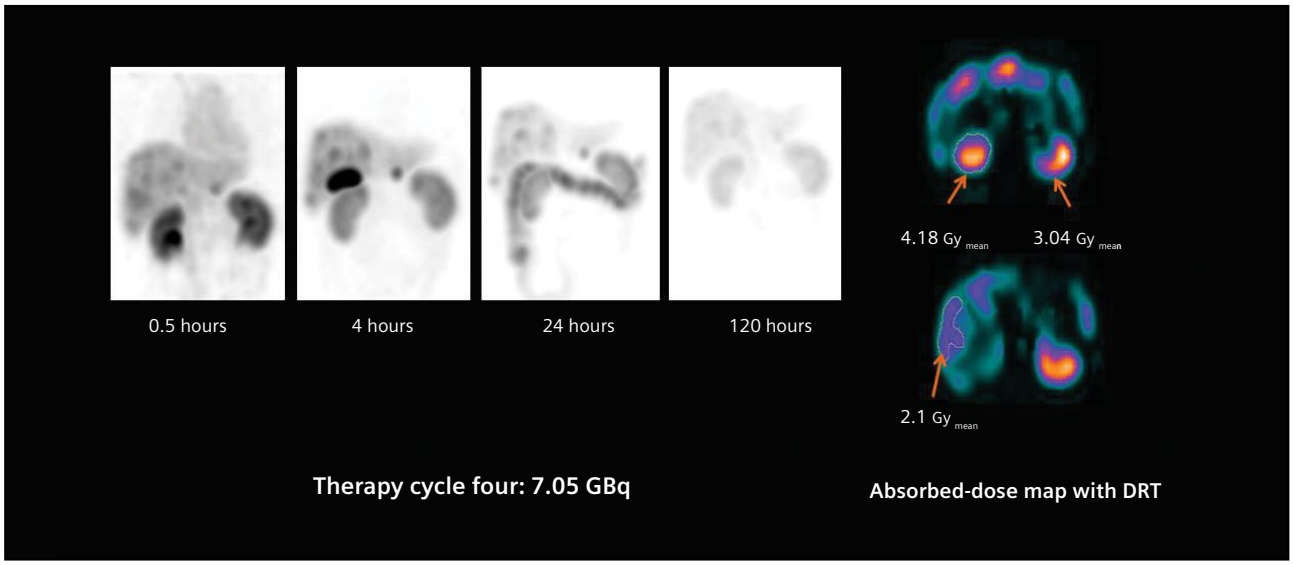

5 Sequential xSPECT Quant MIP images acquired following administration of the fourth therapy cycle of 7.05 GBq of ^{177}Lu DOTATATE.

In summary, from the MIP images (acquired 24 hours after administration of each therapy cycle) it is clear the metastatic lesions show a significant decrease in size and intensity of uptake, thus reflecting strong response to radionuclide therapies. At the time of third cycle, the largest metastatic lesion for which dosimetry was performed
at each cycle has decreased substantially in size and intensity of uptake as evident from the representative images after each therapy cycle. Analyzing the mean tumor dose delivered to this lesion, it is apparent that there is a progressive decrease in mean dose delivered to the lesion which changes from 10.1 Gy after the first cycle to 4.3 Gy after second cycle to 2.1 Gy after the fourth cycle. This can be explained by a decrease in tumor size and intensity of uptake reflecting loss of functioning tumor tissue secondary to positive response to radionuclide therapy.

The renal dose increases slightly after the second therapy reflecting increase in circulating tracer for clearance via kidneys secondary to decrease in tumor uptake following response to first therapy.

The DRT calculations indicate the cumulative dose to the left and right kidneys was 15.3 Gy and 16.18 Gy respectively, which is significantly lower than the 23 Gy limit for renal cortical dose in order to avoid renal toxicity.

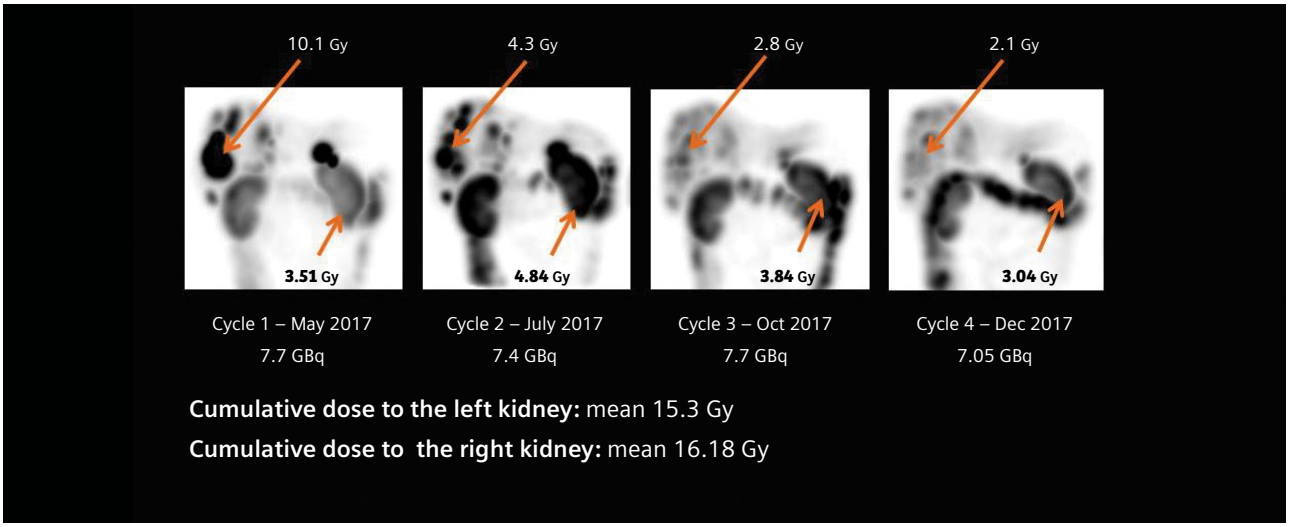

6 MIP images of xSPECT Quant acquired 24 hours after administration of each therapy cycle compare the tumor size and uptake after every cycle. The mean absorbed dose to the largest liver metastases and the left renal cortex is also displayed.

Comments

This study shows excellent tumor response using four therapy cycles with overall low levels of cumulative renal cortical dose. This suggests the possibility of increasing administered dose for the initial therapies without risk of undue renal toxicity. Since tumor dose in subsequent therapies progressively decreases due to shrinkage and loss of functioning tumor cells with consequent lower tumor uptake in delayed therapy cycles, it is conceivable to administer higher initial doses during the first or second cycle in order to delivery higher tumor dose and obtain an earlier response.

xSPECT Quant enables accurate evaluation of absolute tracer concentration within tumor and critical organs across multiple time-point studies in order to compute tumor and renal total radioactivity concentration and residence times which enables accurate dosimetry. The DRT is capable of utilizing the quantitative SPECT/CT data to perform automated organ segmentation and 3D voxel-based dosimetry to generate absorbed-dose maps and dose volume histograms in addition to generating mean-dose values from tumor and organ VOIs without a need for cumbersome dosimetry calculations. Seamless integration of quantitative SPECT/CT (xSPECT Quant) with 3D voxel-based dosimetry software produces absorbed-dose maps including dose color wash, which demonstrates not only the tumor and critical organ dose variations across multiple therapies but also the heterogeneity of the dose distribution within the same organ or tumor VOI. In tumors with heterogeneous distribution of functioning malignant cells, there is substantial heterogeneity of absorbed dose and response within the same tumor may vary and this variability is well reflected on absorbed-dose maps obtained from voxel-based dosimetry.

In this case, the liver metastases all show high tracer uptake in the first study and substantial radiation dose was delivered to tumor, as evident from the dosimetry calculations and subsequent response levels. A similar study evaluated correlated cumulative tumor-absorbed dose and best response in 24 lesions treated with 2 to 6 cycles of 7.4 Gy ^{177}Lu DOTATATE.[1] The tumor response was in the range of 4.5-57% using RECIST criteria with the cumulative absorbed dose ranging between 20 and 340 Gy for tumors larger than 2.2 cm. The cumulative dose of at least 40 Gy was associated with best response and there was significant correlation between tumor-absorbed dose and overall response levels.

In the present study, absorbed dose was calculated using Siemens Healthineers' Dosimetry Research Tool in which the largest lesion showed a mean absorbed dose of 10 Gy after the first therapy. The mean cumulative dose of 19.6 Gy in this lesion appears low when compared to the previously mentioned study. The lower level of mean absorbed dose to tumor in the second, third, and fourth studies, reflect a major decrease in tumor size and uptake secondary to response after the first therapy cycle. The initial absorbed dose to the tumor and the response following the initial therapy were the main drivers of tumor response in this particular patient.

Another study performed quantitative SPECT/CT at 0.5, 4, 24, and 96 hours after no carrier-added ^{177}Lu DOTATATE administration in 13 patients with metastatic neuroendocrine tumors, each receiving three cycles with an average dose of 7.8 GBq per cycle.[2] The mean renal dose of 3.1 +/- 1.0 Gy

per cycle (range 1.1-5.4 Gy) or 0.40 +/- 0.13 mGy/MBq in this patient population is comparable to the mean renal-absorbed dose in this particular patient also from the same institution.

Evaluation of renal- and tumor-absorbed dose across multiple therapies of fixed dose ^{177}Lu DOTATATE in a 200-patient study was performed using sequential SPECT/CT with the aim of optimizing the number of therapies based on cumulative renal- and bone marrow-absorbed dose estimation.[3] Fixed-dose (7.4 GBq/cycle) cycles were repeated until the absorbed dose to the kidneys reached 23 Gy unless therapy required to be stopped for other reasons. Almost half of the patients (49%) received 5-9 cycles (7.4 GBq each) in order to reach cumulative renal dose of 23 Gy. None of the patients reached the maximum bone marrow dose of 2 Gy. Out of all the patients, 23.5% had a partial response and 67.5% had stable disease. The objective tumor response was seen in 30.9% of patients, who reached a renal dose of 23 Gy and was also seen only in 13% of patients who did not reach 23 Gy.

It is evident from this study that substantial higher cumulative tumor dose can be achieved using either multiple fixed dose therapies or higher initial therapy doses without crossing renal thresholds, if accurate dosimetry is performed following every cycle and appropriate modifications to therapy approach are performed based on tumor and critical organ dosimetry.

Conclusion

Sequential xSPECT Quant and 3D voxel-based dosimetry, performed after each ^{177}Lu DOTATATE therapy cycle, show normal renal-cortical dose with each therapy cycle and a tendency of slight increase during the late cycles, which reflects a reduction in tumor burden with each successive therapy cycle. The dose delivered to metastases also show a progressive decrease along with reduction in tumor burden. Four therapy cycles resulted in adequate tumor dose to achieve an impressive reduction in tumor burden. The present case example illustrates the reliable value of quantitative SPECT/CT (xSPECT Quant) and 3D voxel-based dosimetry tools for quantitative evaluation of tumor and renal uptake, response evaluation, and accurate estimation of absorbed dose across multiple therapy cycles in order to have a comprehensive understanding of overall patient response. ●

Examination protocol

Scanner: Symbia Intevo 16

SPECT		CT	
Injected dose	Therapy cycle one: 7.7 GBq ^{177}Lu DOTATATE	Tube voltage	130 kV
	Therapy cycle two: 7.4 GBq ^{177}Lu DOTATATE		
	Therapy cycle three: 7.7 GBq ^{177}Lu DOTATATE		
	Therapy cycle four: 7.05 GBq ^{177}Lu DOTATATE		
Acquisition	60 stops at 20 seconds/stop	Tube current	45 eff mAs
		Slice collimation	6 x 1.0 mm
		Slice thickness	3 mm

The Dosimetry Research Tool is an investigational device. Limited by Federal (or United States) law to investigational use. This device is exclusively for clinical investigations. This investigational device does not fulfill all the essential requirements according to the European Medical Device Directive (93/42/EEC) and its national implementations. It is not commercially available in the European Union, or other countries worldwide.

The outcomes achieved by the Siemens customers described herein were achieved in the customer's unique setting. Since there is no "typical" hospital and many variables exist (e.g. hospital size, case mix, level of IT adoption) there can be no guarantee that others will achieve the same results.

References

1 Ilan E, Sandström M, Wassberg C, et al. Dose response of pancreatic neuroendocrine tumors treated with peptide receptor radionuclide therapy using ^{177}Lu-DOTATATE. *J Nucl Med.* 2015;56(2):177–182.

2 Bailey DL, Hennessy TM, Willowson KP, et al. In vivo measurement and characterization of a novel formulation of [^{177}Lu]-DOTA-Octreotate. *Asia Ocean J Nucl Med Biol*. 2016;4(1):30-37.

3 Garske-Román U, Sandström M, Fröss Baron K, et al. Prospective observational study of ^{177}Lu-DOTA-octreotate therapy in 200 patients with advanced metastasized neuroendocrine tumours (NETs): feasability and impact of a dosimetry-guided study protocol on outcome and toxicity. *Eur J Nucl Med Mol Imaging*. 2018; doi:10.1007/s00259-018-3945-z.

Whole-body parametric PET imaging in metastatic lung cancer

By Damita L. Thomas, MD
Data courtesy of University of Tennessee, Knoxville, Tennessee, USA

History

A 60-year-old woman with adenosquamous cell carcinoma of the lung was treated with resection of the primary disease and adjuvant chemotherapy. Seven months following initial therapy, the patient developed recurrent disease in the form of brain metastases. She subsequently underwent resection of the metastatic cerebral lesions, but developed a second recurrence in the brain approximately seven months later. Spectroscopic MRI was performed, however the results were equivocal as radiation necrosis could not be definitively excluded. Dynamic PET imaging to obtain additional parametric indices of glucose uptake was acquired in order to further assess the lesion.

Findings

Dynamic whole-body PET imaging was performed with Siemens Healthineers' FlowMotion™ Multiparametric PET Suite using the following imaging protocol. With the patient on the system table, 10.5 mCi (388.5 MBq) of Fludeoxyglucose F 18 injection (^{18}F FDG)[a] was intravenously administered. This was immediately followed by a 6 minute, single bed, list-mode (LM) acquisition centered over the heart to obtain data used to generate an image-derived input function: a non-invasive alternative to arterial blood sampling. Whole-body scanning then commenced with continuous bed motion using FlowMotion, allowing data acquisition during both the forward and reverse passes of the gantry bed. A total of 19 whole-body passes were acquired: 4 passes at 2 minutes per pass and 15 passes at 5 minutes. Total imaging time was 89 minutes. Images from whole-body passes 14-19 corresponded to 60-90 minutes post-injection and were summed for the SUV and used for Patlak image reconstructions.

Standard SUV images demonstrated an area of discrete photopenia in the right frontal lobe with hypermetabolic activity along its periphery (Figure 1A). Patlak MR_{FDG} (slope) images, reflecting tissues actively metabolizing ^{18}F FDG, demonstrate the same intensely metabolically active, rim-enhancing photopenic lesion in the right frontal lobe (Figure 1B). Patlak distribution volume (DV or intercept) images, reflecting the ratio of free non-metabolized ^{18}F FDG in tissue versus plasma, demonstrate increased activity in the right frontal lobe as well. However, the pattern of activity is markedly different from that seen on the SUV and MR_{FDG} images as there are low levels along the periphery and high levels in the center of the lesion (Figure 1C).

Given the increased activity seen on the MR_{FDG} images, which reflects tissue that is actively metabolizing ^{18}F FDG, the findings are highly suggestive of residual disease in the right frontal lobe lesion along the periphery of a necrotic core. DV images, however, demonstrate activity within the center of this lesion, which has low MR_{FDG} values. This is an interesting finding because it reflects the accumulation

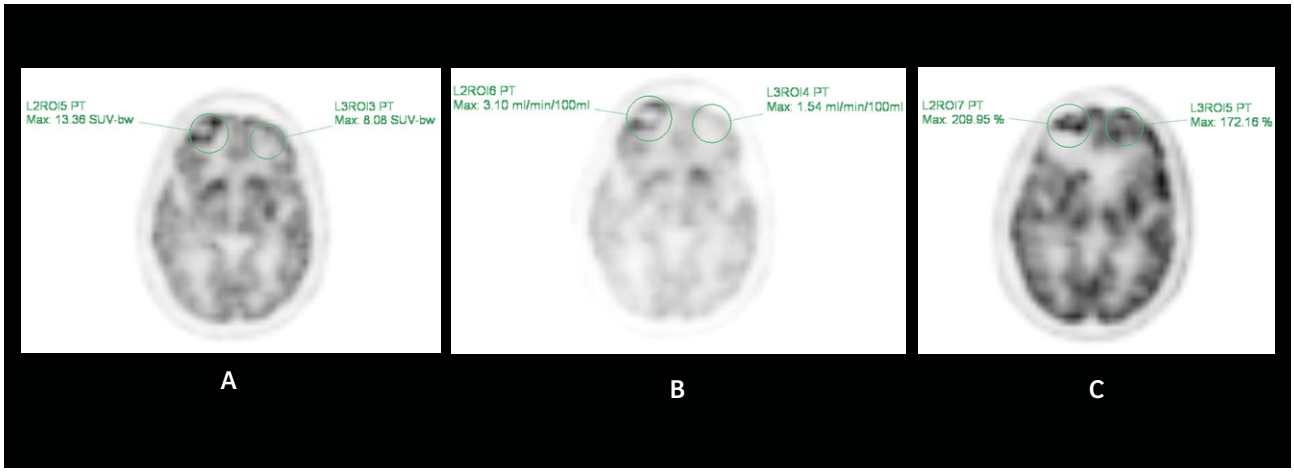

1 **Images from dynamic parametric ^{18}F FDG PET/CT demonstrating uptake in the right frontal lobe lesion and normal contralateral brain parenchyma. A) Conventional summed SUV image demonstrating intense metabolic activity in a ring-like pattern along the periphery of an area of photopenia. B) the MR_{FDG} image reflecting actual ^{18}F FDG metabolism within the region of interest (ROI), matching the ring-like distribution pattern of the tracer as seen on the SUV image (A). C) DV images represent the ratio of non-metabolized ^{18}F FDG in the tissue versus the plasma, and show high values in the center of the lesion, which is in contrast to the SUV and MR_{FDG} images.**

of free, non-metabolized tracer at the center of this lesion. Clinically, this could possibly reflect the physiological role of blood flow or blood pooling that occurs in the process of necrosis following therapy.

Given the equivocal MR results and the parametric PET findings that were highly suspicious for residual disease, a subsequent biopsy was performed, which did demonstrate disease.

Comments

^{18}F FDG PET/CT is well established in oncology as a means to not only initially stage disease, but to also assess therapeutic response and evaluate recurrent disease. Despite its widespread use, its accuracy in performing the latter two tasks is somewhat limited. Metabolic activity secondary to post-therapeutic inflammatory changes can be misinterpreted as residual disease whereas the relative lack of activity in a mass can be erroneously interpreted as absence of residual disease. These limitations in metabolic PET/CT imaging are, in part, due to the methods of image acquisition. The origins of metabolic imaging were acquired dynamically, which allowed assessment of radiotracer kinetics from the time of injection. This type of dynamic acquisition and kinetic assessment translated to the direct measurement of ^{18}F FDG metabolism in a volume of tissue (MR_{FDG}).[1] This method of imaging provided true quantitative data regarding physiologic and tumoral radiotracer activity. However, dynamic imaging proved time consuming, tedious, and uncomfortable for patients with its requirement for prolonged image acquisitions. Challenging post-processing and mathematical analysis, as well as sampling of arterial blood via arterial line insertions to measure radiotracer concentrations in the blood over time posed additional challenges. As such, dynamic imaging was supplanted by the more convenient method of delayed post-injection imaging. This method of imaging allowed PET/CT to become more amenable to routine clinical use and dynamic imaging, from that time forward, was largely confined to investigational research studies.

In today's practice, the acqusition of metabolic imaging follows a specified time delay after the intravenous injection of the radiotracer. Evaluation of physiologic and malignant tissue is via the standardized uptake value (SUV), a measure that quantitates radiotracer activity within a given area of tissue normalized to the distribution of the tracer throughout the body. The SUV, however, is only a rough estimate of ^{18}F FDG metabolism in tissue because the components that comprise its measurement are variable (eg, the patient's metabolic status at time of imaging and weight) and it does not factor in the plasma kinetics of a tracer that can markedly differ between patients.[2] As such, the SUV is semi-quantitative and does not accurately characterize actual tumoral ^{18}F FDG metabolism: a limitation that poses a challenge, particularly when it comes to

Fludeoxyglucose F 18 5-10mCi as an IV injection Indications and Usage

Fludeoxyglucose F 18 Injection is indicated for positron emission tomography (PET) imaging in the following settings:
- Oncology: For assessment of abnormal glucose metabolism to assist in the evaluation of malignancy in patients with known or suspected abnormalities found by other testing modalities, or in patients with an existing diagnosis of cancer.
- Cardiology: For the identification of left ventricular myocardium with residual glucose metabolism and reversible loss of systolic function in patients with coronary artery disease and left ventricular dysfunction, when used together with myocardial perfusion imaging.
- Neurology: For the identification of regions of abnormal glucose metabolism associated with foci of epileptic seizures.

Important Safety Information

- Radiation Risks: Radiation-emitting products, including Fludeoxyglucose F 18 Injection, may increase the risk for cancer, especially in pediatric patients. Use the smallest dose necessary for imaging and ensure safe handling to protect the patient and health care worker.
- Blood Glucose Abnormalities: In the oncology and neurology setting, suboptimal imaging may occur in patients with inadequately regulated blood glucose levels. In these patients, consider medical therapy and laboratory testing to assure at least two days of normoglycemia prior to Fludeoxyglucose F 18 Injection administration.
- Adverse Reactions: Hypersensitivity reactions with pruritus, edema and rash have been reported; have emergency resuscitation equipment and personnel immediately available. Full prescribing information for Fludeoxyglucose F 18 Injection can be found at the conclusion of this publication.

Dosage Forms and Strengths

Multiple-dose 30 mL and 50 mL glass vial containing 0.74 to 7.40 GBq/mL (20 to 200 mCi/mL) of Fludeoxyglucose F 18 injection and 4.5 mg of sodium chloride with 0.1 to 0.5% w/w ethanolas a stabilizer (approximately 15 to 50 mL volume) for intravenous administration. Fludeoxyglucose F 18 injection is manufactured by Siemens' PETNET Solutions, 810 Innovation Drive, Knoxville, TN 39732

---

characterizing a lesion following treatment. As illustrated in this case, the additional indices derived from parametric imaging allow a more accurate characterization of the right frontal lobe brain lesion. Although the lesion demonstrates prominent activity on the conventional SUV image, this activity could very well reflect post-procedural or post-surgical inflammatory changes and not disease. With the additional information provided by the MR_{FDG} image (which reflects actual ^{18}F FDG metabolism in a volume of tissue) it becomes clear that this lesion still bears residual disease along the periphery of a necrotic core. A subsequent biopsy confirmed the suspicion of disease.

Although post-therapy timing conventions help an interpreting physician discern whether activity seen on a post-therapy scan is inflammatory or actual disease (i.e. 10-14 days following chemotherapy, 6-8 weeks following radiotherapy), they are based more so on multiple anecdotal experiences as opposed to concrete data and conclusions from well-controlled clinical trials. Another factor to consider is the wide array of various chemotherapeutic agents and radiotherapy regimens. As it is likely that each affect cellular kill at different rates based on cancer type, histological grading, and intra-patient heterogeneity of lesions, it is also very likely that these loose guidelines either underestimate or overestimate the time needed for post-procedural inflammatory changes to resolve.

With the introduction of FlowMotion Multiparametric PET Suite, dynamic imaging and the additional measurements are now more convenient to incorporate into a clinical setting. This innovation addresses the challenges of dynamic PET imaging while providing true and reproducible quantitative data regarding physiologic and malignant tissue. It uses the well-established Patlak graphical analysis of a two-compartmental model for evaluation of radiotracer kinetics, allowing derivation of truly quantitative MR_{FDG} and DV values. The convenience of FlowMotion allows data image acquisition in a full body sweep with both forward and backward movement of the table gantry. Also, the dedicated six-minute cardiac acquisition to indirectly measure activity within the arterial blood pool from automatically placed regions of interests (ROIs) over the aortic or left ventricle negates the

need for painful, and often laborious, arterial blood line insertions. These innovations will not only make dynamic PET imaging considerably more convenient for clinical research applications, but will hopefully find its way back into routine clinical practice. As there is a plethora of literature[3-7] demonstrating the clinical utility of parametric imaging in various cancer types, it is feasible that parametric imaging can be utilized for particularly challenging cases where additional kinetic information may be useful in reaching the final diagnosis.

Conclusion

As opposed to semi-quantitative SUV measures, ^{18}F FDG PET/CT parametric imaging provides additional quantitative indices that allow for the measurement of radiotracer kinetics, which more accurately characterizes tumoral metabolic activity. As illustrated in this case study, parametric imaging can aid in the differentiation of post-procedural changes, which ultimately affects patient management. ●

Examination protocol

Scanner: Biograph 64 mCT Flow

PET		CT	
Injected dose	Fludeoxyglucose F 18 injection (^{18}F FDG) 10.5 mCi (388.5 MBq)	Tube voltage	120 kV
Scan Delay	No Delay	Tube current	13 mAs
Scan acquisition	Whole-body, dynamic continuous bed motion (CBM) Patlak	Slice thickness	5 mm

References

1 Dimitrakopoulou-Strauss A, Pan L, Strauss LG. Quantitative approaches of dynamic FDG-PET and PET/CT studies (dPET/CT) for the evaluation of oncological patients. *Cancer Imaging*. 2012;12:283-289.

2 Karakatsanis NA, Lodge MA, Tahari AK, Zhou Y, Wahl RL, Rahmim A. Dynamic whole body PET parametric imaging: I. Concept, acquisition protocol optimization and clinical application. *Phys Med Biol.* 2013;58(20):7391-7418.

3 Dimitrakopoulou-Strauss A, Strauss LG, Egerer G, et al. Impact of dynamic 18F-FDG PET on the early prediction of therapy outcome in patients with high-risk soft-tissue sarcomas after neoadjuvant chemotherapy: a feasibility study. *J Nucl Med.* 2010;51:551-558.

4 Dimitrakopoulou-Strass A, Strauss LG, Burger C, et al. Prognostic aspects of 18F-FDG PET kinetics in patients with metastatic colorectal carcinoma receiving FOLFOX chemotherapy. *J Nucl Med*. 2004;45:1480-1487.

5 Spence AM, Muzi M, Mankoff DA, et al. 18F-FDG PET of gliomas at delayed intervals: improved distinction between tumor and normal gray matter. *J Nucl Med.* 2004;45:1653-1659.

6 Dimitrakopoulou-Strass A, Strauss LG, Schwarzbach M, et al. Dynamic PET 18F-FDG studies in patients with primary recurrent soft-tissue sarcomas: impact on diagnosis and correlation with grading. *J Nucl Med*. 2001;42(5):713-720.

7 Dunnwald LK, Gralow JR, Ellis GK, et al. Tumor metabolism and blood flow changes by positron emission tomography: relation to survival in patients treated with neoadjuvant chemotherapy for locally advanced breast cancer. *J Clin Oncol.* 2008:26(27):4449-4457.

[a] For indications and important safety information for Fludeoxyglucose F 18 injection (^{18}F FDG) see page 60. For full prescribing information see pages 80-82.

The statements by Siemens Healthineers customers described herein are based on results that were achieved in the customer's unique setting. Since there is no "typical" hospital and many variables exist (e.g., hospital size, case mix, level of IT adoption) there can be no guarantee that other customers will achieve the same results.

FlowMotion Multiparametric PET Suite is not commercially available in all countries. Due to regulatory reasons, its future availability cannot be guaranteed. Please contact your local Siemens organization for further details.

Evaluation of a retropharyngeal metastasis from papillary carcinoma of the thyroid

By Gustavo Gomez, MD
Data courtesy of Nucléos, Brasilia, Brazil

History

A 26-year-old female with a history of papillary carcinoma of the thyroid was treated with a total thyroidectomy with neck dissection in September 2014. The histopathology showed a 2.5 cm classic papillary carcinoma in the left lobe. Out of 96 dissected neck nodes, 36 were metastatic on histopathological examination.

The patient underwent large-dose ^{131}I therapy (200 mCi) in December 2014. A post-therapy ^{131}I whole-body scan showed a focal area of increased uptake in the retropharynx and cervical region. The patient suffered severe sialoadenitis following iodine therapy and was on follow-up for 10 months. The patient then underwent serum thyroglobulin assay in October 2015, which showed a high value of 32.7 ng/ml. In view of the suspicion of nodal recurrence in the thyroid bed or neck, a neck ultrasound was performed in February 2016 that revealed an enlarged level III left cervical node, which was strongly suspicious for metastasis. Surgical removal of the left cervical lymph node was performed in March 2016 and the histopathology revealed a nodal metastasis from papillary thyroid carcinoma. A diagnostic whole-body ^{131}I scan performed in June 2016 was negative, although a repeat serum thyroglobulin performed at the same time showed persistent high values (serum thyroglobulin in June 2016 was 27.8 ng/ml). In view of the lack of ^{131}I-avid nodal metastases, and the patient's refusal to undergo further large-dose iodine therapy due to complications from the first therapy, plans for a second radioiodine therapy were abandoned.

Thyroid carcinoma often expresses somatostatin receptors and (^{111}In or ^{99m}Tc octreotide) somatostatin receptor scintigraphy or PET can be positive in patients with iodine-negative thyroid carcinoma.[1] Based on this consideration, the patient was referred for a ^{99m}Tc octreotide somatostatin receptor SPECT/CT in August 2016. The octreo scan images showed positive focal uptake in the retropharynx, which was suggestive of a somatostatin receptor-positive, radioiodine-negative metastases. In view of the presence of somatostatin receptor-positive retropharyngeal metastases, the patient was given four cycles of ^{177}Lu DOTATATE therapy, each dose being approximately 200 mCi between October 2016 to June 2017.

A repeat serum thyroglobulin performed in August 2017 showed a high value of 20.6 ng/ml. The patient was subsequently referred for Fludeoxyglucose F 18 injection (^{18}F FDG)[a] PET/CT followed by ^{68}Ga DOTATOC PET/CT to assess the status of the retropharyngeal metastasis and to evaluate for new lesions.

The patient was initially evaluated with ^{18}F FDG PET/CT in August 2017 and a ^{68}Ga DOTATOC PET/CT was performed the following day. Following intravenous (IV) administration of 7.7 mCi (287 MBq) of ^{18}F FDG and 65 minutes post-injection delay, a whole-body PET/CT was performed using low-dose CT (110 kV, 125 ref mAs, 16 x 1.2 mm collimation, 3 mm slice thickness) followed by a PET acquisition at 2 minutes per bed position on Biograph™ Horizon. A dedicated single bed position PET/CT study for the head and neck region was subsequently performed with a low-dose CT (110 kV, 34 eff mAs, 16 x 1.2 mm collimation, 3 mm slice thickness), followed by a PET acquisition of 4 minutes. PET was acquired using time of flight (ToF) and an ultraHD reconstruction of PET data (a reconstruction technique combining ToF with point spread function (PSF)) was fused with CT for evaluation of both whole-body and dedicated head-and-neck PET/CT. PET/CT using ^{68}Ga DOTATATE was performed the following day. One hour following administration of 3.3 mCi (125 MBq) of ^{68}Ga DOTATOC, a low-dose whole-body CT (110 kV, 125 ref mAs, 16 x 1.2 mm collimation, 2 mm slice thickness) was followed by a whole-body PET acquisition at 3 minutes per bed. A dedicated single bed position PET/CT study for the head and neck region was also acquired with a protocol similar to that of the ^{18}F FDG study.

Findings

As shown in Figure 1, an increased glucose metabolism in the right palatine tonsillar mass is suggestive of a glucose-avid metastasis from papillary carcinoma of the thyroid, which corresponds to the lesion previously delineated on the ^{99m}Tc octreotide somatostatin receptor scintigraphy.

^{68}Ga DOTATOC PET/CT (Figure 2) correlates with the diagnosis of a pharyngeal somatostatin receptor-positive, radioiodine-negative metastasis originating from

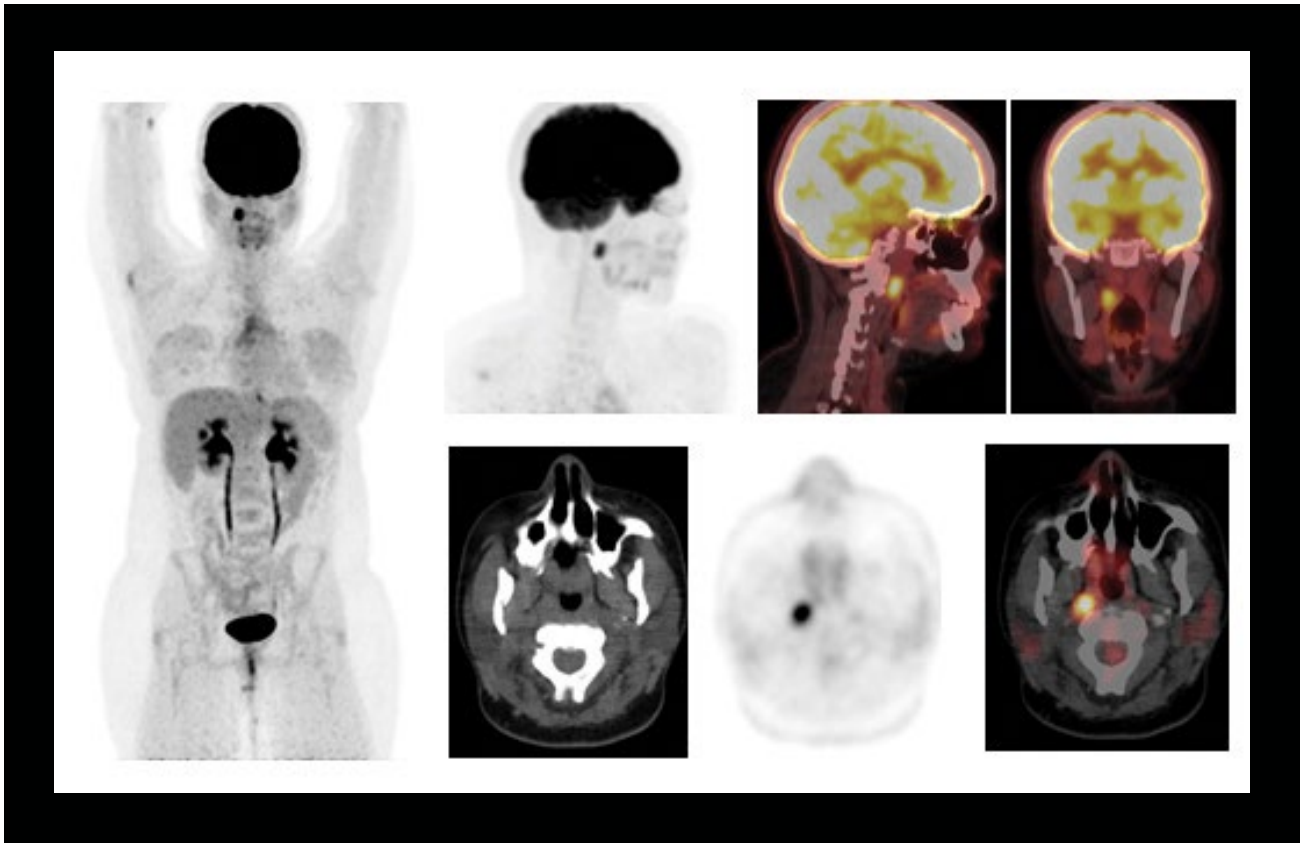

1 **^{18}F FDG whole-body PET maximum intensity projection (MIP) image, CT, and fused PET/CT images show a hypermetabolic mass in the right posterior pharyngeal wall involving the palatine tonsil. No other focal hypermetabolic lymph nodal lesion or evidence of local spread was visualized and the rest of the body shows normal distribution of the tracer.**

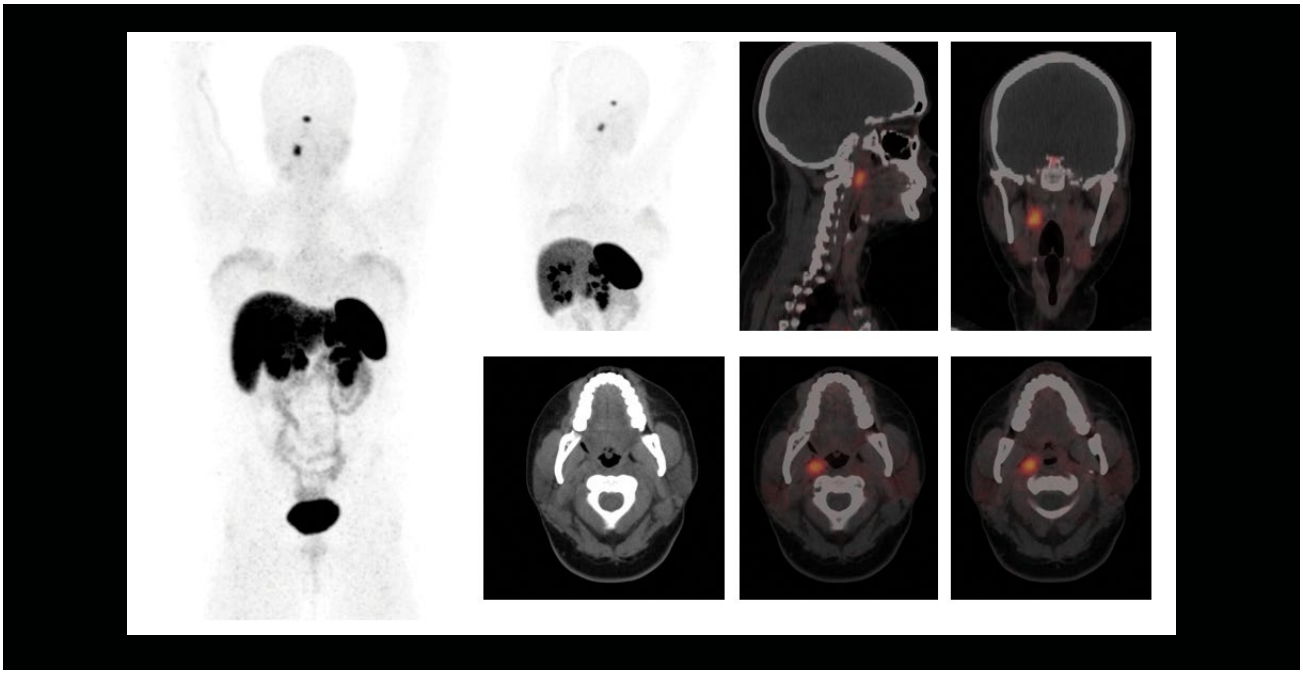

2 **^{68}Ga DOTATOC PET MIP, along with fused PET/CT images, show high uptake within the right palatine tonsillar mass. Such an uptake is suggestive of a somatostatin receptor-positive metastasis, which correspond and confirm the presence of a ^{111}In octreotide-avid metastasis seen in the previous octreoscan study. No other receptor-positive metastases were visualized. Physiological distribution of the tracer is visualized in the pituitary gland, liver, spleen, kidney, and intestines.**

papillary thyroid carcinoma, based on the previous somatostatin receptor scintigraphy.

As seen in Figures 1 and 2, as well as the comparison of ^{18}F FDG and ^{68}Ga DOTATOC uptake within the pharyngeal metastasis, the lesion shows a similar high level of uptake of both tracers that is possibly suggestive of an aggressive, poorly differentiated glucose-avid metastasis with significant somatostatin receptor positivity. The high level of ^{68}Ga DOTATOC uptake even after four previous therapy cycles of ^{177}Lu DOTATATE opens up the possibility of further therapy cycles.The patient underwent a follow-up scan again in July 2018 and the serum thyroglobulin was measured at 17.4 ng/ml, which was slightly lower than the value measured in August 2017. The patient also underwent ^{18}F FDG and ^{68}Ga DOTATOC PET/CT studies with a similar acquisition protocol as the previous study. Both ^{18}F FDG and ^{68}Ga DOTATOC PET/CT studies showed the presence of the pharyngeal metastasis with slightly lower SUV_{max} (^{18}F FDG SUV_{max} 7.9 and ^{68}Ga DOTATOC SUV_{max} 8.9) as compared to the previous study. No new metastases were visualized. The slight reduction of serum thyroglobulin and lesion SUV_{max} is a possible effect of the previous radionuclide therapy with ^{177}Lu DOTATATE.

Comments

Although differentiated thyroid carcinoma is usually ^{131}I-avid and can be effectively treated with radioiodine, some metastatic lesions become dedifferentiated and lose their capacity to accumulate radioiodine. ^{18}F FDG PET/CT has been shown to be sensitive in the detection of radioiodine-negative metastases in differentiated thyroid carcinoma with elevated serum thyroglobulin levels. The sensitivity of ^{18}F FDG PET/CT increases with stimulated Tg levels and reaches 100% sensitivity at stimulated Tg > 28.5 ng/ml.[2] Thyroid carcinoma expresses somatostatin receptors and (^{111}In-octreotide) somatostatin receptor scintigraphy has shown high sensitivity

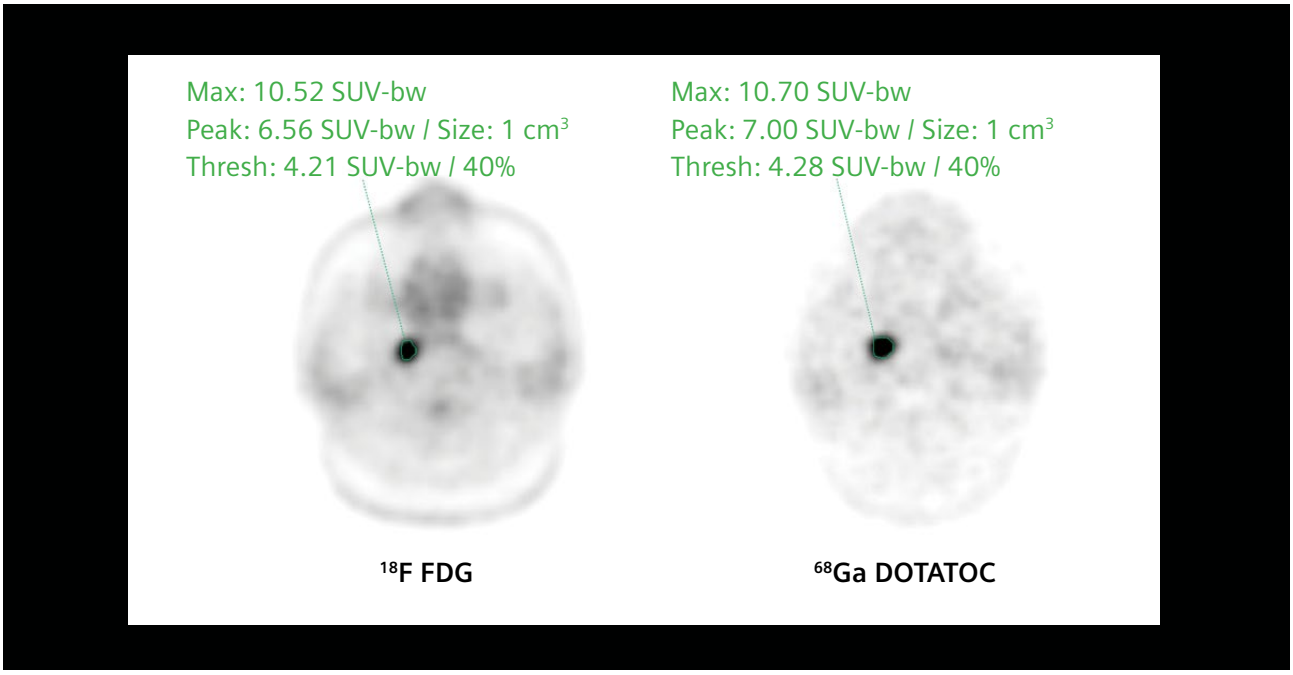

3 **Correlation of maximum and peak SUV within the lesion for the ^{18}F FDG and ^{68}Ga DOTATOC PET images show comparable values, which suggests similar and high levels of uptake.**

in the detection of radioiodine-negative thyroid carcinoma metastases.[1] Expression of somatostatin receptors in thyroid carcinoma cells is the rationale behind usage of ^{68}Ga DOTATOC PET/CT for the detection of somatostatin receptor-positive thyroid carcinoma metastases, particularly for radioiodine-negative metastases, which often pose a diagnostic challenge.

A study compared ^{18}F FDG PET to ^{68}Ga DOTATOC PET in a series of 17 patients with differentiated thyroid cancer.[3] Out of 104 malignant lesions, ^{18}F FDG PET showed an only slightly higher detection rate than ^{68}Ga DOTATOC PET in radioiodine-positive lesions (28/31 versus 25/31), whereas ^{18}F FDG was significantly more sensitive in radioiodine-negative metastatic lesions (70/73 versus 26/73). Three out of 104 lesions were visible using ^{68}Ga DOTATOC PET only.

Although this study shows ^{18}F FDG PET to have a higher sensitivity compared to somatostatin-receptor PET in radioiodine-negative thyroid cancer, studies show the value of ^{68}Ga DOTATOC PET in the detection of thyroid carcinoma metastases, which were radioiodine negative as well as ^{18}F FDG PET negative.[4] In this study, ^{68}Ga DOTATOC was positive in 33% of patients who had metastases that were radioiodine and ^{18}F FDG negative where most of these lesions were poorly differentiated. The rate of somatostatin receptor positivity in ^{18}F FDG and radioiodine negative-differentiated papillary and follicular carcinomas was lower.

Somatostatin receptor positivity in ^{111}In octreotide SPECT and ^{68}Ga DOTATOC PET in patients with radioiodine-negative thyroid carcinoma metastases has lead to therapy options using somatostatin receptor-seeking therapeutic radio-pharmaceuticals like ^{177}Lu DOTATATE. A study performed radionuclide therapy with two cycles of 200 mCi of ^{177}Lu DOTATATE in a patient with ^{18}F FDG- and ^{68}Ga DOTATOC-positive metastases in the lung, mediastinal lymph node, ribs, and muscle with a significant decrease in serum Tg (609 ng/ml pre therapy to 9 ng/ml after 200 mCi ^{177}Lu DOTATATE therapy cycles) after two cycles.[5]

Conclusion

The present case highlights the synergy that may be achieved by combining ^{18}F FDG and ^{68}Ga DOTATOC PET/CT in patients with elevated thyroglobulin and negative radioiodine whole-body scans. Although ^{18}F FDG PET/CT detected the hypermetabolic pharyngeal metastasis with high contrast, the high uptake of ^{68}Ga DOTATOC with SUV_{max} levels similar to that of ^{18}F FDG suggested the need to continue ^{177}Lu DOTATATE therapy. The follow-up PET/CT study performed in July 2018 demonstrated a decrease in lesion SUV for both ^{18}F FDG and ^{68}Ga DOTATATE PET/CT with no fresh metastatic lesion, which reflects the effect of previously delivered radionuclide therapy.

In a patient where all other therapy options were exhausted or rejected by the patient due to toxicity concerns, ^{177}Lu DOTATATE therapy offered an alternative, which led to a slight decrease in serum thyroglobulin as well as a significant reduction in lesion uptake, as evident in the follow-up study. ●

Examination protocol

Scanner: Biograph Horizon

PET		CT	
Injected dose	Fludeoxyglucose F 18 Injection (^{18}F FDG) 7.7 mCi	Tube voltage	110 kV
Acquisition	Whole-body PET/CT followed by PET at 2 minutes per bed	Tube current	125 ref mAs
		Tube collimation	16 x 1.2 mm

The outcomes achieved by the Siemens customers described herein were achieved in the customer's unique setting. Since there is no "typical" hospital and many variables exist (e.g. hospital size, case mix, level of IT adoption) there can be no guarantee that others will achieve the same results.

References

1 Christian JA, Cook CJR, Harmer C. Indium-111-labelled octreotide scintigraphy in the diagnosis and management of non-iodine avid metastatic carcinoma of the thyroid. *British Journal of Cancer.* 2003;89:258–261.

2 Trybek T, Kowalska A, Lesiak J, Mlynarczyk J. The role of 18F-Fluorodeoxyglucose Positron Emission Tomography in patients with suspected recurrence or metastatic differentiated thyroid carcinoma with elevated serum thyroglobulin and negative I-131 whole body scan. *Nuclear Medicine Review*. 2014;17(2):87–93.

3 Middendorp M, Selkinski I, Happel C, Kranert WT, Grunwald F. Comparison of positron emission tomography with [(18)F] FDG and [(68)Ga]DOTATOC in recurrent differentiated thyroid cancer: preliminary data. *Q J Nucl Med Mol Imaging*. 2010;54(1):76-83.

4 Binse I, Poeppel TD, Ruhlmann M, et al. 68Ga-DOTATOC PET/CT in Patients with Iodine- and 18F-FDG-Negative Differentiated Thyroid Carcinoma and Elevated Serum Thyroglobulin. *J Nucl Med*. 2016;57:1512–1517.

5 Elboga U, Ozkaya M, Sayiner ZA, Celen YZ. Lu-177 labelled peptide treatment for radioiodine refractory differentiated thyroid carcinoma. *BMJ Case Rep*. 2016. doi:10.1136/bcr-2015-213627.

[a] For indications and important safety information for Fludeoxyglucose F 18 injection (^{18}F FDG) see page 60. For full prescribing information, please see pages 80-82.

Detection of solitary pelvic lymph node metastasis in a patient with primary prostate cancer

By Walter Noordzij, MD, PhD; Ronald Borra, MD, PhD; and Partha Ghosh, MD
Data courtesy of University Medical Center Groningen, Groningen, The Netherlands

History

A 78-year-old male with a medical history of lower urinary tract symptoms, referred for primary staging of his newly-diagnosed Gleason 3+4 prostate cancer, underwent a ^{68}Ga PSMA PET/CT for initial staging on Biograph Vision™. The patient was intravenously injected with 2.7 mCi (100 MBq) of ^{68}Ga PSMA, and the PET/CT study was performed 1 hour and 45 minutes post injection. The examination began with an ultra low-dose CT (100 kV, 16 eff mAs, 32 x 1.2 mm collimation) followed by a PET acquisition with continuous bed motion (FlowMotion™ technology), at a constant table speed of 1.0 mm/sec. The PET study was reconstructed with a 220 x 220 matrix using time of flight (ToF) and point spread function (PSF).

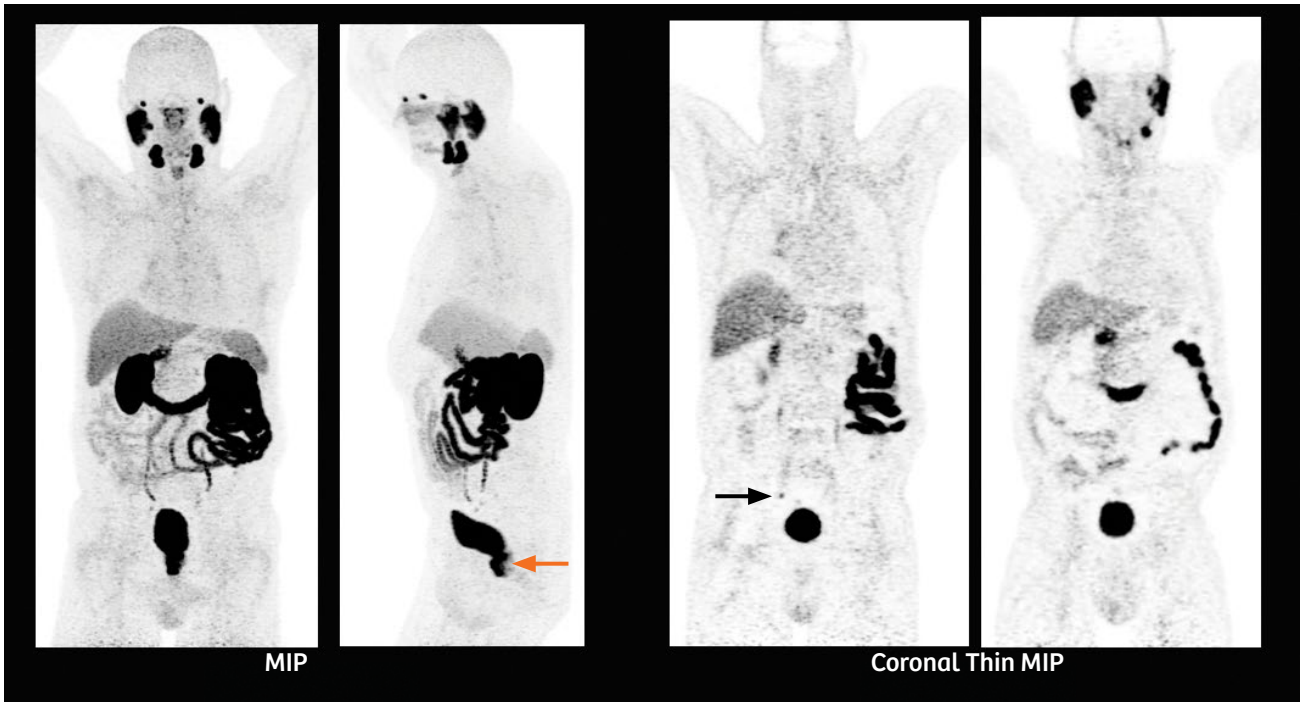

1 **Left panel: coronal and sagittal ^{68}Ga PSMA PET maximum intensity projection (MIP) images. Lobulated and intense tracer uptake in the ventral part of the prostate (orange arrow) reflect the primary tumor. Right panel: coronal thin MIP images show a small focal uptake in the right pelvis (black arrow) that is distinct from the ureter, which is suggestive of a solitary lymph node metastasis. No other tracer-avid lymph nodal lesions are visualized. Salivary and lacrimal glands, liver, kidneys, and intestines show physiological uptake, with physiological excretion through the ureters towards the urine bladder. Additionally, no skeletal lesion is visualized.**

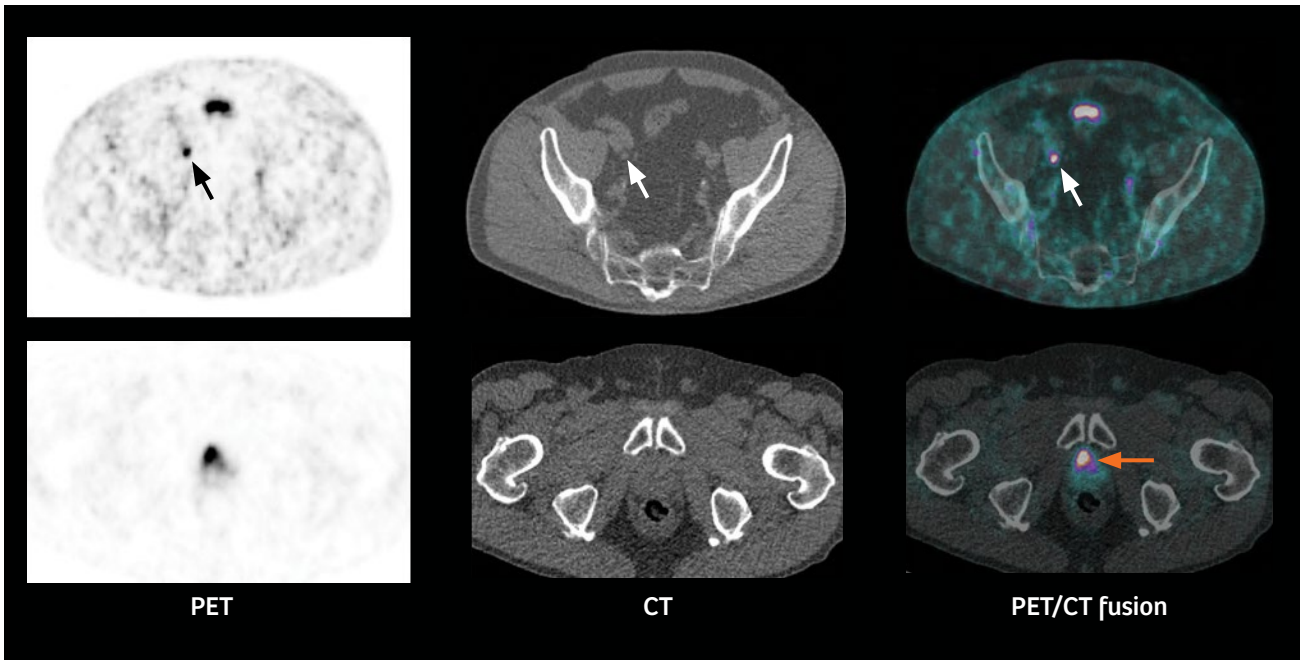

2 **Axial slices through PET (left), CT (center), and fused images (right) at the level of the prostate (bottom row) and the pelvic nodal lesion (top row) showing high uptake of ^{68}Ga PSMA in the primary prostatic tumor (orange arrow) and lymph node metastasis along the right external iliac artery (white and black arrows). The size of this solitary right external iliac lymph node on CT is still within normal range.**

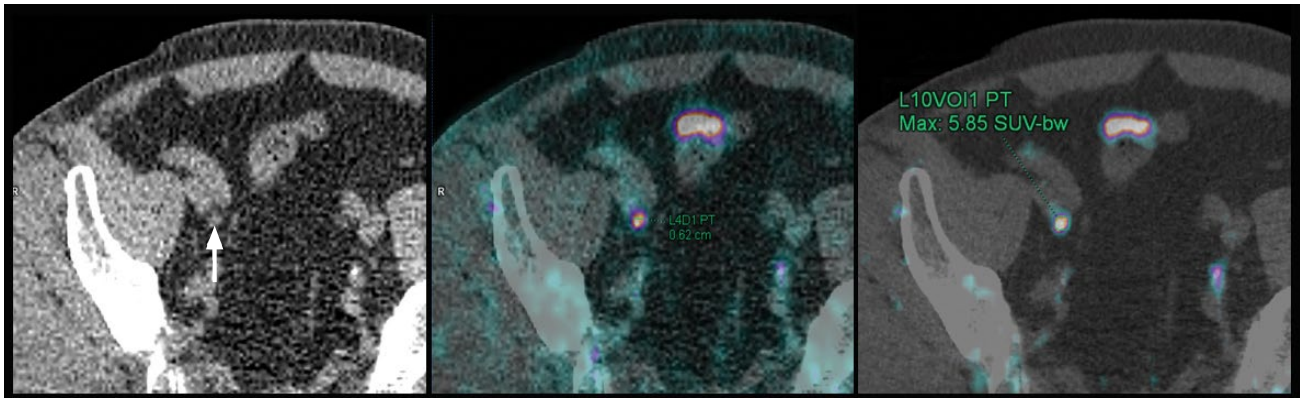

3 **Enlarged views of CT (left) and fused PET/CT images (both center and right) highlight the solitary right external iliac lymph node metastasis, which is approximately 6 mm in diameter on CT and has a SUV_{max} of 5.8.**

Findings

The ^{68}Ga PSMA PET/CT (Figures 1-3) shows a solitary right external iliac lymph node metastasis along with the PSMA-avid primary prostatic tumor without evidence of any other skeletal, soft tissue, or extrapelvic nodal metastases. The primary prostatic tumor showed a high-intensity uptake of ^{68}Ga PSMA with a SUV_{max} of 41.2. The 6 mm solitary pelvic nodal metastasis had a SUV_{max} of 5.8 with with high lesion-to-background ratio seen on the PET images, which helped differentiate the lesion from surrounding uptake in the ureter and intestines. The ^{68}Ga PSMA PET/CT was instrumental in detecting a solitary pelvic lymph node metastasis in this patient with primary prostate cancer who otherwise had no clinical or radiological suspicion of metastases. Detection of a single metastatic lymph node puts the patient in stage IV, irrespective of the Gleason score or PSA level.

Comments

The ^{68}Ga PSMA PET/CT was instrumental in accurately staging this patient who was otherwise clinically considered free of nodal or distant metastases. Detection of a solitary PSMA-expressing nodal metastasis by the ^{68}Ga PSMA PET/CT scan places the patient in stage IV; such staging leads to a significant change in therapy approach regarding the use of androgen deprivation therapy (ADT). The detection of a small lymph node metastasis (6 mm in diameter on CT) reflects the high sensitivity of the ^{68}Ga PSMA PET/CT for detection of nodal metastases. High ToF performance on Biograph Vision demonstrates a possible key relevance for such sharp delineation of a 6 mm lymph node metastasis with high lesion-to-background ratio. Increased contrast to background in any nodal lesion helps distinguish a metastasis from adjacent soft tissue and physiological uptake in the intestines. Excellent ToF performance, high resolution, and count-rate capability available with Biograph Vision should have a positive impact in improving the accuracy of staging since the detectability of small metastatic lesions is a key driver in the staging of prostate cancer.

The primary prostatic tumor in this patient shows high PSMA avidity with a high SUV_{max} of 41.2. Primary tumors with higher PSMA uptake and SUV have been shown to be associated with higher serum PSA levels and a higher Gleason score.[1] In this case, the 41.2 SUV_{max} in the primary tumor probably reflects a higher Gleason score.

^{68}Ga PSMA PET/CT has shown high sensitivity for detection of nodal metastases, as reflected by a study, which demonstrated detection rates of 57.9% in patients with mild post-surgery PSA increase to the level of 0.2-0.5 ng/ml.[2] In another study involving 50 newly diagnosed prostate cancer patients without any previous treatment history, ^{68}Ga-PSMA-11 PET/CT detected lymph node metastases in 16% of patients and distant metastases in 10% of patients.[3] In 13 of these 50 patients (26%), there was a change in staging with 11 of the 13 patients (84%) upstaged based on ^{68}Ga PSMA PET/CT. There was an alteration in the treatment plan in 44% of this patient group.

The present report reflects the sensitivity of ^{68}Ga PSMA PET/CT for the detection of lymph node metastases and the potential impact on staging and management. Technological improvements in PET/CT, such as the incorporation of Silicon Photomultiplier (SiPM) technology—which leads to an improvement in ToF performance—may potentially prove instrumental in demonstrating PET/CT's impact in staging and managing prostate cancer.

Biograph Vision, with 214-picosecond timing resolution, enables high lesion contrast to background with standard acquisition time in spite of low injected dose and long post-injection delay. Such a high lesion-to-background ratio improves small metastatic lymph node detectability. Partial volume effect can impact the detection of lymph node metastases as small as 6 mm with low uptake demonstrated by a relatively small SUV_{max} of 5.8, as seen in this case. The 3.2 mm crystals in Biograph Vision provide high spatial resolution, which help minimize partial volume effects thereby providing sharp delineation of such a small lesion along with a high lesion-to-background ratio for excellent small lesion visibility and quantitative accuracy.

Conclusion

The sharp definition and high lesion-to-background ratio provided by advanced SiPM PET/CT technology, enables the visualization of a solitary 6 mm pelvic lymph node metastasis with relatively low uptake of ^{68}Ga PSMA in a patient with primary prostate cancer. The ability to visualize a singular lymph nodal metastasis led to a major change in the patient's staging-associated therapy implications. ●

References

1 Rowe SP, Gage KL, Faraj SF, et al. 18F-DCFBC PET/CT for PSMA-Based Detection and Characterization of Primary Prostate Cancer. *J Nucl Med.* 2015;56(7):1003–1010.

2 Eiber M, Maurer T, Souvatzoglou M, et al. Evaluation of Hybrid ^{68}Ga-PSMA Ligand PET/CT in 248 Patients with Biochemical Recurrence After Radical Prostatectomy. *J Nucl Med.* 2015;56(5):668-674.

3 Koerber SA, Will L, Kratochwil C, et al. ^{68}Ga-PSMA-11 PET/CT in Primary and Recurrent Prostate Carcinoma: Implications for Radiotherapeutic Management in 121 Patients. *J Nucl Med.* 2018. doi:10.2967/jnumed.118.211086.

Examination protocol

Scanner: Biograph Vision

PET	
Injected dose	2.7 mCi (100 MBq)
Acquisition	FlowMotion 1.0 mm/sec, 220 x 220 matrix
CT	
Slice collimation	32 x 1.2 mm
Tube voltage	100 kV
Tube current	16 eff mAs
Slice thickness	3 mm

SPECT/CT delineation of patellar and femorotibial overload after knee arthroplasty

By Christian Waldherr, MD and Partha Ghosh, MD
Data and images courtesy of Engereid Hospital, Bern, Switzerland

History

A 52-year-old woman with a history of right total-knee arthroplasty (TKA) presented with persistent right knee pain. An inconclusive radiographic led to a ^{99m}Tc-MDP three-phase bone scan, which was followed by SPECT/CT imaging to evaluate knee pathology.

After an intravenous injection of 600 MBq of ^{99m}Tc-MDP, the three-phase bone scan was initiated. Initial dynamic planar perfusion images were followed by planar bloodpool images of both knee joints. Delayed-phase planar whole-body images were acquired three hours post injection accompanied by a SPECT/CT of both knees, which was performed on a Symbia Intevo™ 6. CT and fused SPECT/CT images were reviewed together for final evaluation.

Findings

The prior radiographic information was inconclusive (Figure 1) since there was no sign of loosening (lysis), periprosthetic fracture, or particle disease. In patients with painful joints after arthroplasty, functional evaluation is key to identifying the cause of pain.

The perfusion and bloodpool images show synovitis and osseous hypervascularization of the right knee, right patella, and medial tibial epipysis (along the medial tibial plateau). In correlation, late-phase planar and SPECT/CT images demonstrate osseous hyper-metabolism in the right patella and the medial femoro-tibial joint reflecting bone stress and bone marrow edema. Varus deformity of the right knee joint with the mechanical axis of the right femur (line between head of the right femur and midpoint between two femoral condyles) is slightly in variance to the tibial shaft axis (line through the tibial shaft). Varus deformity developing following TKA leads to overload stress at various points in the right knee, especially the medial femoral and tibial compartments, as is reflected in the pattern of hypermetabolism.

SPECT/CT delineated the overload stress pattern secondary to a varus deformity delineated on the whole-body planar images.

The various orientations of CT and SPECT/CT images (Figures 4 to 7) clearly demonstrate the bony-overload stress in the patella, medial femoral condyle, and medial tibial plateau. The CT images show osteolysis in the patella, medial femoral condyle, and cystic zone of osteolysis in the lateral femoral condyle, reflecting periprosthetic bone loss. There is no visible evidence of prosthetic loosening, misalignment of articular surfaces, or patellar misalignment. The synovitis involving the entire knee joint is reflected in the mild hyperperfusion and hypervascularity seen in the dynamic perfusion and bloodpool images. The Insall-Salvati (IS) ratio, as well as tibial tuberosity (TT)-trochlear groove (TG) distance of the right knee, is within normal limits (Figures 8 and 9), which reflects absence of misalignment of patella and prosthetic articular components. This finding, along with absence of loosening, confirms the mild varus deformity of the right knee to be the principal cause of the patellar and medial femoral condylar and medial tibial plateau overload stress, which are identified as the source of the pain.

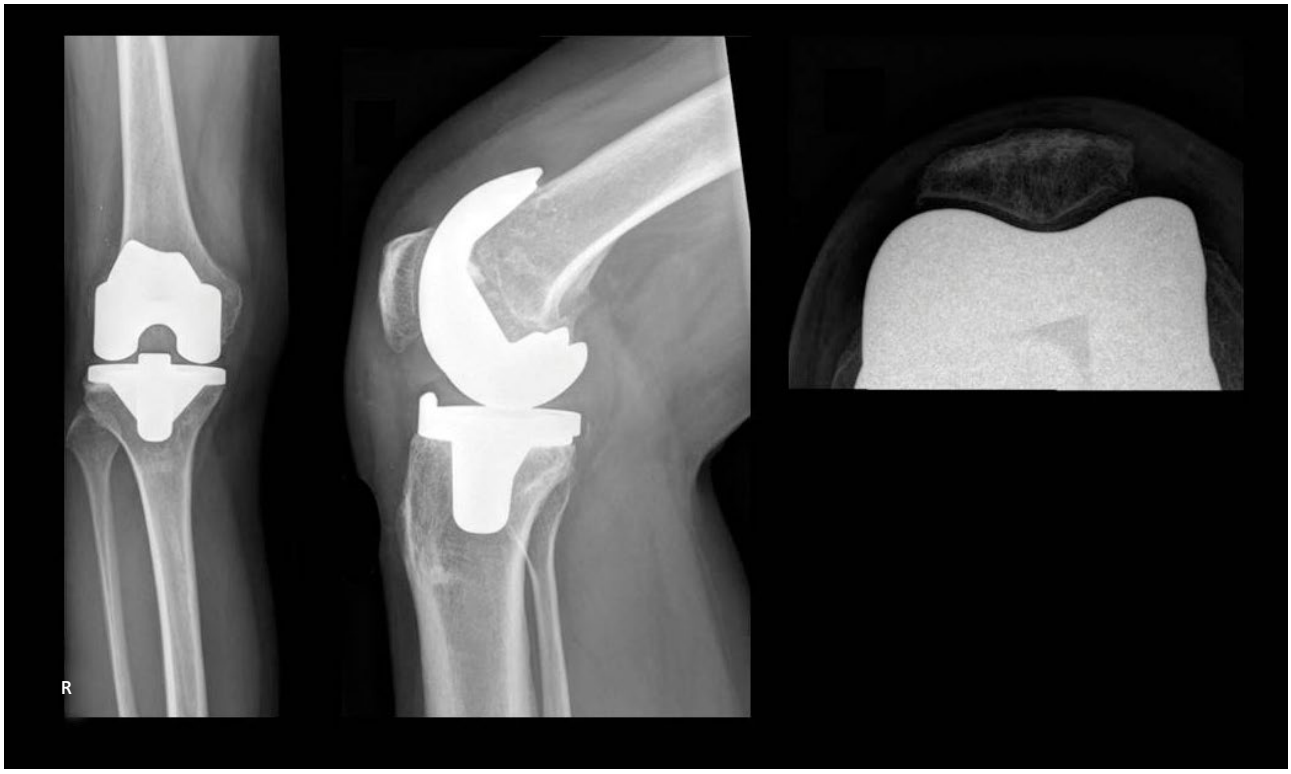

1 Anterior, lateral, and end-on radiographs of the right knee suggest correct axial and vertical positioning of the patella and absence of lysis among the components of TKA, which reflect absence of patellar misload and absence of radiographic signs of loosening or fracture. The periprosthetic femur shows slight radiolucency, which reflects erosion of the bone. The patella is undisplaced with normal concavity of the articular surfaces but shows significant radiolucency, which reflects periarticular bone loss. The radiograph suggest a slight varus mal-alignment when compared to the opposite knee (not shown).

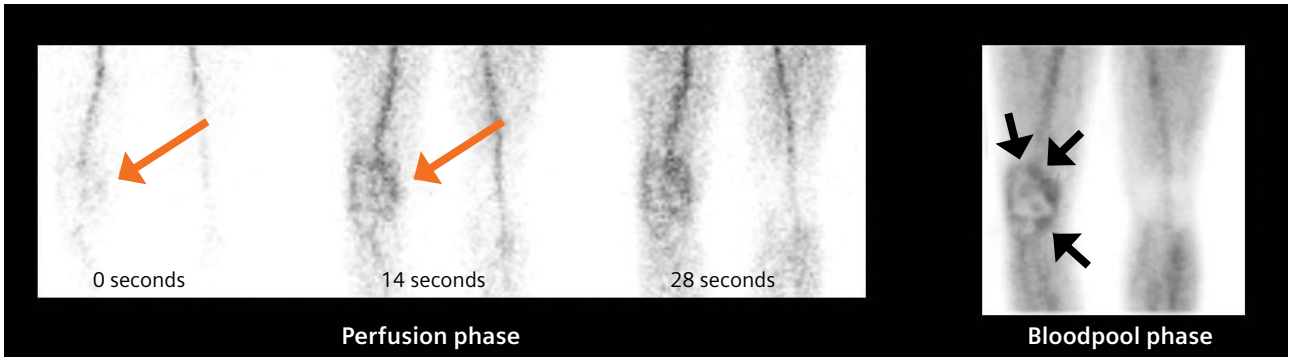

2 Arterial phase and bloodpool images show hypervascularization of bone and soft tissue , especially increased blood flow to the patella as well as the medial part of the knee (orange arrows). The bloodpool images show synovitis in the right knee with hypervascularity in the patella as well as in the medial tibial plateau (black arrows).

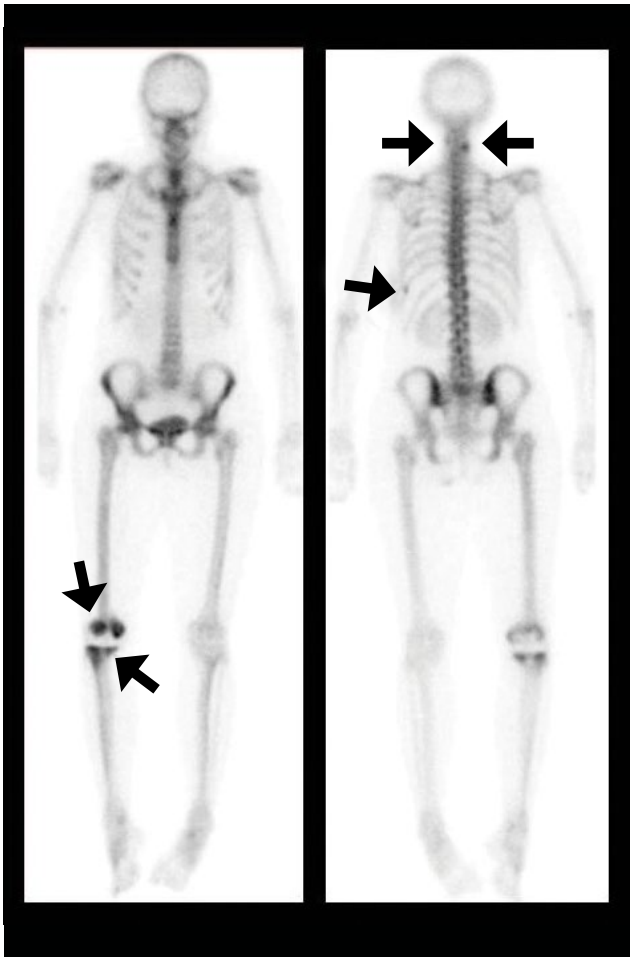

3 Anterior and posterior whole-body planar images show areas of focal hypermetabolism in the right knee joint, especially in the right patella and medial compartment of the tibia (arrows) correlating with the perfusion images. There is a slightly lower level of hypermetabolism in the medial femoral condyle and lateral tibial compartment. These focal areas of increased tracer uptake reflect bone stress related to the right TKA prosthesis. The right knee shows a slight varus deformity with the mechanical axis of the femur not perfectly aligned to the tibial shaft axis. Focal hypermetabolism is also seen in the cervical spine and left 10th rib, which may be related to degenerative changes and trauma. Additionally, there is no active bone stress in the hips or ankle.

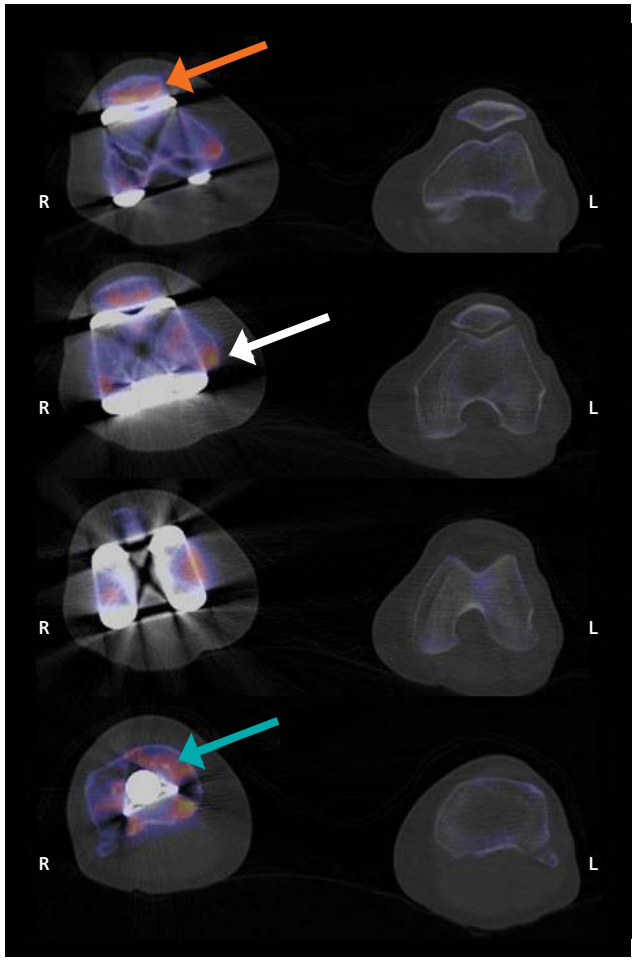

4 Fused SPECT/CT axial images show focal hypermetabolism in the patella, predominantly in the periarticular zone adjacent to the patellar articulating surface articulating with the femoral component of the TKA prosthesis (orange arrow), which reflects patellar-overload stress, secondary to arthroplasty. Focal hypermetabolism in the medial femoral condyle (white arrow), just medial to the prosthesis margin, reflects bone stress. Increased uptake in the medial tibial plateau (blue arrow), just medial to the prosthesis margin, also demonstrates bone stress. There is no evidence of loosening or displacement of prosthesis and the patella appears to be in proper position without misalignment.

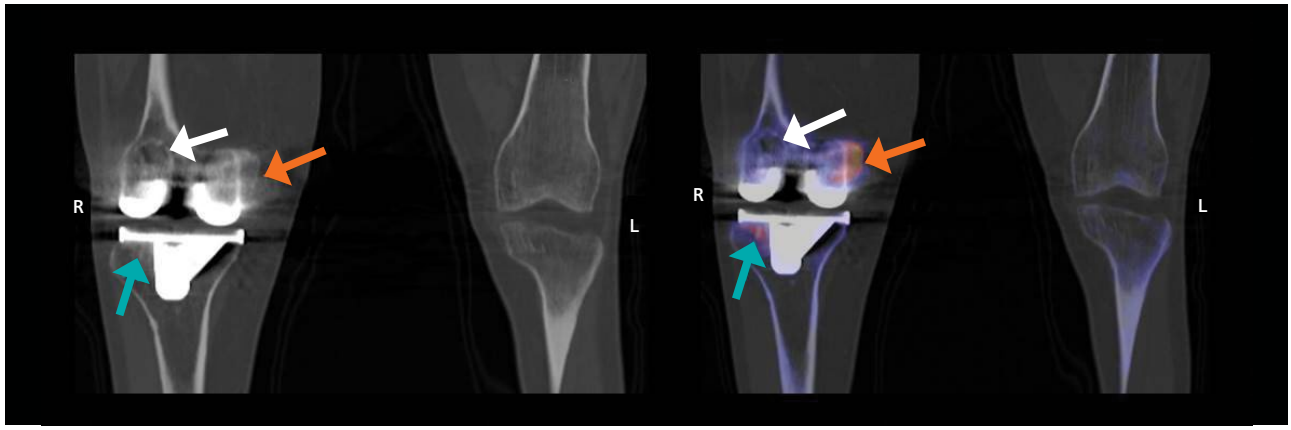

5 Coronal CT and fused SPECT/CT images show increased bone resorption in the medial femoral condyle with corresponding hypermetabolism (orange arrow). This reflects bony stress possibly related to an overload, secondary to slight, varus deformity with alteration of the angle between the mechanical axis of the right femur to the tibial shaft axis, secondary to arthroplasty. The lateral femoral condyle shows a cystic zone of osteolysis (white arrow), which does not demonstrate hypermetabolism. The lateral tibial plateau, just below the prosthetic tibial articular plate, shows minor sclerosis with mild hypermetabolism (blue arrows), which appears reactive in nature but does not appear related to loosening. No gap between bone and prosthetic margins is visualized, which suggests an absence of loosening. Interarticular space is normal with no displacement between the femoral and tibial articular surfaces of the TKA prosthesis.

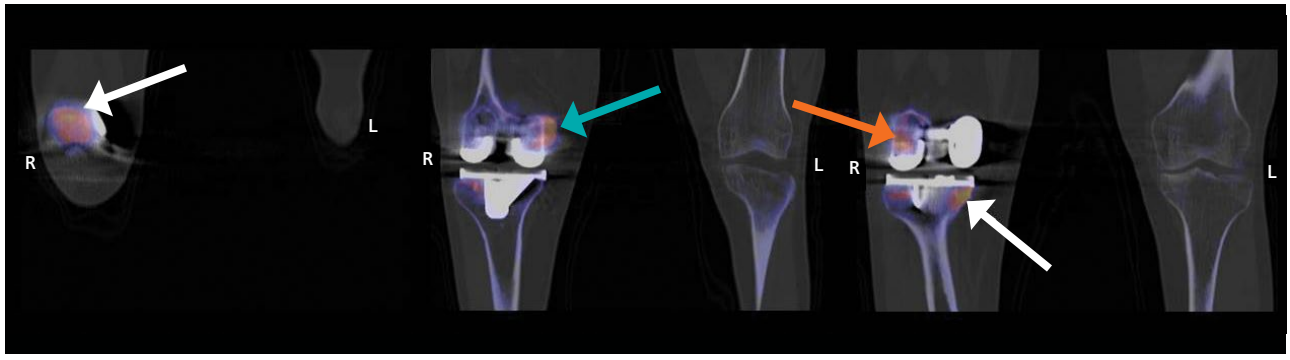

6 Coronal-fused SPECT/CT slices, captured from anterior to posterior, show patellar hypermetabolism (white arrows), bony overload stress in the medial femoral condyle (blue arrow), and hypermetabolism in the lateral femoral condyle adjacent to the prosthesis margin (orange arrow), all of which reflect bone stress. The medial tibial plateau, just below the medial edge of the articular surface of the tibial component of the TKA prosthesis, shows hypermetabolism, which is also related to overload stress related to the slight varus deformity of the right knee following arthroplasty.

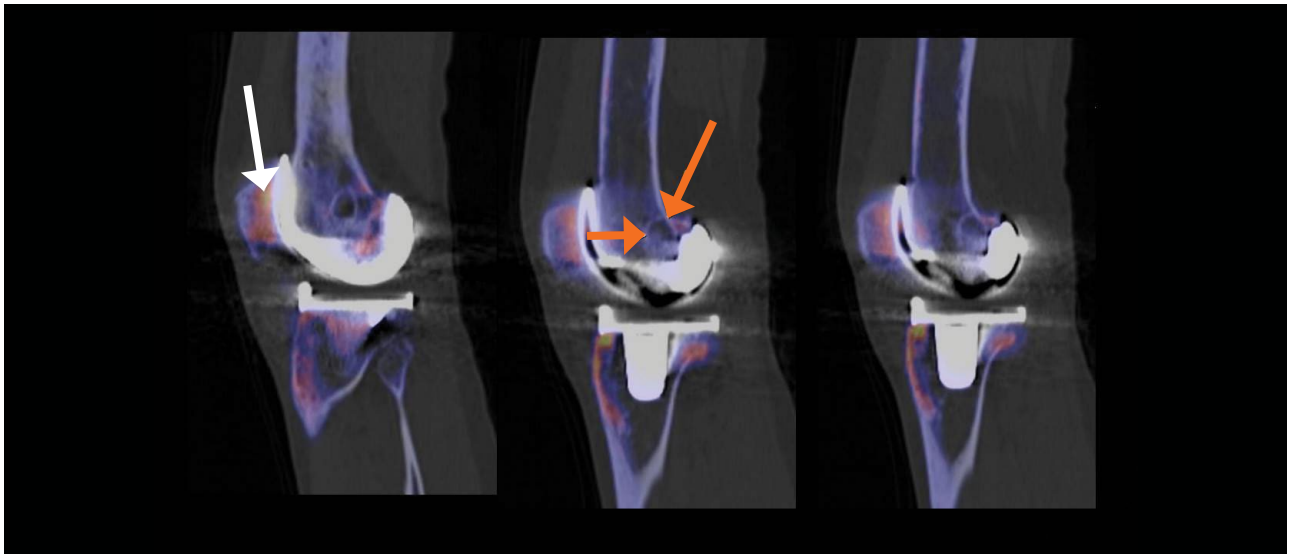

7 Sagittal-fused SPECT/CT slices through the right knee joint, from medial to lateral, show patellar hypermetabolism (white arrow) as well as cystic radiolucency in the lateral femoral condyle (orange arrows). As no gap is visible between the prosthetic margin and adjacent bone in either the femoral and tibial component, and there is proper alignment of the prosthetic articular surfaces, these results are suggestive of an absence of prosthetic loosening, misalignment, or displacement of articular surfaces.

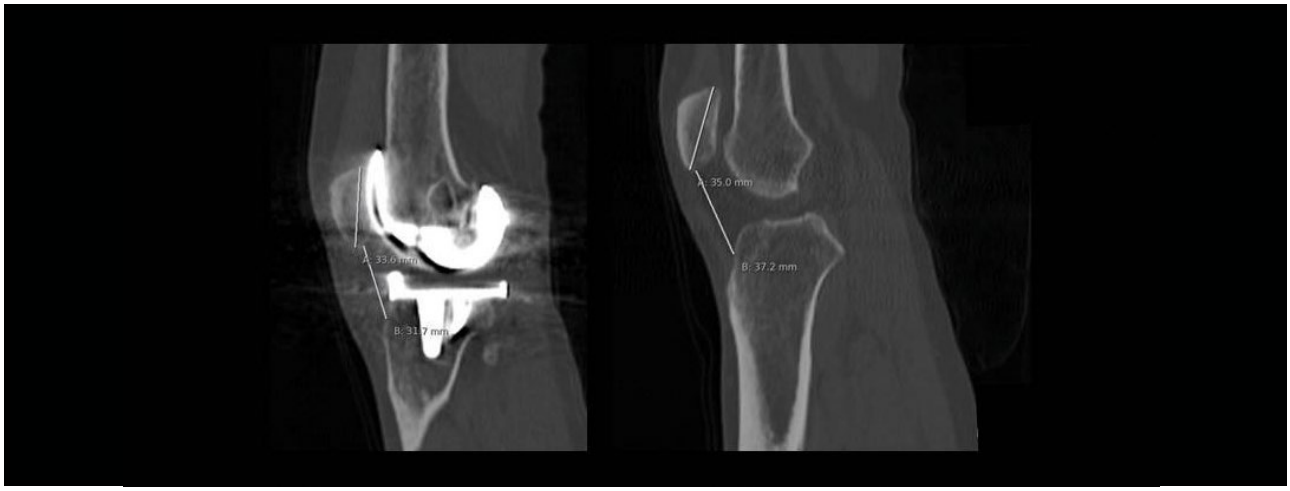

8 Sagittal CT slices of right and left (normal) knee joints used for determination of IS ratio of both knee joints. Both knees show normal IS ratio of < 1. Normal IS ratio is 0.8 to 1.2.

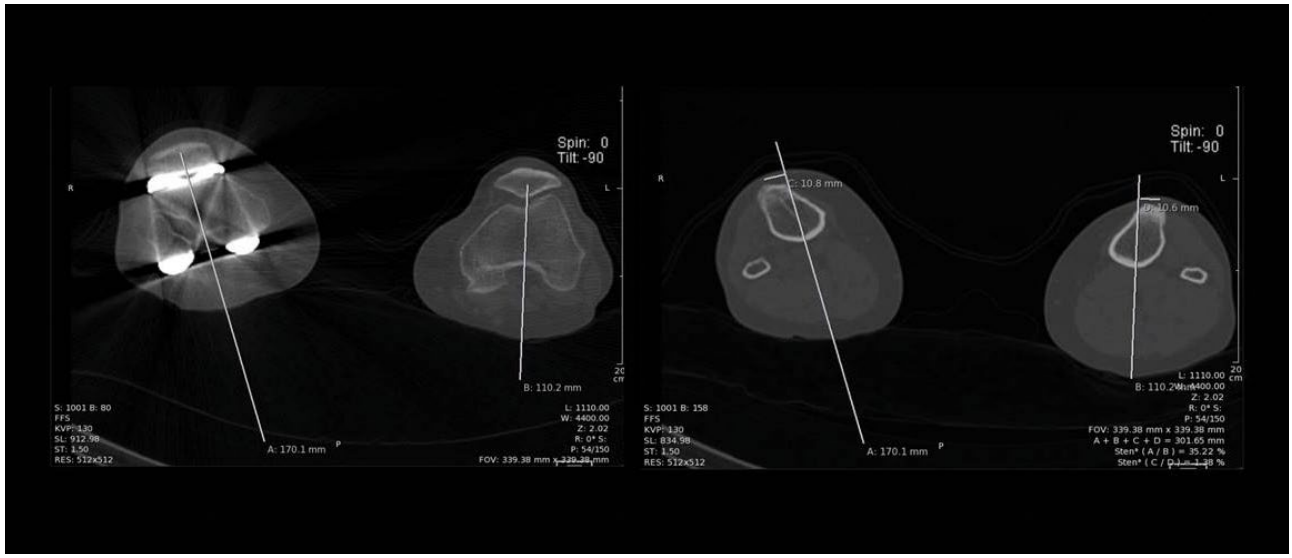

9 Axial CT slices through both knee joints at the level of TG of femur (left) and the TT (right), taken in order to measure the distance between the TT to the TG or patellar transition distance. The TT-TG distance in both knees is 1.1 cm and is within normal limits (< 15 mm).

Discussion

The most frequent cause of pain and implant loosening in arthroplasty patients is overload/misload of periprosthetic bone and patella, which is reflected as hyper-metabolism related to bone stress on bone SPECT/CT. In this case this was instrumental in accurately defining the focal areas of periprosthetic bony stress in the right knee joint as related to overload stress caused by mild varus deformity secondary to TKA in absence of any prosthetic loosening, malalignment, or articular displacement or periprosthetic fracture. Bony stress-related hypermetabolism in the medial femoral condyle and medial tibial plateau delineated on SPECT/CT correlates with varus deformity visible on the planar whole-body and coronal SPECT/CT images, which causes atypical stress to the medial compartment of the right knee joint. The level of hypermetabolism is lower than that of the patella and is likely not the principal cause of pain. The patellar hypermetabolism in absence of any patellar misalignment, malrotation, or displacement suggest patellar overload secondary to genu varum deformity. The normal IS ratio and TT-TG distance in the right knee also suggests stable patella with proper position of patellar articular surface in the trochlear groove of the femoral component of the TKA prosthesis. This rules out patellar malalignment or maltracking as a cause of the patellar hypermetabolism, thereby confirming patellar overload stress caused by varus deformity of right knee.

Patellar overload without malposition is most likely due to scarring of the patellar ligaments, the likely reason for acute pain. The CT shows perfect alignment of the prosthetic margins with periprosthetic bone without any gap—which rules out loosening. Even without loosening, the osseous overload of medial part of the tibial component with genu varum deformity is likely to be the biomechanical reason for eventual loosening. The reasons for patella overload are frequently axial patella shift (medial or lateral), high or low riding patella, and tibial malrotation to the femur that leads to patella maltracking) or scarring of the patella ligaments. Various measurements in the SPECT/CT images show the orthopedic surgeon how to correct the mal-positioning. Comparison with the other side (knee) is essential because knee alignment, patella positioning, and tilt varies from patient to patient. Measurements of patella shift, tilt, vertical position, and TT-TG are key to explain the reasons for overload. Chronic stress to the arthroplasty will eventually lead to loosening with CT evidence of lysis, which reflects instability caused by a moving prothesis. in such situations the management decision is between waiting until the arthroplasty becomes loose or earlier realignment of the joint. This depends on the pain profile of the patient.

Conclusion

Since focal bony stress may be associated with changes visualized on CT, like focal lysis or sclerosis (which are non-specific), evaluation of bone metabolism in the joint—with correlation to evidence of instability, deformity, malalignment, or loosening using bone SPECT/CT—is vital for proper evaluation of post-arthroplasty pain or movement restriction. Although an MRI can delineate bone edema related to focal bone stress, it is often difficult to interpret in the presence of a prosthesis. As shown in this particular case study, SPECT/CT with accurate co-registration of bony metabolic abnormalities to joint and prosthetic morphology can be of vital clinical value. The high-quality CT, combined with the high-resolution SPECT provided by Symbia Intevo are key to diagnostic accuracy and confidence. ●

Examination protocol

Scanner: Symbia Intevo 6

SPECT		**CT**	
Injected dose	600 MBq ^{99m}Tc-MPD	Tube voltage	130 kV
Acquisition	30 frames, 20 seconds per frame with Flash 3D reconstruction	Tube current	25 mAs
		Slice thickness	3 mm

The outcomes achieved by the Siemens customers described herein were achieved in the customer's unique setting. Since there is no "typical" hospital and many variables exist (e.g. hospital size, case mix, level of IT adoption) there can be no guarantee that others will achieve the same results.

From innovations to clinical results

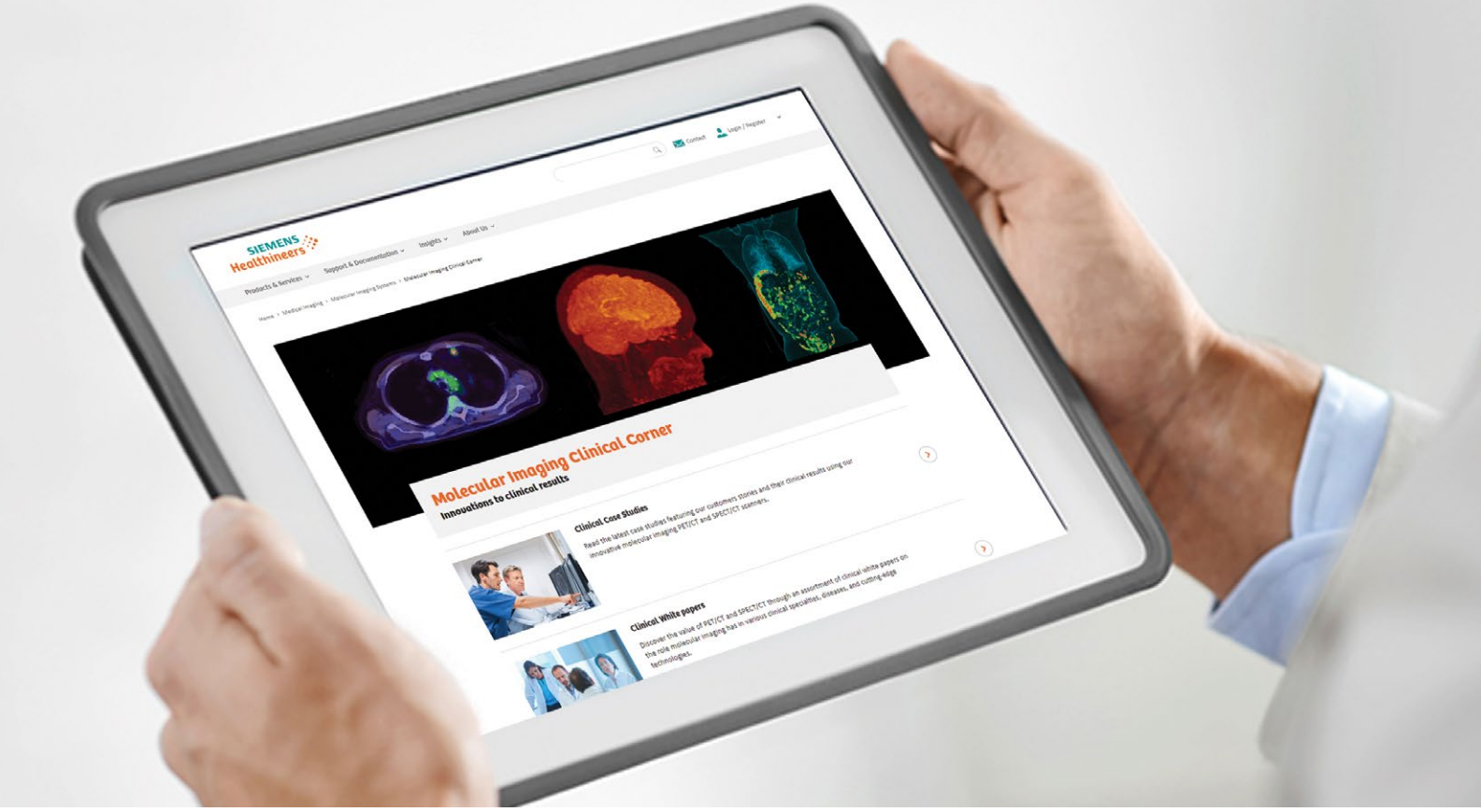

Discover the latest in molecular imaging with the Molecular Imaging Clinical Corner.

Read case studies from international healthcare institutions.

Discover the value of PET and SPECT technologies through an assortment of clinical white papers.

Expand your clinical knowledge through a wide range of archived continuing education (CE) webinars.[a]

Access current clinical information anytime, anywhere:
siemens-healthineers.com/miclinicalcorner

[a] CE webinars offer one free CE credit upon successful completion of the webinar. You can download certificates from the webinar console upon completion.

Images courtesy of University of Tennessee Medical Center, Knoxville, TN, USA; University of Groningen Medical Center, Groningen, The Netherlands; Keio University Hospital, Keio, Japan.

Imaging Life

Imaging Life is your resource for molecular imaging innovation. Read about the latest trends, best practices, news, and more from leading healthcare professionals around the world.

Connect with us on:
Facebook, Twitter, LinkedIn
or online: siemens-healthineers.com

facebook.com/siemenshealthineers

@SiemensHealth
#ImagingLife

linkedin.com/siemenshealthineers

Imaging Life online

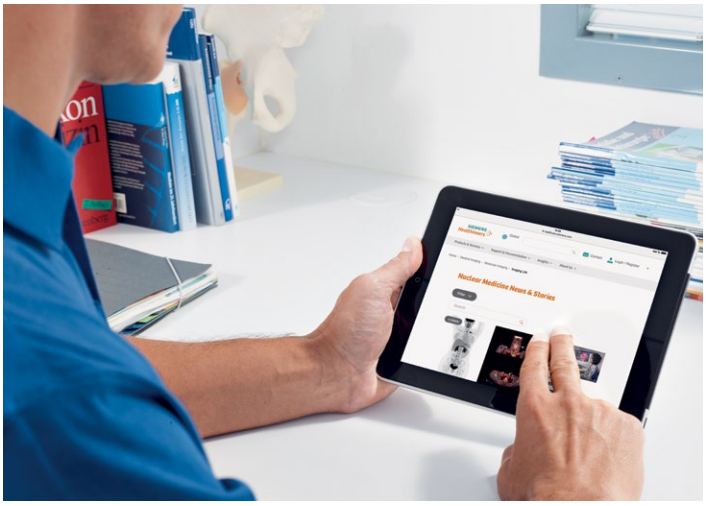

Your resource for molecular imaging innovation is now online! Access and enjoy nuclear medicine news, stories, and clinical cases on our webpage.

siemens-healthineers.com/NMNS

Imprint

Publisher
Siemens Medical Solutions USA, Inc.
2501 N. Barrington Road
Hoffman Estates, IL 60192-2061
USA
Phone: +1 847-304-7700
siemens-healthineers.com/mi

Editor
Kathryn J. McCullough
kathryn.mccullough@siemens-healthineers.com

Journalists
Erika Claessens
Univ.-Prof. Dr. Marcus Hacker
Bill Hinchberger
Claudette Lew
Kathryn J. McCullough
Colleen R. Smith

Photographers
Miquel Gonzalez
Ronald Patrick
Peter J. Reese
Alex Teuscher

Illustrations
Dmitri Broido

Text & Photographic Contribution
Primafila AG, Zurich, Switzerland/
Primafila Correspondents
independent Medien-Design, Munich, Germany
M Health, LLC, Pennsylvania, USA

Layout
Clint Poy Design, Georgia, USA

Printer
Master Print, Virginia, USA
The YGS Group, Pennsylvania, USA

***Imaging Life* is available online:**
siemens-healthineers.com/NMNS

Some of the imaging biomarkers in this publication are not currently recognized by the U.S. Food and Drug Administration (FDA) or other regulatory agencies as being safe and effective, and Siemens does not make any claims regarding their use.

DISCLAIMERS: *Imaging Life*: "The information presented in this magazine is for illustration only and is not intended to be relied upon by the reader for instruction as to the practice of medicine. Healthcare practitioners reading this information are reminded that they must use their own learning, training and expertise in dealing with their individual patients. This material does not substitute for that duty and is not intended by Siemens Healthcare GmbH to be used for any purpose in that regard." Contrast agents: "The drugs and doses mentioned herein are consistent with the approved labeling for uses and/or indications of the drug. The treating physician bears the sole responsibility for the diagnosis and treatment of patients, including drugs and doses prescribed in connection with such use. The operating instructions must always be strictly followed when operating your Siemens system. The source for the technical data is the corresponding data sheets." Trademarks: "All trademarks mentioned in this document are property of their respective owners." Results: "The outcomes achieved by the Siemens customers described herein were achieved in the customer's unique setting. Since there is no "typical" hospital and many variables exist (e.g., hospital size, case mix, level of IT adoption), there can be no guarantee that others will achieve the same results."

HIGHLIGHTS OF PRESCRIBING INFORMATION

These highlights do not include all the information needed to use Fludeoxyglucose F 18 Injection safely and effectively. See full prescribing information for Fludeoxyglucose F 18 Injection.

Fludeoxyglucose F 18 Injection, USP
For intravenous use
Initial U.S. Approval: 2005

RECENT MAJOR CHANGES

Warnings and Precautions (5.1, 5.2)	7/2010
Adverse Reactions (6)	7/2010

INDICATIONS AND USAGE

Fludeoxyglucose F18 Injection is indicated for positron emission tomography (PET) imaging in the following settings:

- Oncology: For assessment of abnormal glucose metabolism to assist in the evaluation of malignancy in patients with known or suspected abnormalities found by other testing modalities, or in patients with an existing diagnosis of cancer.
- Cardiology: For the identification of left ventricular myocardium with residual glucose metabolism and reversible loss of systolic function in patients with coronary artery disease and left ventricular dysfunction, when used together with myocardial perfusion imaging.
- Neurology: For the identification of regions of abnormal glucose metabolism associated with foci of epileptic seizures (1).

DOSAGE AND ADMINISTRATION

Fludeoxyglucose F 18 Injection emits radiation. Use procedures to minimize radiation exposure. Screen for blood glucose abnormalities.

- In the oncology and neurology settings, instruct patients to fast for 4 to 6 hours prior to the drug's injection. Consider medical therapy and laboratory testing to assure at least two days of normoglycemia prior to the drug's administration (5.2).
- In the cardiology setting, administration of glucose-containing food or liquids (e.g., 50 to 75 grams) prior to the drug's injection facilitates localization of cardiac ischemia (2.3).

Aseptically withdraw Fludeoxyglucose F 18 Injection from its container and administer by intravenous injection (2).

The recommended dose:

- for adults is 5 to 10 mCi (185 to 370 MBq), in all indicated clinical settings (2.1).
- for pediatric patients is 2.6 mCi in the neurology setting (2.2).

Initiate imaging within 40 minutes following drug injection; acquire static emission images 30 to 100 minutes from time of injection (2).

DOSAGE FORMS AND STRENGTHS

Multi-dose 30mL and 50mL glass vial containing 0.74 to 7.40 GBq/mL (20 to 200 mCi/mL) Fludeoxyglucose F 18 Injection and 4.5mg of sodium chloride with 0.1 to 0.5% w/w ethanol as a stabilizer (approximately 15 to 50 mL volume) for intravenous administration (3).

CONTRAINDICATIONS

None (4)

WARNINGS AND PRECAUTIONS

- Radiation risks: use smallest dose necessary for imaging (5.1).
- Blood glucose adnormalities: may cause suboptimal imaging (5.2).

ADVERSE REACTIONS

Hypersensitivity reactions have occurred; have emergency resuscitation equipment and personnel immediately available (6).

To report SUSPECTED ADVERSE REACTIONS, contact PETNET Solutions, Inc. at 877-473-8638 or FDA at 1-800-FDA-1088 or www.fda.gov/medwatch.

USE IN SPECIFIC POPULATIONS

Pregnancy Category C: No human or animal data. Consider alternative diagnostics; use only if clearly needed (8.1).

- Nursing mothers: Use alternatives to breast feeding (e.g., stored breast milk or infant formula) for at least 10 half-lives of radioactive decay, if Fludeoxyglucose F 18 Injection is administered to a woman who is breast-feeding (8.3).
- Pediatric Use: Safety and effectiveness in pediatric patients have not been established in the oncology and cardiology settings (8.4).

See 17 for PATIENT COUNSELING INFORMATION

Revised: 1/2016

FULL PRESCRIBING INFORMATION: CONTENTS*

* Sections or subsections omitted from the full prescribing information are not listed.

FULL PRESCRIBING INFORMATION

1 INDICATIONS AND USAGE

Fludeoxyglucose F 18 Injection is indicated for positron emission tomography (PET) imaging in the following settings:

1.1 Oncology

For assessment of abnormal glucose metabolism to assist in the evaluation of malignancy in patients with known or suspected abnormalities found by other testing modalities, or in patients with an existing diagnosis of cancer.

1.2 Cardiology

For the identification of left ventricular myocardium with residual glucose metabolism and reversible loss of systolic function in patients with coronary artery disease and left ventricular dysfunction, when used together with myocardial perfusion imaging.

1.3 Neurology

For the identification of regions of abnormal glucose metabolism associated with foci of epileptic seizures.

2 DOSAGE AND ADMINISTRATION

Fludeoxyglucose F 18 Injection emits radiation. Use procedures to minimize radiation exposure. Calculate the final dose from the end of synthesis (EOS) time using proper radioactive decay factors. Assay the final dose in a properly calibrated dose calibrator before administration to the patient [see Description (11.2)].

2.1 Recommended Dose for Adults

Within the oncology, cardiology and neurology settings, the recommended dose for adults is 5 to 10 mCi (185 to 370 MBq) as an intravenous injection.

2.2 Recommended Dose for Pediatric Patients

Within the neurology setting, the recommended dose for pediatric patients is 2.6 mCi, as an intravenous injection. The optimal dose adjustment on the basis of body size or weight has not been determined [see *Use in Special Populations (8.4)*].

2.3 Patient Preparation

- To minimize the radiation absorbed dose to the bladder, encourage adequate hydration. Encourage the patient to drink water or other fluids (as tolerated) in the 4 hours before their PET study.
- Encourage the patient to void as soon as the imaging study is completed and as often as possible thereafter for at least one hour.
- Screen patients for clinically significant blood glucose abnormalities by obtaining a history and/or laboratory tests [see *Warnings and Precautions (5.2)*]. Prior to Fludeoxyglucose F 18 PET imaging in the oncology and neurology settings, instruct patient to fast for 4 to 6 hours prior to the drug's injection.
- In the cardiology setting, administration of glucose-containing food or liquids (e.g., 50 to 75 grams) prior to Fludeoxyglucose F18 Injection facilitates localization of cardiac ischemia

2.4 Radiation Dosimetry

The estimated human absorbed radiation doses (rem/mCi) to a newborn (3.4 kg), 1-year old (9.8 kg), 5-year old (19 kg), 10-year old (32 kg), 15-year old (57 kg), and adult (70 kg) from intravenous administration of Fludeoxyglucose F 18 Injection are shown in Table 1. These estimates were calculated based on human[2] data and using the data published by the International Commission on Radiological Protection[4] for Fludeoxyglucose ^{18}F. The dosimetry data show that there are slight variations in absorbed radiation dose for various organs in each of the age groups. These dissimilarities in absorbed radiation dose are due to developmental age variations (e.g., organ size, location, and overall metabolic rate for each age group). The identified critical organs (in descending order) across all age groups evaluated are the urinary bladder, heart, pancreas, spleen, and lungs.

Table 1. Estimated Absorbed Radiation Doses (rem/mCi) After Intravenous Administration of Fludeoxyglucose F-18 Injection[a]

Organ	Newborn (3.4 kg)	1-year old (9.8 kg)	5-year old (19 kg)	10-year old (32 kg)	15-year old (57 kg)	Adult (70 kg)
Bladder wall[b]	4.3	1.7	0.93	0.60	0.40	0.32
Heart wall	2.4	1.2	0.70	0.44	0.29	0.22
Pancreas	2.2	0.68	0.33	0.25	0.13	0.096
Spleen	2.2	0.84	0.46	0.29	0.19	0.14
Lungs	0.96	0.38	0.20	0.13	0.092	0.064
Kidneys	0.81	0.34	0.19	0.13	0.089	0.074
Ovaries	0.80	0.8	0.19	0.11	0.058	0.053
Uterus	0.79	0.35	0.19	0.12	0.076	0.062
LLI wall *	0.69	0.28	0.15	0.097	0.060	0.051
Liver	0.69	0.31	0.17	0.11	0.076	0.058
Gallbladder wall	0.69	0.26	0.14	0.093	0.059	0.049
Small intestine	0.68	0.29	0.15	0.096	0.060	0.047
ULI wall **	0.67	0.27	0.15	0.090	0.057	0.046
Stomach wall	0.65	0.27	0.14	0.089	0.057	0.047
Adrenals	0.65	0.28	0.15	0.095	0.061	0.048
Testes	0.64	0.27	0.14	0.085	0.052	0.041
Red marrow	0.62	0.26	0.14	0.089	0.057	0.047
Thymus	0.61	0.26	0.14	0.086	0.056	0.044
Thyroid	0.61	0.26	0.13	0.080	0.049	0.039
Muscle	0.58	0.25	0.13	0.078	0.049	0.039
Bone surface	0.57	0.24	0.12	0.079	0.052	0.041
Breast	0.54	0.22	0.11	0.068	0.043	0.034
Skin	0.49	0.20	0.10	0.060	0.037	0.030
Brain	0.29	0.13	0.09	0.078	0.072	0.070
Other tissues	0.59	0.25	0.13	0.083	0.052	0.042

[a] MIRDOSE 2 software was used to calculate the radiation absorbed dose. Assumptions on the biodistribution based on data from Gallagher et al.[1] and Jones et al.[2]

[b] The dynamic bladder model with a uniform voiding frequency of 1.5 hours was used. *LLI = lower large intestine; **ULI = upper large intestine

2.5 Radiation Safety – Drug Handling

- Use waterproof gloves, effective radiation shielding, and appropriate safety measures when handling Fludeoxyglucose F 18 Injection to avoid unnecessary radiation exposure to the patient, occupational workers, clinical personnel and other persons.
- Radiopharmaceuticals should be used by or under the control of physicians who are qualified by specific training and experience in the safe use and handling of radionuclides, and whose experience and training have been approved by the appropriate governmental agency authorized to license the use of radionuclides.
- Calculate the final dose from the end of synthesis (EOS) time using proper radioactive decay factors. Assay the final dose in a properly calibrated dose calibrator before administration to the patient [see *Description (11.2)*].
- The dose of Fludeoxyglucose F 18 used in a given patient should be minimized consistent with the objectives of the procedure, and the nature of the radiation detection devices employed.

2.6 Drug Preparation and Administration

- Calculate the necessary volume to administer based on calibration time and dose.
- Aseptically withdraw Fludeoxyglucose F 18 Injection from its container.
- Inspect Fludeoxyglucose F 18 Injection visually for particulate matter and discoloration before administration, whenever solution and container permit.
- Do not administer the drug if it contains particulate matter or discoloration; dispose of these unacceptable or unused preparations in a safe manner, in compliance with applicable regulations.
- Use Fludeoxyglucose F 18 Injection within 12 hours from the EOS.

2.7 Imaging Guidelines

- Initiate imaging within 40 minutes following Fludeoxyglucose F 18 Injection administration.
- Acquire static emission images 30 to 100 minutes from the time of injection.

3 DOSAGE FORMS AND STRENGTHS

Multiple-dose 30 mL and 50 mL glass vial containing 0.74 to 7.40 GBq/mL (20 to 200 mCi/mL) of Fludeoxyglucose F 18 Injection and 4.5 mg of sodium chloride with 0.1 to 0.5% w/w ethanol as a stabilizer (approximately 15 to 50 mL volume) for intravenous administration.

4 CONTRAINDICATIONS

None

5 WARNINGS AND PRECAUTIONS

5.1 Radiation Risks

Radiation-emitting products, including Fludeoxyglucose F 18 Injection, may increase the risk for cancer, especially in pediatric patients. Use the smallest dose necessary for imaging and ensure safe handling to protect the patient and health care worker [see *Dosage and Administration (2.5)*].

5.2 Blood Glucose Abnormalities

In the oncology and neurology setting, suboptimal imaging may occur in patients with inadequately regulated blood glucose levels. In these patients, consider medical therapy and laboratory testing to assure at least two days of normoglycemia prior to Fludeoxyglucose F 18 Injection administration.

6 ADVERSE REACTIONS

Hypersensitivity reactions with pruritus, edema and rash have been reported in the post-marketing setting. Have emergency resuscitation equipment and personnel immediately available.

7 DRUG INTERACTIONS

The possibility of interactions of Fludeoxyglucose F 18 Injection with other drugs taken by patients undergoing PET imaging has not been studied.

8 USE IN SPECIFIC POPULATIONS

8.1 Pregnancy

Pregnancy Category C

Animal reproduction studies have not been conducted with Fludeoxyglucose F 18 Injection. It is also not known whether Fludeoxyglucose F 18 Injection can cause fetal harm when administered to a pregnant woman or can affect reproduction capacity. Consider alternative diagnostic tests in a pregnant woman; administer Fludeoxyglucose F 18 Injection only if clearly needed.

8.3 Nursing Mothers

It is not known whether Fludeoxyglucose F 18 Injection is excreted in human milk. Consider alternative diagnostic tests in women who are breast-feeding. Use alternatives to breast feeding (e.g., stored breast milk or infant formula) for at least 10 half-lives of radioactive decay, if Fludeoxyglucose F 18 Injection is administered to a woman who is breast-feeding.

8.4 Pediatric Use

The safety and effectiveness of Fludeoxyglucose F 18 Injection in pediatric patients with epilepsy is established on the basis of studies in adult and pediatric patients. In pediatric patients with epilepsy, the recommended dose is 2.6 mCi. The optimal dose adjustment on the basis of body size or weight has not been determined. In the oncology or cardiology settings, the safety and effectiveness of Fludeoxyglucose F 18 Injection have not been established in pediatric patients.

11 DESCRIPTION

11.1 Chemical Characteristics

Fludeoxyglucose F 18 Injection is a positron emitting radiopharmaceutical that is used for diagnostic purposes in conjunction with positron emission tomography (PET) imaging. The active ingredient 2-deoxy-2-[^{18}F]fluoro-D-glucose has the molecular formula of $C_6H_{11}{}^{18}FO_5$ with a molecular weight of 181.26, and has the following chemical structure:

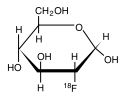

Fludeoxyglucose F 18 Injection is provided as a ready to use sterile, pyrogen free, clear, colorless solution. Each mL contains between 0.740 to 7.40GBq (20.0 to 200 mCi) of 2-deoxy-2-[^{18}F]fluoro-D-glucose at the EOS, 4.5 mg of sodium chloride and 0.1 to 0.5% w/w ethanol as a stabilizer. The pH of the solution is between 4.5 and 7.5. The solution is packaged in a multiple-dose glass vial and does not contain any preservative.

11.2 Physical Characteristics

Fluorine F 18 decays by emitting positron to Oxygen O 16 (stable) and has a physical half-life of 109.7 minutes. The principal photons useful for imaging are the dual 511 keV gamma photons, that are produced and emitted simultaneously in opposite direction when the positron interacts with an electron (Table 2).

Table 2. Principal Radiation Emission Data for Fluorine F18

Radiation/Emission	% Per Disintegration	Mean Energy
Positron (b+)	96.73	249.8 keV
Gamma (±)*	193.46	511.0 keV

*Produced by positron annihilation

From: Kocher, D.C. Radioactive Decay Tables DOE/TIC-I 1026, 89 (1981)

The specific gamma ray constant (point source air kerma coefficient) for fluorine F 18 is 5.7 R/hr/mCi (1.35 x 10^{-6} Gy/hr/kBq) at 1 cm. The half-value layer (HVL) for the 511 keV photons is 4 mm lead (Pb). The range of attenuation coefficients for this radionuclide as a function of lead shield thickness is shown in Table 3. For example, the interposition of an 8 mm thickness of Pb, with a coefficient of attenuation of 0.25, will decrease the external radiation by 75%.

Table 3. Radiation Attenuation of 511 keV Photons by lead (Pb) shielding

Shield thickness (Pb) mm	Coefficient of attenuation
0	0.00
4	0.50
8	0.25
13	0.10
26	0.01
39	0.001
52	0.0001

For use in correcting for physical decay of this radionuclide, the fractions remaining at selected intervals after calibration are shown in Table 4.

Table 4. Physical Decay Chart for Fluorine F18

Minutes	Fraction Remaining
0*	1.000
15	0.909
30	0.826
60	0.683
110	0.500
220	0.250

*calibration time

12 CLINICAL PHARMACOLOGY

12.1 Mechanism of Action

Fludeoxyglucose F 18 is a glucose analog that concentrates in cells that rely upon glucose as an energy source, or in cells whose dependence on glucose increases under pathophysiological conditions. Fludeoxyglucose F 18 is transported through the cell membrane by facilitative glucose transporter proteins and is phosphorylated within the cell to [^{18}F] FDG-6-phosphate by the enzyme hexokinase. Once phosphorylated it cannot exit until it is dephosphorylated by glucose-6-phosphatase. Therefore, within a given tissue or pathophysiological process, the retention and clearance of Fludeoxyglucose F 18 reflect a balance involving glucose transporter, hexokinase and glucose-6-phosphatase activities. When allowance is made for the kinetic differences between glucose and Fludeoxyglucose F 18 transport and phosphorylation (expressed as the ‚lumped constant" ratio), Fludeoxyglucose F 18 is used to assess glucose metabolism.

In comparison to background activity of the specific organ or tissue type, regions of decreased or absent uptake of Fludeoxyglucose F 18 reflect the decrease or absence of glucose metabolism. Regions of increased uptake of Fludeoxyglucose F 18 reflect greater than normal rates of glucose metabolism.

12.2 Pharmacodynamics

Fludeoxyglucose F 18 Injection is rapidly distributed to all organs of the body after intravenous administration. After background clearance of Fludeoxyglucose F 18 Injection, optimal PET imaging is generally achieved between 30 to 40 minutes after administration.

In cancer, the cells are generally characterized by enhanced glucose metabolism partially due to (1) an increase in activity of glucose transporters, (2) an increased rate of phosphorylation activity, (3) a reduction of phosphatase activity or, (4) a dynamic alteration in the balance among all these processes. However, glucose metabolism of cancer as reflected by Fludeoxyglucose F 18 accumulation shows considerable variability. Depending on tumor type, stage, and location, Fludeoxyglucose F 18 accumulation may be increased, normal, or decreased. Also, inflammatory cells can have the same variability of uptake of Fludeoxyglucose F 18.

In the heart, under normal aerobic conditions, the myocardium meets the bulk of its energy requirements by oxidizing free fatty acids. Most of the exogenous glucose taken up by the myocyte is converted into glycogen. However, under ischemic conditions, the oxidation of free fatty acids decreases, exogenous glucose becomes the preferred myocardial sub strate, glycolysis is stimulated, and glucose taken up by the myocyte is metabolized immediately instead of being converted into glycogen. Under these conditions,

phosphorylated Fludeoxyglucose F 18 accumulates in the myocyte and can be detected with PET imaging.

In the brain, cells normally rely on aerobic metabolism. In epilepsy, the glucose metabolism varies. Generally, during a seizure, glucose metabolism increases. Interictally, the seizure focus tends to be hypometabolic.

12.3 Pharmacokinetics

Distribution: In four healthy male volunteers, receiving an intravenous administration of 30 seconds induration, the arterial blood level profile for Fludeoxyglucose F 18 decayed triexponentially. The effective half-life ranges of the three phases were 0.2 to 0.3 minutes, 10 to 13 minutes with a mean and standard deviation (STD) of 11.6 (±) 1.1 min, and 80 to 95 minutes with a mean and STD of 88 (±) 4 min.

Plasma protein binding of Fludeoxyglucose F 18 has not been studied.

Metabolism: Fludeoxyglucose F 18 is transported into cells and phosphorylated to [^{18}F]-FDG-6- phosphate at a rate proportional to the rate of glucose utilization within that tissue. [F18]-FDG-6-phosphate presumably is metabolized to 2-deoxy-2-[F18]fluoro-6-phospho-D-mannose([F 18]FDM-6-phosphate).

Fludeoxyglucose F 18 Injection may contain several impurities (e.g., 2-deoxy-2-chloro-D-glucose (ClDG)). Biodistribution and metabolism of ClDG are presumed to be similar to Fludeoxyglucose F 18 and would be expected to result in intracellular formation of 2-deoxy-2-chloro-6-phospho-D-glucose (ClDG-6-phosphate) and 2-deoxy-2-chloro-6-phospho-D-mannose (ClDM-6-phosphate). The phosphorylated deoxyglucose compounds are dephosphorylated and the resulting compounds (FDG, FDM, ClDG, and ClDM) presumably leave cells by passive diffusion. Fludeoxyglucose F 18 and related compounds are cleared from non-cardiac tissues within 3 to 24 hours after administration. Clearance from the cardiac tissue may require more than 96 hours. Fludeoxyglucose F 18 that is not involved in glucose metabolism in any tissue is then excreted in the urine.

Elimination: Fludeoxyglucose F 18 is cleared from most tissues within 24 hours and can be eliminated from the body unchanged in the urine. Three elimination phases have been identified in the reviewed literature. Within 33 minutes, a mean of 3.9% of the administrated radioactive dose was measured in the urine. The amount of radiation exposure of the urinary bladder at two hours post-administration suggests that 20.6% (mean) of the radioactive dose was present in the bladder.

Special Populations:

The pharmacokinetics of Fludeoxyglucose F 18 Injection have not been studied in renally-impaired, hepatically impaired or pediatric patients. Fludeoxyglucose F 18 is eliminated through the renal system. Avoid excessive radiation exposure to this organ system and adjacent tissues.

The effects of fasting, varying blood sugar levels, conditions of glucose intolerance, and diabetes mellitus on Fludeoxyglucose F 18 distribution in humans have not been ascertained [*see Warnings and Precautions (5.2)*].

13 NONCLINICAL TOXICOLOGY

13.1 Carcinogenesis, Mutagenesis, Impairment of Fertility

Animal studies have not been performed to evaluate the Fludeoxyglucose F 18 Injection carcinogenic potential, mutagenic potential or effects on fertility.

14 CLINICAL STUDIES

14.1 Oncology

The efficacy of Fludeoxyglucose F 18 Injection in positron emission tomography cancer imaging was demonstrated in 16 independent studies. These studies prospectively evaluated the use of Fludeoxyglucose F 18 in patients with suspected or known malignancies, including non-small cell lung cancer, colo-rectal, pancreatic, breast, thyroid, melanoma, Hodgkin's and non-Hodgkin's lymphoma, and various types of metastatic cancers to lung, liver, bone, and axillary nodes. All these studies had at least 50 patients and used pathology as a standard of truth. The Fludeoxyglucose F 18 Injection doses in the studies ranged from 200 MBq to 740 MBq with a median and mean dose of 370 MBq.

In the studies, the diagnostic performance of Fludeoxyglucose F 18 Injection varied with the type of cancer, size of cancer, and other clinical conditions. False negative and false positive scans were observed. Negative Fludeoxyglucose F 18 Injection PET scans do not exclude the diagnosis of cancer. Positive Fludeoxyglucose F 18 Injection PET scans can not replace pathology to establish a diagnosis of cancer. Non-malignant conditions such as fungal infections, inflammatory processes and benign tumors have patterns of increased glucose metabolism that may give rise to false-positive scans. The efficacy of Fludeoxyglucose F 18 Injection PET imaging in cancer screening was not studied.

14.2 Cardiology

The efficacy of Fludeoxyglucose F 18 Injection for cardiac use was demonstrated in ten independent, prospective studies of patients with coronary artery disease and chronic left ventricular systolic dysfunction who were scheduled to undergo coronary revascularization. Before revascularization, patients underwent PET imaging with Fludeoxyglucose F 18 Injection (74 to 370 MBq, 2 to 10 mCi) and perfusion imaging with other diagnostic radiopharmaceuticals. Doses of Fludeoxyglucose F 18 Injection ranged from 74 to 370 MBq (2 to 10 mCi). Segmental, left ventricular, wall-motion assessments of asynergic areas made before revascularization were compared in a blinded manner to assessments made after successful revascularization to identify myocardial segments with functional recovery.

Left ventricular myocardial segments were predicted to have reversible loss of systolic function if they showed Fludeoxyglucose F 18 accumulation and reduced perfusion (i.e., flow-metabolism mismatch). Conversely, myocardial segments were predicted to have irreversible loss of systolic function if they showed reductions in both Fludeoxyglucose F 18 accumulation and perfusion (i.e., matched defects).

Findings of flow-metabolism mismatch in a myocardial segment may suggest that successful revascularization will restore myocardial function in that segment. However, false-positive tests occur regularly, and the decision to have a patient undergo revascularization should not be based on PET findings alone. Similarly, findings of a matched defect in a myocardial segment may suggest that myocardial function will not recover in that segment, even if it is successfully revascularized. However, false-negative tests occur regularly, and the decision to recommend against coronary revascularization, or to recommend a cardiac transplant, should not be based on PET findings alone. The reversibility of segmental dysfunction as predicted with Fludeoxyglucose F 18 PET imaging depends on successful coronary revascularization. Therefore, in patients with a low likelihood of successful revascularization, the diagnostic usefulness of PET imaging with Fludeoxyglucose F 18 Injection is more limited.

14.3 Neurology

In a prospective, open label trial, Fludeoxyglucose F 18 Injection was evaluated in 86 patients with epilepsy. Each patient received a dose of Fludeoxyglucose F 18 Injection in the range of 185 to 370 MBq (5 to 10 mCi). The mean age was 16.4 years (range: 4 months to 58 years; of these, 42 patients were less than 12 years and 16 patients were less than 2 years old). Patients had a known diagnosis of complex partial epilepsy and were under evaluation for surgical treatment of their seizure disorder. Seizure foci had been previously identified on ictal EEGs and sphenoidal EEGs. Fludeoxyglucose F 18 Injection PET imaging confirmed previous diagnostic findings in 16% (14/87) of the patients; in 34% (30/87) of the patients, Fludeoxyglucose F 18 Injection PET images provided new findings. In 32% (27/87), imaging with Fludeoxyglucose F 18 Injection was inconclusive. The impact of these imaging findings on clinical outcomes is not known.

Several other studies comparing imaging with Fludeoxyglucose F 18 Injection results to subsphenoidal EEG, MRI and/or surgical findings supported the concept that the degree of hypometabolism corresponds to areas of confirmed epileptogenic foci. The safety and effectiveness of Fludeoxyglucose F 18 Injection to distinguish idiopathic epileptogenic foci from tumors or other brain lesions that may cause seizures have not been established.

15 REFERENCES

1. Gallagher B.M., Ansari A., Atkins H., Casella V., Christman D.R., Fowler J.S., Ido T., MacGregor R.R., Som P., Wan C.N., Wolf A.P., Kuhl D.E., and Reivich M. "Radiopharmaceuticals XXVII. ^{18}F-labeled 2-deoxy-2-fluoro-d-glucose as a radiopharmaceutical for measuring regional myocardial glucose metabolism in vivo: tissue distribution and imaging studies in animals," J Nucl Med, 1977; 18, 990-6.
2. Jones S.C., Alavi, A., Christman D., Montanez, I., Wolf, A.P., and Reivich M. "The radiation dosimetry of 2 [F-18] fluoro-2-deoxy-D-glucose in man," J Nucl Med, 1982; 23, 613-617.
3. Kocher, D.C. "Radioactive Decay Tables: A handbook of decay data for application to radiation dosimetry and radiological assessments," 1981, DOE/TIC-I 1026, 89.
4. ICRP Publication 53, Volume 18, No. l-4,1987, pages 75-76.

16 HOW SUPPLIED/STORAGE AND DRUG HANDLING

Fludeoxyglucose F 18 Injection is supplied in a multi-dose, capped 30 mL and 50 mL glass vial containing between 0.740 to 7.40GBq/mL (20 to 200 mCi/mL), of no carrier added 2deoxy-2-[F 18] fluoro-D-glucose, at end of synthesis, in approximately 15 to 50 mL. The contents of each vial are sterile, pyrogen-free and preservative-free.

NDC 40028-511-30; 40028-511-50

Receipt, transfer, handling, possession, or use of this product is subject to the radioactive material regulations and licensing requirements of the U.S. Nuclear Regulatory Commission, Agreement States or Licensing States as appropriate.

Store the Fludeoxyglucose F 18 Injection vial upright in a lead shielded container at 25°C (77°F); excursions permitted to 15-30°C (59-86°F).

Store and dispose of Fludeoxyglucose F 18 Injection in accordance with the regulations and a general license, or its equivalent, of an Agreement State or a Licensing State.

The expiration date and time are provided on the container label. Use Fludeoxyglucose F 18 Injection within 12 hours from the EOS time.

17 PATIENT COUNSELING INFORMATION

Instruct patients in procedures that increase renal clearance of radioactivity. Encourage patients to:

- drink water or other fluids (as tolerated) in the 4 hours before their PET study.
- void as soon as the imaging study is completed and as often as possible thereafter for at least one hour.

Manufactured by: PETNET Solutions Inc.
810 Innovation Drive
Knoxville, TN 37932

Distributed by: PETNET Solutions Inc.
810 Innovation Drive
Knoxville, TN 37932

PETNET Solutions

Legal information: On account of certain regional limitations of sales rights and service availability, we cannot guarantee that all products included in this publication are available through the Siemens sales organization worldwide. Availability and packaging may vary by country and is subject to change without prior notice. Some/all of the features and products described herein may not be available in the United States.

The information in this document contains general technical descriptions of specifications and options as well as standard and optional features, which do not always have to be present in individual cases.

Siemens reserves the right to modify the design, packaging, specifications, and options described herein without prior notice.

Please contact your local Siemens sales representative for the most current information.

Note: Any technical data contained in this document may vary within defined tolerances. Original images always lose a certain amount of detail when reproduced.

Siemens Healthineers Headquarters
Siemens Healthcare GmbH
Henkestr. 127
91052 Erlangen
Germany
Phone: +49 9131 84-0
siemens-healthineers.com

Published by
Siemens Medical Solutions USA, Inc.
2501 N. Barrington Road
Hoffman Estates, IL 60192-2061
USA
Phone: +1 847-304-7700
siemens-healthineers.com/mi

Order No. A91MI-10497-M1-7600 | Printed in USA | MI-4547.KM.CP.SNMMI.13K

siemens-healthineers.com/NMNS